STYRELSEN FÖR

VINTERSJÖFARTSFORSKNING

WINTER NAVIGATION RESEARCH BOARD

Research Report No 45

BEPERS

(Bothnian Experiment in Preparation for ERS-1)
PILOT STUDY. DATA REPORT

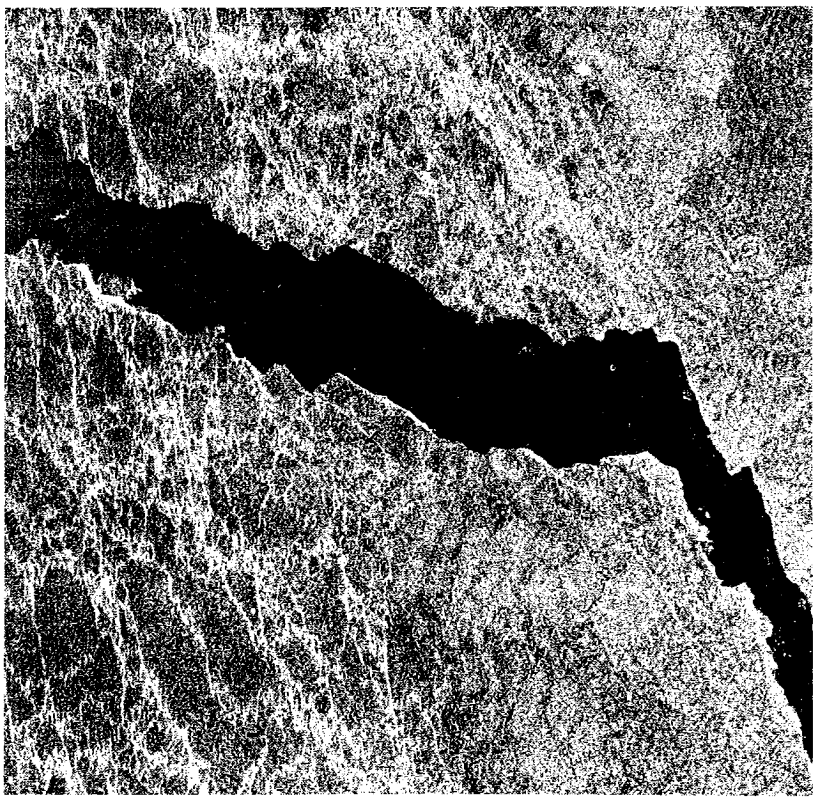

C.N.E.S. VARAN-S X-BAND SAR
SEA OF BOTHNIA 2 APRIL 1987
IMAGE SIZE 10 × 10 KM

Sjöfartsstyrelsen
Finland

Finnish Board of Navigation

Sjöfartsverket
Sverige

Swedish Administration
of Shipping and Navigation

STYRELSEN FÖR
VINTERSJÖFARTSFORSKNING

WINTER NAVIGATION RESEARCH BOARD

Research Report No 45

BEPERS

(Bothnian Experiment in Preparation for ERS-1)

PILOT STUDY. DATA REPORT

Helsinki 1988

ISBN 951-47-1278-1

VAPK Kampin VALTIMO 1988

FOREWORD

The Winter Navigation Research Board presents its report No. 45. This report belongs to the BEPERS (Bothnian Experiment in Preparation for ERS-1) programme, a joint Finnish and Swedish research programme for learning to use the data of ERS-1 satellite of ESA in operative ice mapping and in ice research. This report presents the data and preliminary results of BEPERS Pilot Study which was performed in the Gulf of Bothnia and Northern Baltic Sea Proper during 30 March - 3 April 1987. The principal object of BEPERS Pilot Study was the use of Synthetic Aperture Radar (SAR) in remote sensing of brackish water pack ice.

The following institutes participated in the experiment: Finnish Institute of Marine Research, Helsinki University of Technology, Technical Research Centre of Finland VTT, University of Helsinki, Chalmers Technical University, Swedish Defense Research Institute FOA3, Lund Institute of Technolocy, Swedish Meteorological and Hydrological Institute SMHI, and Swedish Space Corporation. Most valuable contribution in the operational level was also given by the Army Map Service, Board of Navigation and National Board of Survey from Finland and the Coast Guard from Sweden. SAR imaging was performed by GDTA (Groupement pour le Développement de la Télédetection Aérospatiale), Toulouse, France and funded by Technology Development Centre (TEKES) in Finland.

The Winter Navigation Research Board expresses its thanks to all who have taken part in this field experiment.

Helsinki and Norrköping, January 1988

Jan-Erik Jansson

Kaj Janérus

BEPERS (Bothnian Experiment in Preparation for ERS-1) PILOT STUDY. DATA REPORT

In: BEPERS Pilot Study. Data Report. Styrelsen för Vintersjöfartsforskning/Winter Navigation Research Board, Rep. No 45, p. 1-15. Helsinki 1988.

I OVERVIEW OF BEPERS PILOT STUDY

By Matti Leppäranta[1)] and Risto Kuittinen[2)]

1) Finnish Institute of Marine Research
P.O. Box 33, SF-00931 Helsinki, Finland

2) Technical Research Centre of Finland VTT, Vuorimiehentie 5
02150 Espoo, Finland

ABSTRACT

An overview of a field experiment BEPERS Pilot Study on use of Synthetic Aperture Radar (SAR) in sea ice remote sensing is given. This experiment is a part of the BEPERS (Bothnian Experiment in Preparation for ERS-1) programme to learn to use ERS-1 data in the Baltic Sea. It was organized by the Technical Research Centre of Finland and the Finnish Institute of Marine Research, and it was carried through in the Baltic Sea during 30 March - 3 April 1987. There were four separate study areas. French Varan-S SAR imaged these areas on 2 April. Ground truth observations were made at three bases, and supporting remote sensing data were obtained for all study areas.

1. INTRODUCTION

In the Baltic Sea the length of ice season is about half a year. The winter traffic is, however, intensive, and with the help of 25-30 icebreakers all the main harbours are kept open throughout

the year. It is very important to the economics of navigation to map and predict the ice conditions properly. In Finland and in Sweden a lot of effort has been put on ice research in support of the winter shipping (e.g. Leppäranta, 1986).

Remote sensing methods are largely used in operative ice mapping in the Baltic Sea. Presently the main remote sensing tools are NOAA images and visual reconnaissance. It is expected that the next significant improvement in sea ice remote sensing will come true in next decade with satellite Synthetic Aperture Radars (SAR). The first satellite carrying SAR will be ERS-1 of the European Space Agency (ESA) to be launched in 1990. To prepare for ERS-1, a joint research programme BEPERS (Bothnian Experiment in Preparation for ERS-1) has been prepared by Finland and Sweden. The aim of this programme is learning for the use of SAR in the Baltic Sea ice conditions. It is worth mentioning that Baltic Sea has an important part in the PIPOR (A Programme for International Polar Oceans Research) ERS-1 proposal to ESA (PIPOR Group, 1985). The main field effort of BEPERS programme is planned to be made in March 1988 (Thompson and Leppäranta, 1987).

In Finland it was considered very necessary to carry through a pilot study in 1987. This experiment, BEPERS Pilot Study, was then made during 30 March-3 April largely along the lines of BEPERS-88 plan but with a smaller field programme. For the SAR data the French VARAN-S X-band SAR was chartered from GDTA (Groupement pour le Développement de la Télédetection Aérospatiale) which carried it through together with IGN (Institut Géographique National) and CNES (Centre National d'Etudes Spatiales). Four study areas were chosen in the northern part of the Baltic Sea. In each area intensive ground and remote sensing observations were made for correct interpretation of the SAR images. The Swedish group joined in the experiment and made ground measurements in one study area and organized SLAR (Side Looking Airborne Radar) and infrared scanner observations.

BEPERS Pilot Study was very successful and no major drawbacks occurred. Even the weather was very good providing the possibility to carry through the whole ground truth program and aerial photography and to acquire good quality satellite data to verify the SAR images.

2. ORGANIZATION OF THE EXPERIMENT

2.1 Timing

The period of the experiment was 30 March - 3 April 1987, and the operation day of the SAR flight was 2 April as had been scheduled. The whole period was used for ground observations and additional remote sensing measurements. Prior to the flight the image areas were marked. The weather conditions were very good during the experiment.

2.2 Bases and study areas

In this experiment four study areas were chosen in the northern part of the Baltic Sea (Fig. 1). Three of the study areas had field groups in bases. Helsinki airport was an additional base for coordination of the remote sensing flights in Finland. The coordination centre of the whole experiment was R/V Aranda in area II.

In each study area I-IV SAR imaging was performed along a straight strip which was 40-70 km long and 10 km wide. These strips are shown in Fig. 1. Additional remote sensing observations and ground measurements were made in and around SAR strips. Helsinki-Vantaa airport was the base of the SAR plane and aerial photography plane.

The study areas were located in quite different ice conditions. The most thick and rough ice occurs in area I. The ice pack becomes thinner and smoother southward, and finally, the ice edge is located in area IV. For more, the salinity of the ice increases southward from less than one per mille in area I to around three in area IV.

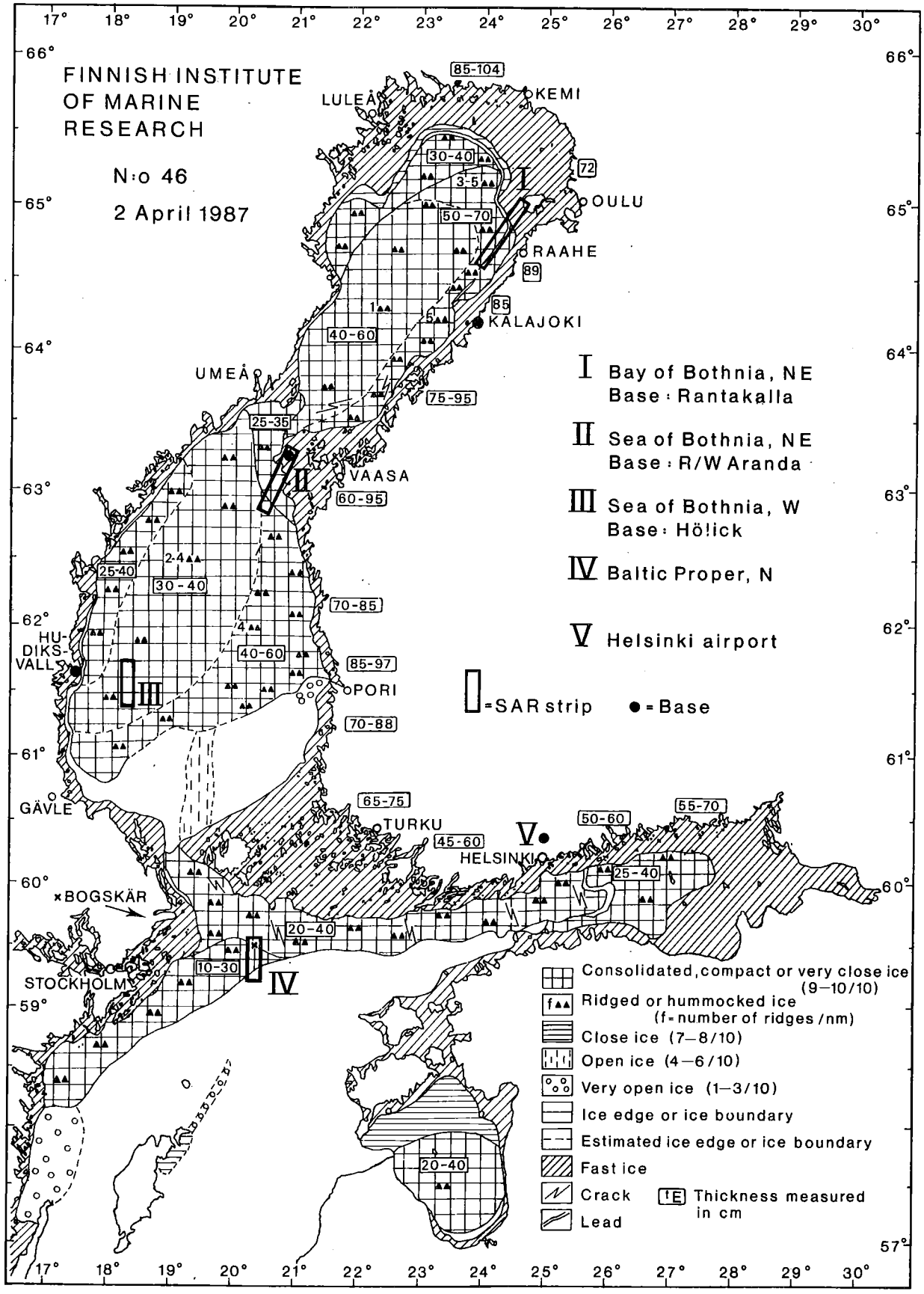

Figure 1. Baltic Sea ice chart, 2 April 1987 (FIMR, 1987). Also shown are the locations of the bases and study areas in BEPERS Pilot Study.

Six Finnish and six Swedish institutes took part in this experiment. They are listed below

Finland:	Army Map Service	AMS
	Finnish Institute of Marine Research	FIMR
	Helsinki University of Technology	HUT
	National Board of Survey	NBS
	Technical Research Centre of Finland	VTT
	University of Helsinki	UH
Sweden:	Chalmers Technical University	CTU
	Coast Guard	CG
	Lund Institute of Technology	LIT
	Swedish Defense Research Institute	FOA3
	Swedish Meteorological and Hydrological Institute	SMHI
	Swedish Space Corporation	SSC

Field work in areas I and II was organized by FIMR and in area III by CTU and SMHI. VTT and SSC were responsible for organizing the remote sensing flights.

The bases and study areas are described briefly below:

I Bay of Bothnia, NE

The base was a coastal hotel Rantakalla in Kalajoki. The helicopter of the Finnish icebreakers in the Bay of Bothnia could be used in marking and field work. Operative days were 1 and 2 April.

The centre line of the SAR image strip was the line Marjaniemi-Nahkiainen of 60 km length (Fig. 1). Both these endpoints are lighthouses. Approximately one-third of the line goes over the fast ice area southwest of the island of Hailuoto.

Chief scientist:	Jouni Vainio	FIMR
Other participants:	Jari Haapala	FIMR
	Henry Söderman	FIMR

II Sea of Bothnia, NE

The base was R/V Aranda which was moored to fast ice at the fast ice boundary in the Vaasa archipelago (Fig. 1). Aranda served as the coordination centre of the experiment. For more, the field group was largest in this area, and Aranda also was the main ground data base. One helicopter was aboard Aranda to be used just for this experiment for the whole period.

Aranda was located in the northern corner of the SAR image strip. This strip extended 60 km to the direction SSW (203° magnetic) from Aranda.

Chief scientist:	Matti Leppäranta	FIMR
Other participants:	Hanna Kemppainen	FIMR
	Pekka Kosloff	FIMR
	Terhikki Manninen	FIMR
	Juhani Rapo	FIMR
	Erkki Palosuo	UH
	Yrjö Rauste	VTT
	Martti Hallikainen	HUT
	Juha Hyyppä	HUT
	Martti Toikka	HUT
	Eva Cronström	SSC
	Roland Johansson	CTU
	Peter Ulriksen	LIT

III Sea of Bothnia, W

The base was here a Swedish pilot station Hölick in Hornslandet (Fig. 1). This area was in the responsibility of the Swedish group.

The centre line of the SAR image strip was defined as 18°15'E. The starting point was 61°43'N and the strip extended 40 km south. There is no land in this area.

Chief scientist:	Thomas Thompson	SMHI
Other participants:	Bertil Håkansson	SMHI
	Jan Askne	CTU
	Lars Ulander	CTU
	Bertil Brusmark	FOA3

IV Baltic Proper, N

There was no field group or base in this area. However, it was considered important to have this area imaged with SAR because the main ice edge in the Baltic Sea was here (Fig. 1). The SAR image can be verified mainly on the basis of aerial photography and routine ice observations made by Finnish and Swedish ice services.

The centre line of the SAR image strip was defined as from 10 km north of Bogskär (lighthouse) to 30 km south of Bogskär (Fig. 1). The orientation of the line was strictly north-south.

V Helsinki airport

Helsinki airport was the base of the French VARAN-S SAR plane (Boeing B-17). In addition, the plane which was used for the aerial photography was also based here. The photography was carried through by the National Board of Survey.

Chief scientist:	Risto Kuittinen	VTT

2.3 Marking of the areas

It is a crucial point to mark the study areas properly. This is first of all needed in order to compare various remote sensing products with each other and with ground measurements.

Geographic coordinates of a few markers are also needed to correct various geometric scaling errors in the remote sensing data.

Land marks were available for SAR strips I, II and IV. In addition four markers were deployed in each of the strips I, II and III. These markers consisted of an aluminium corner reflector for the SAR and a cross or a circle for the aerial photography (Fig. 2). The visual mark was made either by using dye or by showeling snow away from the top of the ice. The geographic coordinates of the markers were obtained with the Decca Navigator system of the helicopters. The relative accuracy of Decca is tens of meters. With this accuracy we also get the geographic coordinates of the markers if the Decca coordinates of a nearby known land mark are also measured then.

3. FIELD PROGRAMME

The principal instrument in this experiment was the synthetic aperture radar (SAR). Other remote sensing observations and ground measurements were made mainly in order to interprete the SAR image correctly.

The weather conditions were very good through the period of the experiment. South-southeasterly flow of mild air was then prevailing in Finland. On March 31 the sky was clear over all the study areas, and this day was the best for satellite imagery. The next day was worse but fortunately the SAR day, April 2, was better again. Fig. 3 shows the weather chart in the afternoon of April 2. The high pressure was getting stronger in northern Finland and the air became clearer in the afternoon. In area I the sky was all clear while in other areas the cloudiness was more than fifty percent. However, the clouds were located at high altitude and did not cause difficulties to aerial photography.

Figure 2. The marking system for SAR and aerial photography in BEPERS Pilot Study.

3.1 SAR image

The French VARAN-S SAR is an X-band SAR (frequency 9.37 GHz). It is installed in Boeing B-17, the "Flying Fortress" of the Second World War. Helsinki airport was the base of the plane.

In this experiment the SAR imaging was performed from north to south, i.e. the strips I-IV were imaged in the order of their numbering. The SAR looked to the right from the flight direction, and the 10-km wide image strip was located at 2-12 km distance from the path of the plane. The flight altitude was 6000 m and thus the incidence angle of the radar beam at the ice surface was 11-62 degrees.

SAR imaging was performed with horizontal polarization. Processed images were of and 3-m and 9-m resolution. Quick-look images were available right after the flight and were

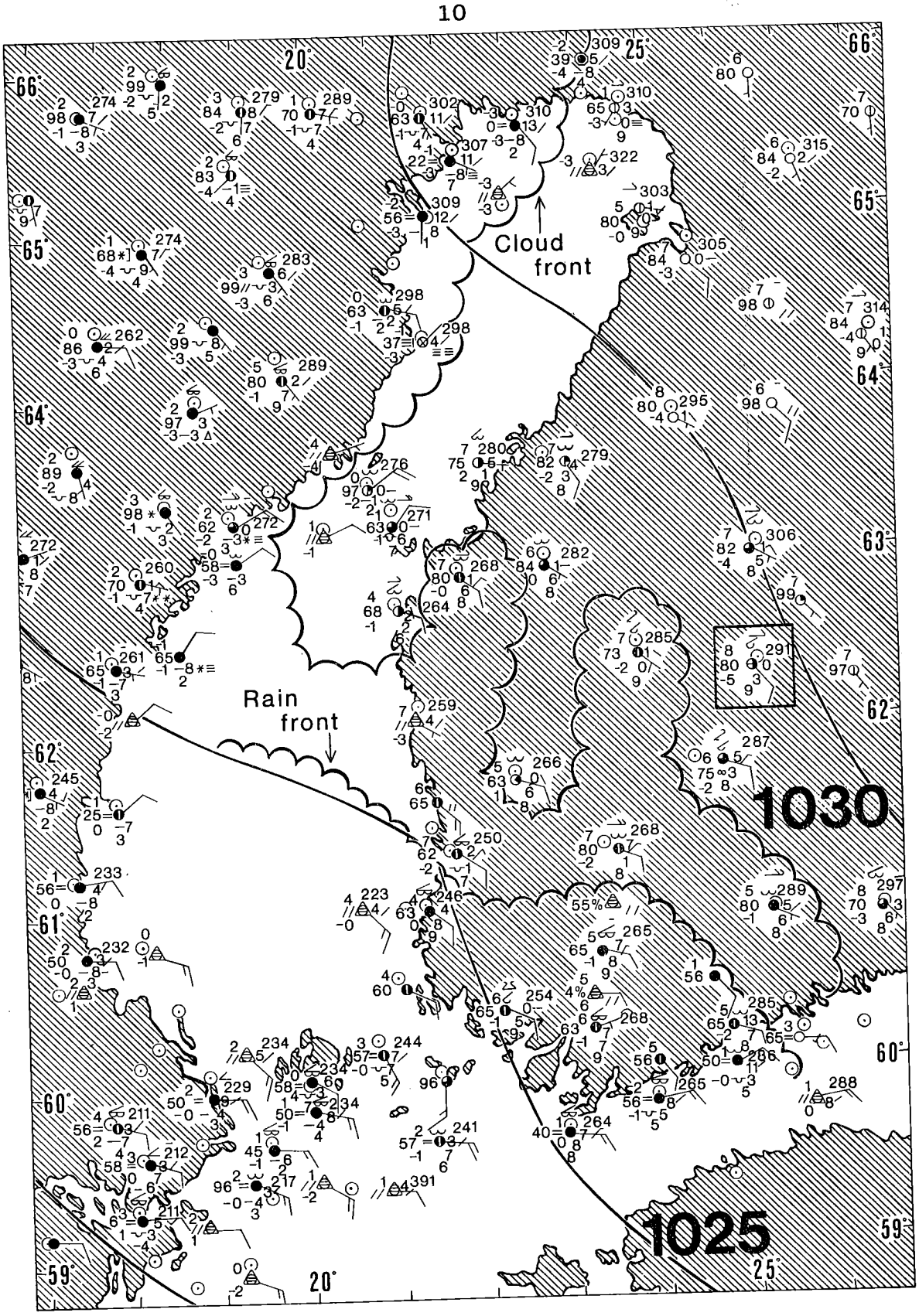

Figure 3. Weather chart on 2 April, 15.00 hrs (1200 UTC). Standard notation. E.g. station at about 62°30'N 25°E (boxed): 8 = air temperature 8°C, 80 = relative humidity 80 %, 291 = air pressure 1029.1 mb, lower circle shows cloudiness of 5/8 and the line on it indicates SE wind, and the upper circle with dot shows the location of the observation station. (Finnish Meteorol. Inst., 1987).

transported to Aranda early 3 April. Raw data processing was made in France, and the processed data were then sent to Finland. This processing time was about six weeks.

3.2 Ground measurements

The ground data programme consisted of a general description of ice conditions in the study areas and detailed measurements at selected (relatively) homogeneous patches. These patches were areas of different representative ice types, and their size was of the order of 1 km x 1 km.

The general description is mainly based on helicopter reconnaissance flights. Routine observations of the Finnish and Swedish ice services could also be used for additional information. The products are presented in ice chart form. These charts are similar to routine ice charts but their scale is naturally larger. The ice charts basically describe ice type and ice thickness.

Detailed measurements were made in the selected homogeneous patches. The observation programme of the study areas I-III is shown in Table 1.

Table 1. Ground measurement programme in BEPERS Pilot Study.

Object	Study area I	II	III
Ice crystal structure		x	
Ice salinity	x	x	x
Air bubbles in ice	x	x	
Ice temperature		x	x
Dielectric properties of ice		x	
Ice thickness	x	x	x
Snow density		x	
Grain size of snow		x	
Free water content of snow		x	
Snow temperature		x	x
Snow thickness	x	x	x
Surface temperature		x	x
Surface topography		x	
Meteorological observations	x	x	x

The field programme could be successfully carried through with no major drawbacks. Although observations could be much made close to the base on foot, skis and ski-do, a critical point in this kind of experiment is the available helicopter time. The weather was good enough for the helicopter to be used 6-12 hours each day. However, it takes time to take samples and do the necessary in-situ observations in the field, and this severely limits the number of data one can get.

3.3 Remote sensing in addition to SAR

Various remote sensing observations were made to verify the SAR images. The most important of these methods is here aerial photography. Below the remote sensing work is briefly described.

Aerial photography

In the study areas I, II and IV strips were photographed over the SAR strips to a scale varying from 1:10000 to 1:31000. This scale variation was due to the visibility conditions; the scale of about 1:30000 would have been large enough for this study but that requires a flight altitude of close to 5 km. The width of the photography strips was 2-7 km. The navigation of the SAR and photography planes succeeded very well so that the strips really overlap. The overlap percentage is 80-90. The availability of land marks was naturally very helpful to the navigation. In addition, in study area II a small patch of 1 km x 0.25 km was streo photographed close to Aranda to a scale of 1:1620.

The aerial photography was carried through by the National Board of Survey (Finland). The base of the plane was Helsinki airport as was of the SAR plane, too. The photography plane took off a couple of hours before the SAR plane and did its work between 11 and 19 hrs. The timing of aerial photographs is within 2-3 hours from the timing of the SAR images. During this time gap there were only minor changes in the ice conditions: the ice was

slowly moving in areas II, III and IV, and the snow was in the stage of melting in all areas.

IR-scanner and SLAR

The Swedish Coast Guard plane Cessna with IR-scanner and SLAR (Side Looking Airborne Radar) was used in study areas II (southern part) and III. This flight was organized by the Swedish Space Corporation.

IR-scanner uses the wavelength 8.5-14 µm. It provides a high spatial resolution (2 m) image of the underlying surface. The accuracy is 0.2°C for ice-snow-water surface which has the infrared emissivity of very close to one. At the time of the measurements the whole surface (ice or snow) was in the stage of melting. SLAR works in the X-band (9.4 GHz) and has a spatial resolution of 75 m.

Pulse radar

A pulse radar was used by Peter Ulriksen from the Lund Institute of Technology to map the thicknesses of ice and snow. In addition to the thicknesses, pulse radar gives the surface topography. The work was done only in the study area II at less than 10-km distance from Aranda. Due to the slush layer at the ice-snow interface the radar signal could not penetrate into the ice.

Satellites

Satellite data for this experiment consist of several NOAA images and one SPOT image. Most of the satellite data are from 31 March because of the weather conditions. However, the ice situation did not change much during 31 March - 2 April.

NOAA images were obtained from the Tromsø Telemetry Station, Norway. A good image of the area I was obtained on 2 April but for the other areas the best usable image is from 31 March. Swedish Space Corporation took care of getting SPOT images of areas II and III. Also these images were taken on 31 March.

4. DISCUSSION

A successful SAR experiment has been carried through in the northern part of the Baltic Sea. A summary list of the data obtained is shown in Table 2.

Table 2. Summary list of BEPERS Pilot Study data.

Data quality	Study area I	II	III	IV	Time (1987)
SAR	x	x	x	x	2 April
Ground truth	x	x	x		30 March - 3 April
Routine ice data	x	x	x	x	30 March - 3 April
Aerial photography	x	x		x	2 April
SLAR		x	x		2 April
IR scanner		x	x		2 April
Pulse radar		x			30 March - 1 April
NOAA	x				2 April
NOAA	x	x	x	x	31 March
SPOT		x	x		31 March

A comprehensive data set has been obtained. These data should teach Finnish and Swedish scientists to use SAR in practical sea ice mapping in the Baltic Sea. It is also anticipated that the results of this experiment aid the general understanding of SAR images of sea ice. In addition this experiment has given most useful practical as well as scientific information for performing BEPERS-88 experiment in March 1988 and PIPOR Baltic Sea calibration/validation experiment early next decade.

5. ACKNOWLEDGEMENTS

This experiment has been financially supported by the Board of Navigation and Technology Development Centre (TEKES) in Finland which is greatly acknowledged.

6. REFERENCES

FIMR, 1987: Baltic Sea ice chart No 46, 2 April 1987. - 1 p. Finnish Institute of Marine Research, Helsinki.

Finnish Meteorological Institute, 1987: Weather chart for the Northern Europe on 2 April 1987, 1200 UTC. - 1 p. Archives of the Finnish Meteorological Institute, Helsinki.

Leppäranta, M. 1986: Ice information systems for marine operations. - POLARTECH'86, Vol. 1, p. 57-70. Technical Research Centre of Finland VTT.

PIPOR Group, 1985: A Programme for International Polar Oceans Research (PIPOR). - ESA SP-1074 (Final Version), 42 p. ESA, Paris.

Thompson, T. and M. Leppäranta, 1987: BEPERS-88 Experiment Plan, 2nd ed. - Styrelsen för Vintersjöfartsforskning/Winter Navigation Research Board, Rep. No. 46 (in press). Swedish Administration of Shipping and Navigation, Norrköping, and Finnish Board of Navigation, Helsinki.

In: BEPERS Pilot Study. Data Report. Styrelsen för Vintersjöfartsforskning/Winter Navigation Research Board, Rep. No 45, p. 17-30. Helsinki 1988.

II SAR- FLIGHT

Risto Kuittinen,

Technical Research Centre of Finland
Vuorimiehentie 5, SF-02150 Espoo, Finland

1 INTRODUCTION

The acquisition and interpretation of radar images were the main goal of the BEPERS Pilot Study, because this kind of images will probaply be used on an operational basis in sea ice monitoring in the next decade when satellites with imaging and other radars are in use (ERS-1, Radarsat, JERS-1). The darkness in winter and the quite frequent cloudiness which prevent the imaging using optical sensors are the main reasons for the interest in using radars in sea ice monitoring.

This experiment was flown using French VARAN-S airborne radar. This radar itself is operated by Centre National d'Etudes Spatiales (CNES) and the aircraft by Institut Geographique National (IGN). The missions are planned and carried out by Groupement pour le Developpement de la Teledetection Aerospatiale (GDTA), France. In the technical team of IGN are pilot in command, first officer, navigator and ground mechanic whereas the team of CNES consists of radar operators. CNES has also scientific interests in radar operations.

The aircraft used was Boeing B-17-G F-BEEA 'Chateau de Verneuil', a four engine aircraft built in 1945 and owned by IGN . The navigation system of this aircraft, apart from the standard instrument flight rules, consists of a Litton 96 gyro-laser Inertial Navigation System, a Global 500 A 3 global navigation system and a Doppler navigation radar. The communication equipment includes two aviation VHF sets, one HF, a marine VHF set and an intercom.Figure 1 shows the aircraft at the Helsinki-Vantaa airport during the mission.

Figure 1. Boeing B-17-G, F-BEEA, Chateau de Verneuil, at Helsinki-Vantaa airport on April 1st, 1987.

2 THE VARAN-S RADAR

The VARAN-S is a high resolution radar working in Real Aperture Radar (RAR) mode or Synthetic Aperture Radar (SAR) mode, Vaillant (1985, 1987). In this experiment only SAR mode was used. The characteristics of the radar are the follows:

-frequency: 9.375 GHz

-wavelength: 3.2 cm

-bandwidth: 70 MHz

-ADC window: 60 us

-pulse rate frequency: 800 Hz

-PRF at ADC: 400 Hz

-pulse length: 10 us

-sampling rate: 50 MHz for 4 bits

-peak power: 6kW

-average power: 50 W

-noise figure: 7 dB

-polarisations: Horozontal (HH), Vertical (VV), HV or VH 2 channels

-the length of antenna: 1 m

-imaging is possible to the left or to the right from the flight direction

-swath width: 11,6 km, Figure 2 shows the measurement geometry of the SAR.

-incidence angle: from 16 to 67 degrees

-samples per line: 6000

-recording: HDDT at 750 kbits/s, CCT's 6250 bpi

-quick look: real time, low resolution video display
70 mm black and white film

-spatial resolution: single look 3x3 m
nine looks 9x9 m

Figure 3 shows the block diagram of the VARAN-S.

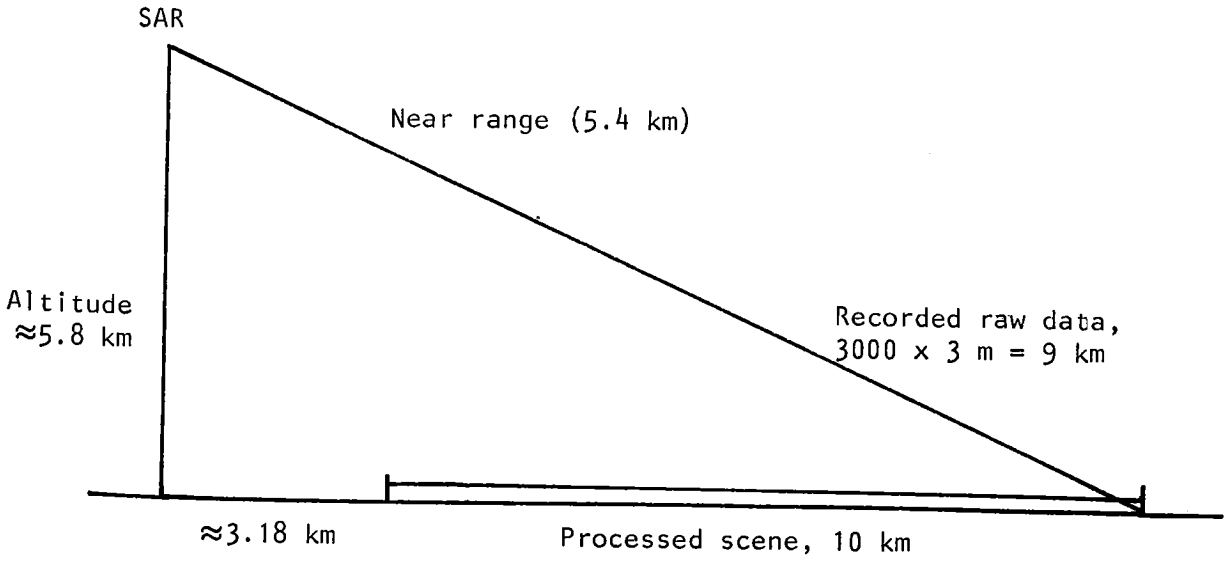

Figure 2. The measuring geometry of the Varan-S SAR.

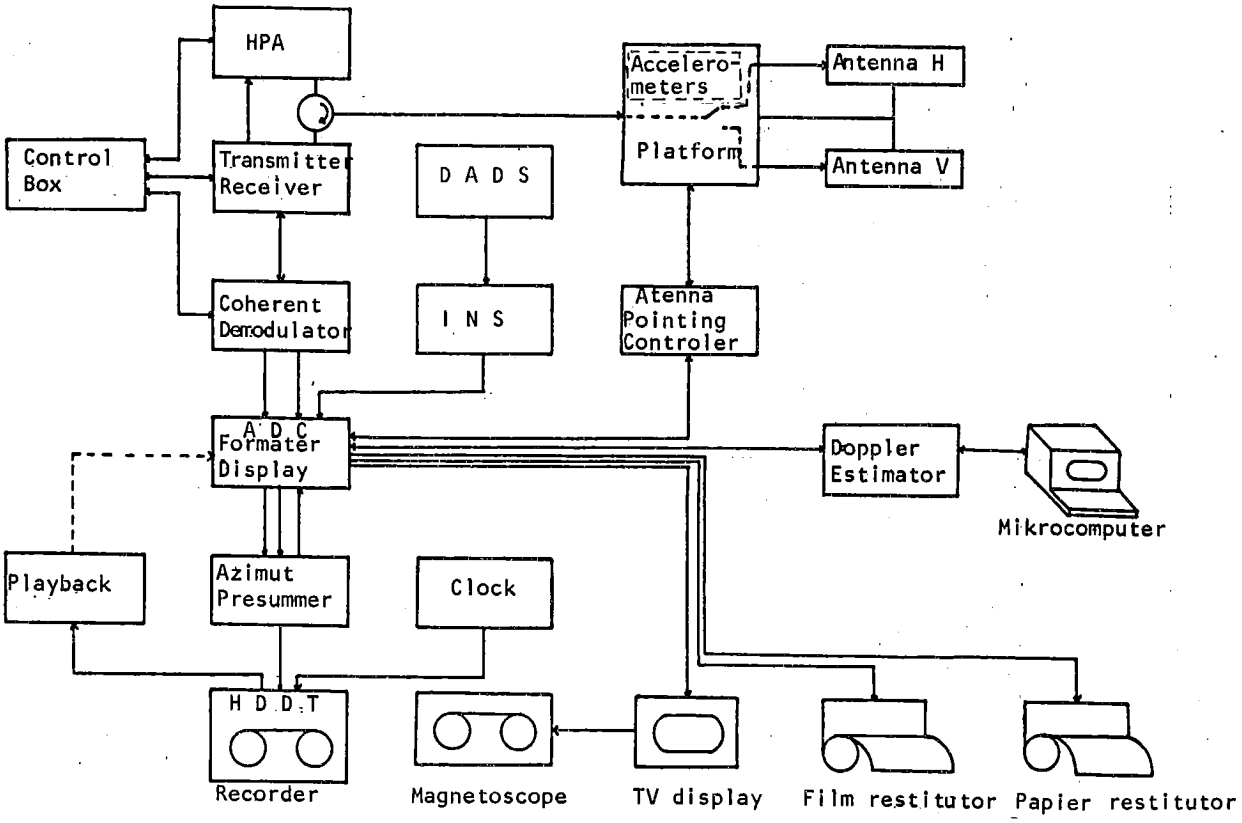

Figure 3. The block diagram of the VARAN-S, Vaillant et.al. (1987).

Quick look images are actually Real Aperture images enhanced with azimuth low pass filtering. Due to the uncorrected backscattered signal strength the images have different contrast and gray level at the sides of the image. This cannot be corrected using printing techniques. However images are very useful in near real time work, because the digital processing itself takes several weeks.

The SAR antenna is stabilized in yaw and roll by using three accelerometers. Drift and roll parameters for these are provided by the inertial navigation system.

Figure 4 shows an example of quick look images produced. The original film was developed by The National Board of Surveying and the prints were made by the Army Map Service.

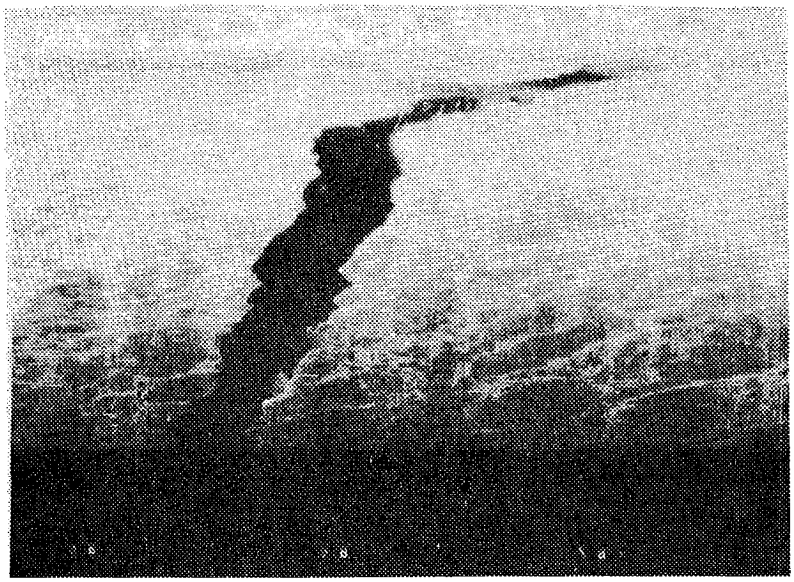

Figure 4. A quick look image of the recorded radar image on 2.4.1987.

3 PRE-PROCESSING OF DATA

3.1 General

In the first step of pre-processing the high density digital tapes (HDDT) are transformed to computer compatible tapes (CCT/6250 ppi).

In the second step azimuth compression and detection are done.

The third step is to convert the slant range to the ground range and after that resampling the lines to correct for ground speed and pitch variations. At last the image is rotated to correct for possible drift.

Processing is made using 'MADIRAN', a 32 bits mini-computer VAX-780 with an attached array processor FPS 5205. The software structure is presented in Figure 5, Vaillant (1985 and 1987).

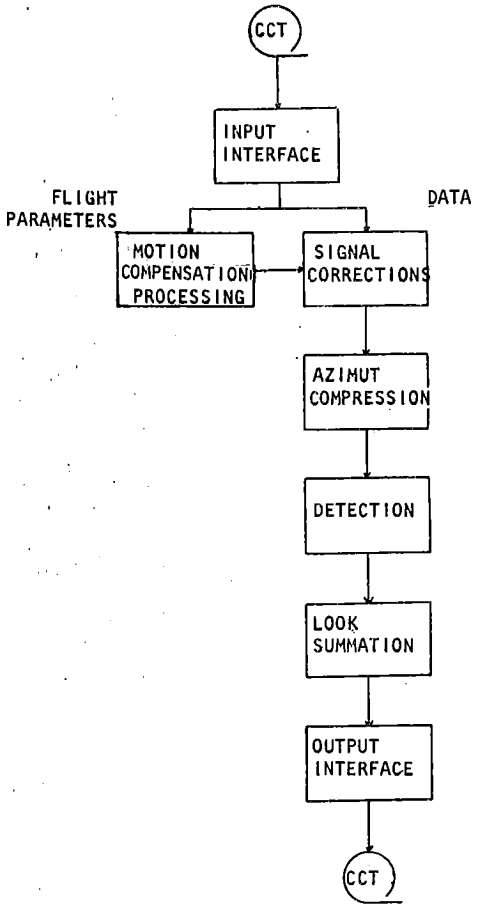

Figure 5. The software structure of VARAN-S data processing.

3.2 Internal calibration

The image is at first processed up to full resolution (3 meters) using 16 bits per pixel. From this data were processed low resolution data (about 9 meters). The low resolution data are calibrated by multiplying the image by the inverse of its mean radiometry, which seems to be valid because the images are quite homogenous. However this processing does not give possibilities to compare the original recorded backscattering which may cause problems in interpreting the data. In the scenes processed up to full resolution this kind of calibration has also been made, but the mean radiometry data has been delivered with the image data. This enables the computation of the original, non-calibrated, pixel values. Interference between the antenna and the aircraft has caused interferometric patterns in images especially in those areas where the backscattering was low. This could not be corrected.

3.2 Geometric corrections

Necessary information for these is recorded during the flight using the navigation systems described, Figures 3 and 5. The readings of the parameters are in the file two in the beginning of the full resolution tapes and the description of these data is available.

4. CARRYING OUT THE MISSION

4.1 General

The aircraft and the team arrived to Finland on 1 April 1987 evening after which detailed plans were made for the fligth of the next day. The mission was carried out on the next day (-2.4.1987). Originally an extra day (3.4.1987) was reserved for possible bad weather conditions or other possible problems. Because the operation time of the aircraft is about 10 hours all study areas were imaged during the same flight. Helsinki-Vantaa airport was the base of the aircraft and Air France carried out the maintenance of the aircraft. JETFLITE Ltd kindly helped in organizing the connections between tha base and the different aircraft operated in the mission (GDTA, National Board of Survey, and Kustbevakning/Coast Guard of Sweden).

The first takeoff of the F-BEEA was at 8.30 but due to some difficulties in steering the SAR antenna the plane had to return to the airport. The measuring flight started at 11.30 and so all imaging was made in the afternoon because the first study area imaged was area I. Figure 6 shows the flight route of the F-BEEA on 2 April 1987.

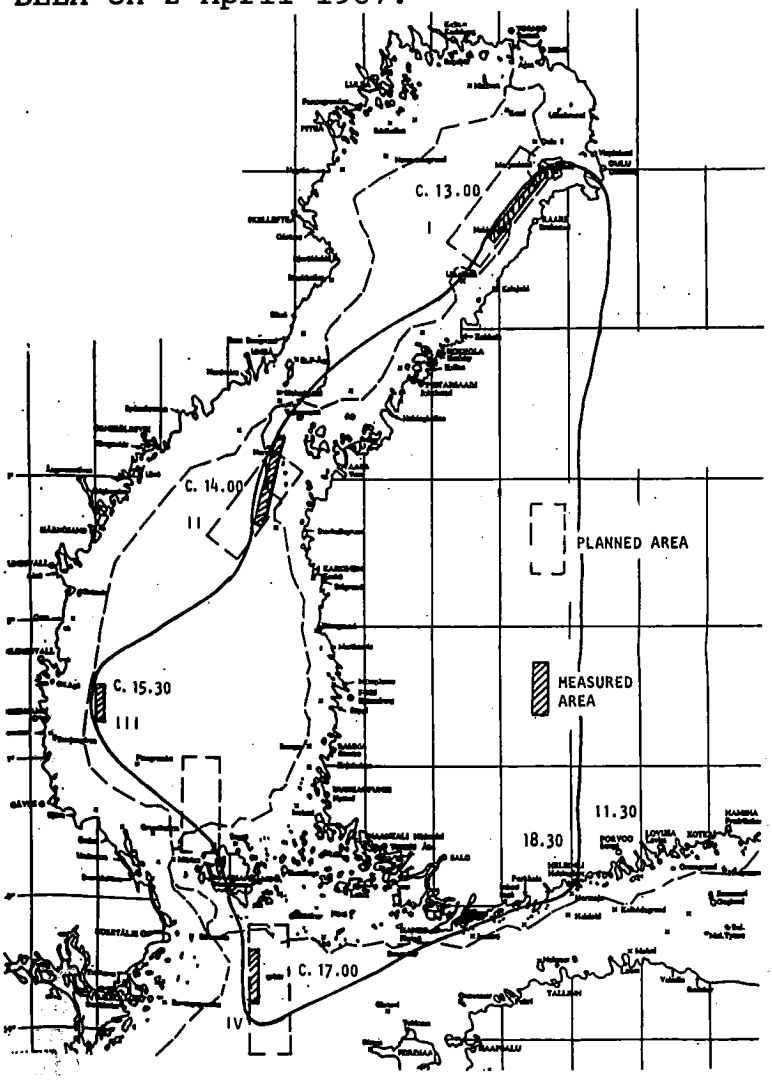

Figure 6. The flight route of the F-BEEA on 2 April 1987.

The flight altitude was about 6000 m and the temperature at that height -21 C. Horizontal polarisation was used in every area.- Area I could be measured also by help of visual navigation, but clouds prevented visual sight over other areas. The navigation was very accurate and the images taken covered exactly the study areas.

4.2 Radar reflectors

Alltogether 12 radar reflectors were made at the Instrument Laboratory ofTechnical Research Centre of Finland. Figure 7 shows the reflector and the way used in placing these reflectors on the ice.

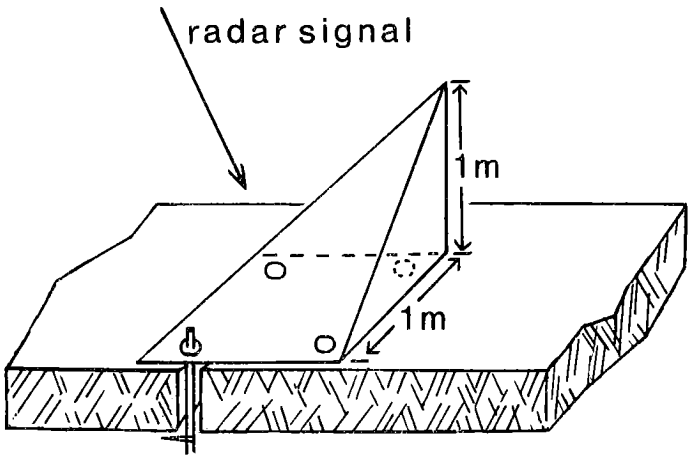

Figure 7. Radar reflector.

These reflectors were installed on the ice in three study areas for the purpose of identifying at least one reflector per study area. The places of reflectors were determined using decca system. Other ground control points needed for rectification of SAR-images consist of small islands at the shoreline ends of the imaged areas.

5 IMAGED AREAS

Alltogether four areas were imaged. Figure 6 shows the location of these areas and figures 8 -11 show closer the areas, the flight axis for every area and the approximate location of the reflectors. In the images there is also marked the location of SAR scenes and the type SAR-data.

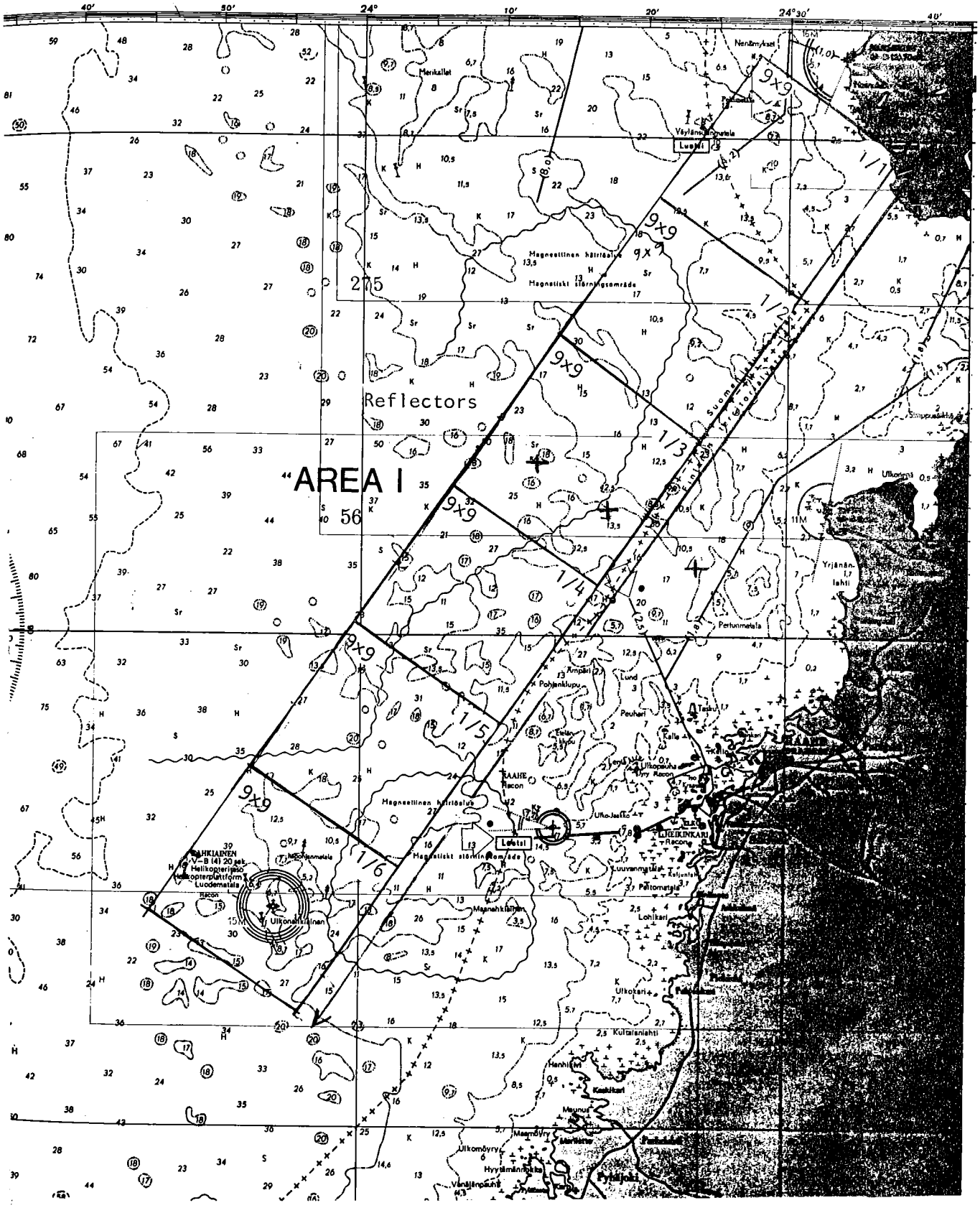

Figure 8. Location of the study area I, Bay of Bothnia.

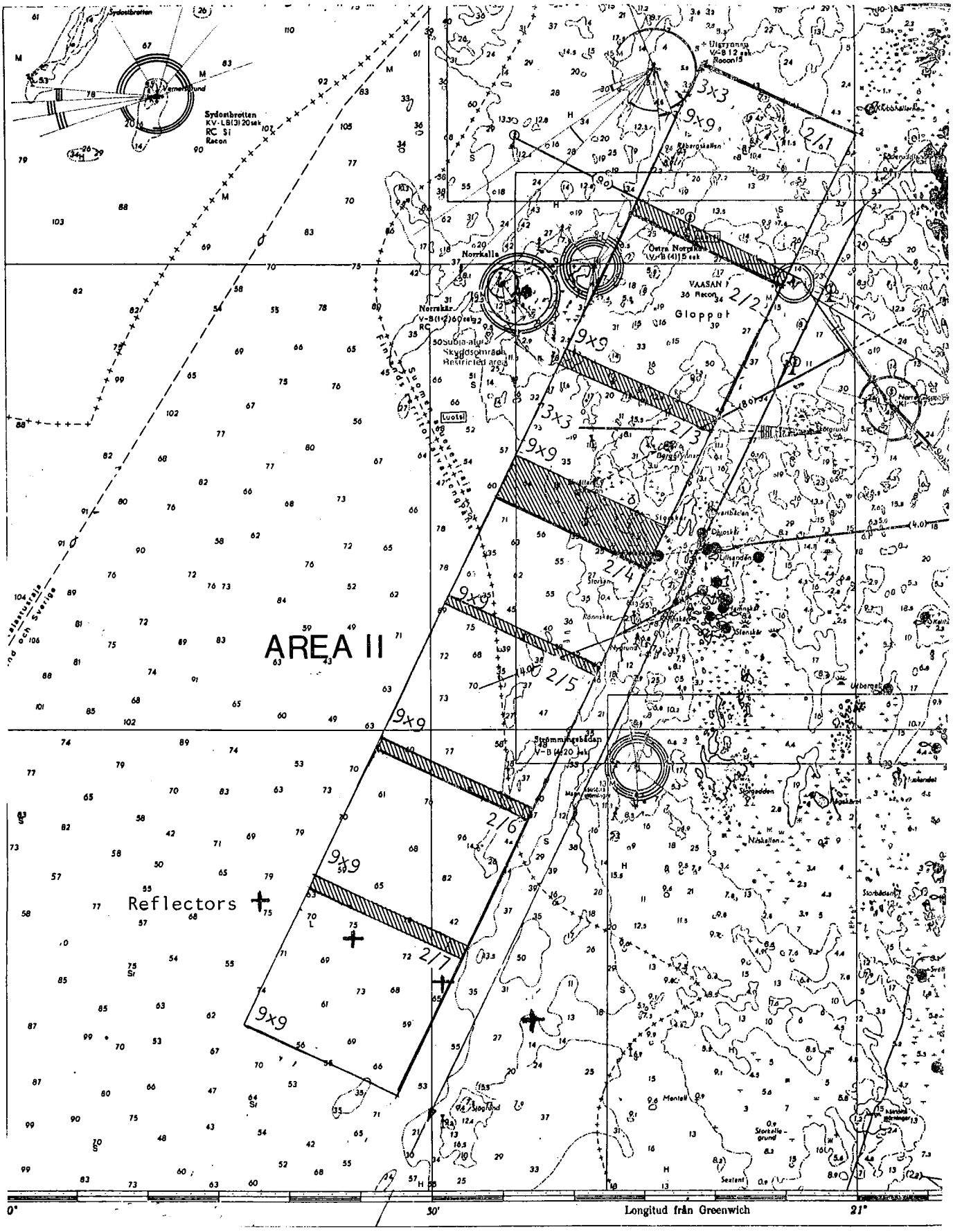

Figure 9. Location of the study area II, Northern Sea of Bothnia.

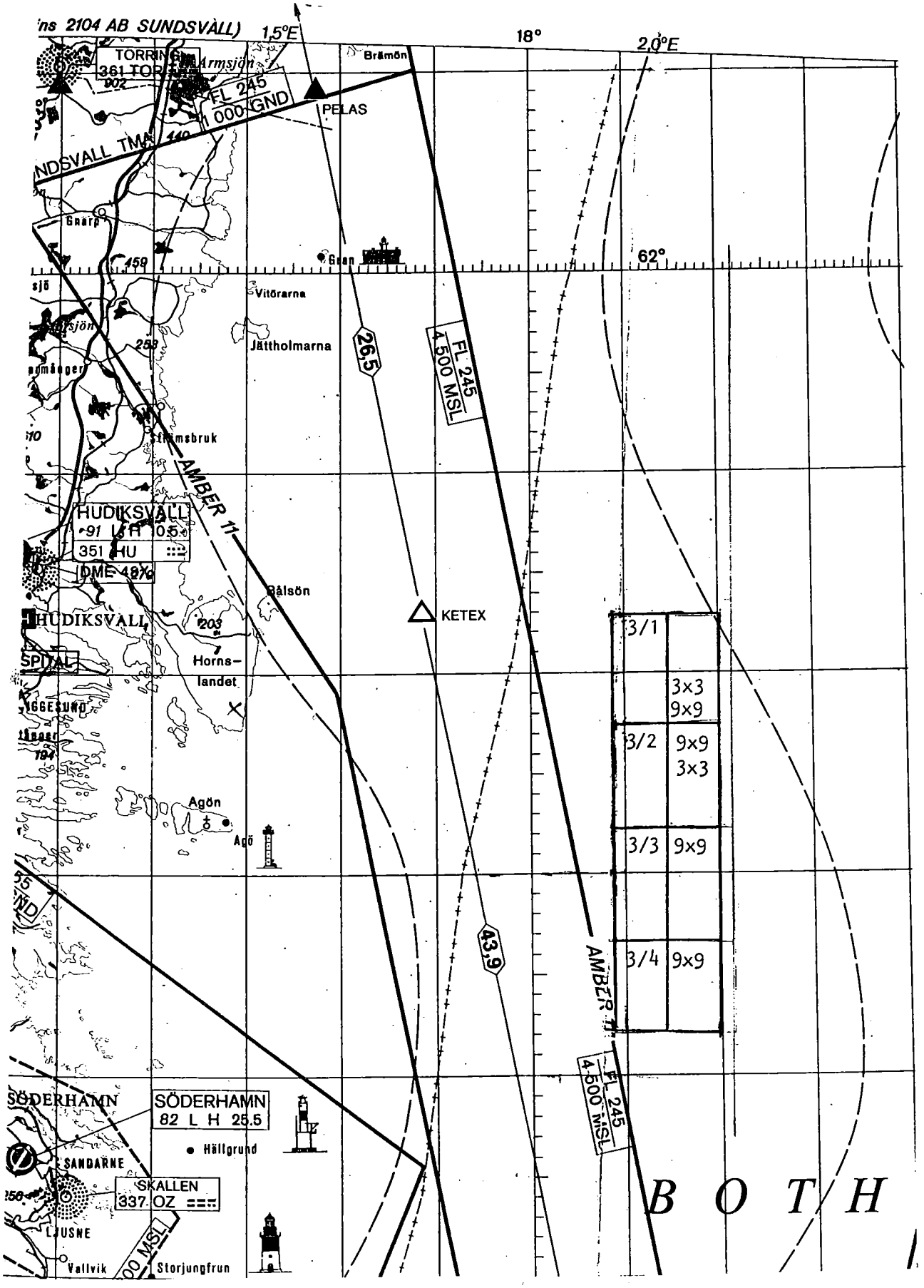

Figure 10. Location of the study area III, Southern Sea of Bothnia.

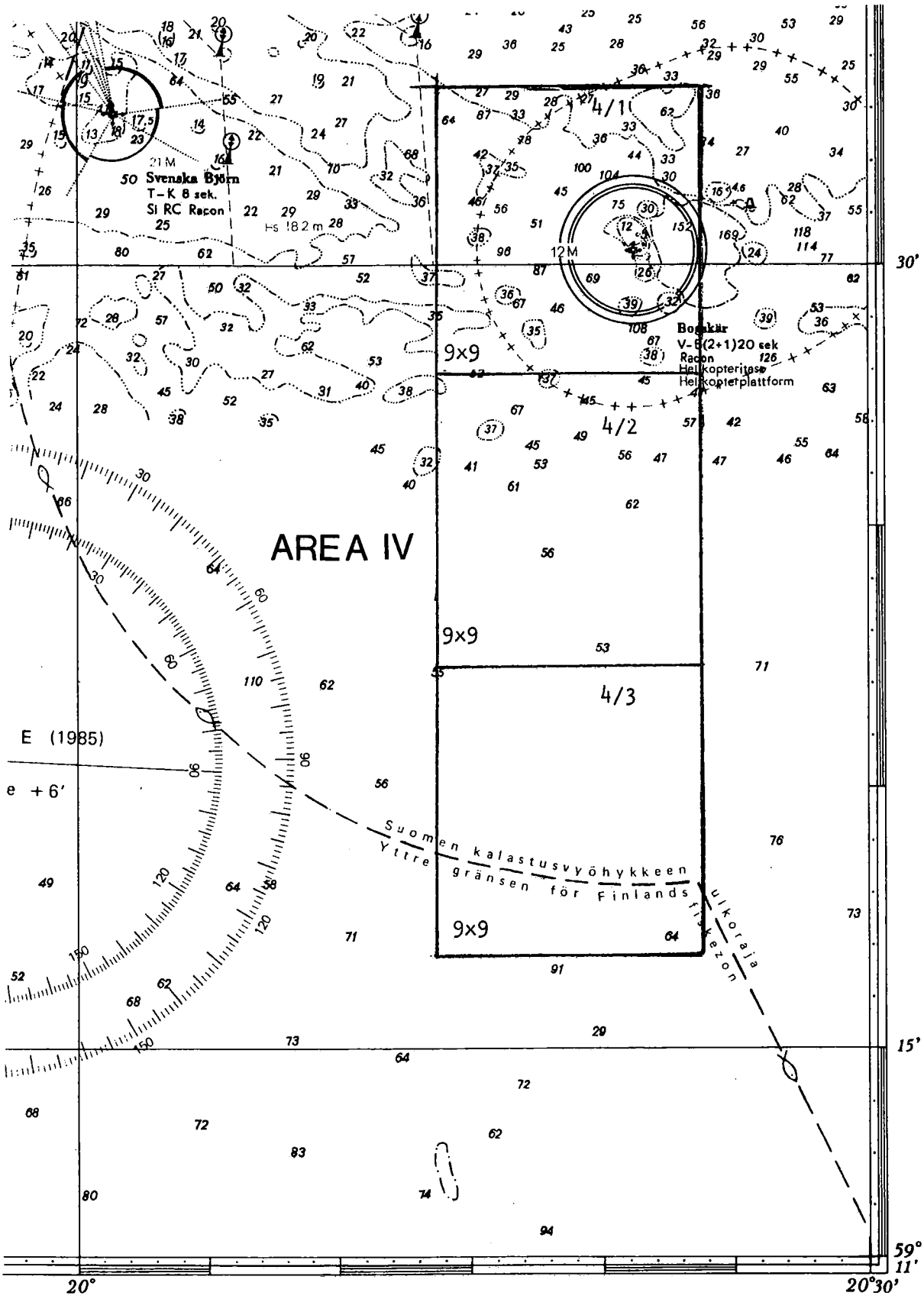

Figure 11. Location of the study area IV, Northern Baltic Proper.

6 DATA

The SAR data set consist of 20 scenes of 9x9 m resolution data and 3 scenes of 3x3 m data in the following way:

AREA	Digital images type	pieces	Photo graphs	Quick Looks
I Bay of Bothnia (Scenes 1/1 -1/6)	9x9 m	6	6	1
II Northern Sea of Bothnia (Scenes 2/1 -2/7 and 2/1 and 2/3)	9x9 m 3x3 m	7 2	7	1
III Southern Sea of Bothnia (Scenses 3C/1-3C/4 and 3C/1 and 3C/2)	9x9 m 3x3 m	4 2	4	1
IV Northern Baltic Proper (Scens 3B/1 - 3B/3)	9x9 m	3	3	1
		24	20	4

The area covered by one scene is 10x10 km2. Photographs mentioned in the above list are negatives from which necessary copies for participating institutions have been made.

7 REFERENCES

Vaillant, D. and Wadsworth A.,1987. Preliminary results of some remote sensing campaigns of the French airborne SAR VARAN-S. To be published in IGARSS'87.Ann Arbor Michigan, USA.

Wadsworth A., Vaillant D. and Grosjean O., 1987. Utilisation operationalle du radar imageur VARAN-S. To be published in FI3G,Lyon France.

Vaillant, D., 1985. VARAN-S: An Airborne Synthetic Aperture Radar for Research in Microwave Remote Sensing. Proc. EARSeL/ESA Symposium on European Remote Sensing Opportunities, ESA SP-233.

Massonnet, D. Conclusion about the campaign over the Gulf of Bothnia.

Wadsworth A. Campaign Suomi'87. Mission report.

ERS-1: European Remote Sensing Satellite

JERS-1: Japanese Earth Resources Satellite

Radarsat: Canadian ramote sensing satellite

In: BEPERS Pilot Study. Data Report. Styrelsen för Vintersjöfartsforskning/Winter Navigation Research Board, Rep. No. 45, p. 31-40. Helsinki 1988.

III GROUND BASE I

By Jouni Vainio

Finnish Institute of Marine Research
P.O.Box 33, SF-00931 Helsinki, Finland

ABSTRACT

At the ground base I, which was situated in the eastern Bay of Bothnia, ice observations were made on the 1st and 2nd of April. A survey of ice conditions on the region was made by helicopter. At this area the ice field was stationary. The air temperature was around 0°C. The ice thickness of snow varied from 0 to 24 cm and snow was dry everywhere at study area I about two hours before the SAR-flight.

1. INTRODUCTION

At the ground base I, which was situated in the Bay of Bothnia between lighthouses Nahkiainen and Marjaniemi, ice observations were made on the 1st and 2nd of April. Four reflectors were deployed in the area. The reflector-line was perpendicular to

the SAR-strip and distances between the reflectors were about 6 km (3.25 nautical miles). The line was situated to the northwest from Raahe (reflectors are numbered from 1 to 4 in Fig. 1). At the each reflector-point the following observations were made:

a) thickness of ice
b) salinity of ice (By taking vertical ice sample, which was divided into pieces of 10 cm. These pieces were melted and salinity was measured from the melt water.)
c) height and number of ridges around the reflector (visual estimate)
d) structure of ice (visual study of the vertical samples in the field)
e) thickness of snow
f) quality of snow (dry><wet, hard><soft)
g) thickness of slush
h) thickness of water layer on the ice
j) temperatures: air, snow, slush, water
k) salinity of surface water

Each reflector-point was marked with dye and with orange-coloured flags. The localization of points based on Decca-system of the helicopter.

A survey of the study area of ground base I was made on the 1st of April. On the 2nd of April observations were completed for three separately chosen points. These points (numbered from 5 to 7 in Fig. 1) represent highly ridged ice, ridged ice and snow-covered fast ice (respectively). The reflector-points were checked during the helicopter-flight. Also a general view over the region was completed.

This article presents the data of the ice and snow geophysics observation programme in the study area I.

2. ICE AND WEATHER CONDITIONS

Ice

A survey of the region was made on the 1st of April between 1100-1130 UTC (1400-1430 local time). The survey was made by helicopter, which flew along the line between lighthouses Marjaniemi and Nahkiainen. The flying altitude was about 400 feet. Ice conditions in the study area I are illustrated in Fig. 1.

Up to 5.5 nautical miles (n.m.) from Nahkiainen lighthouse there was a ridged ice zone. At about 2.6 n.m. from Nahkiainen there was a very small fracture (width 30 m) parallel with the SAR-strip. About 3.3 n.m. from Nahkiainen there was a frozen ice-breaker channel to Raahe. At the area between 7-7.5 n.m. from Nahkiainen ridge frequency was about 5-7 ridges/km (9-13 ridge/n.m.). East from the SAR-strip there was a very small fracture (width 10-20 m) about 8 n.m. from Nahkiainen. There were heavily ridged areas between 8.5-8.7 n.m. and between 9-9.5 n.m. from Nahkiainen and many patches of high ridges which were likely grounded on the west-side of strip. At this area depths are around 15 m.

At the area up to 10-13 n.m. from Nahkiainen there were small openings on the west-side of the strip. Up to 14.5 n.m. from Nahkiainen the ice field was mainly snow-covered, but also bare ice existed. There was also some snow-drift in the ridged ice zone. Bare ice existed at the areas between 14.5-14.8 n.m. and 16.5-18.3 n.m. from Nahkiainen. Ice field was snow-covered from 18.3 n.m. from Nahkiainen to Marjaniemi lighthouse. Ice was ridged also 15.7 n.m. and between 19.5-19.9 n.m. from Nahkiainen lighthouse.

Fast ice boundary was not, except on the northern-most part of the region, in sight from helicopter. The area was covered with consolidated pack ice and floes were small or medium size. Single ridges or ridged ice were observed also in the following

places (distances in nautical miles from Nahkiainen lighthouse): 13, 13.5-14.5, 18.8, 19.2, 20.3, 20.9, 21.1, 21.5, 22.5-22.6, 23.9, 24.3, 26.4 and 27.0. Ridge frequency was about 1-3 ridge/km (2-5 ridge/n.m.).

At our area there was no motion. According to ice-breaker reports the ice field was slowly moving toward southeast at the southern part of the Bay of Bothnia. The speed was about 20 m/h.

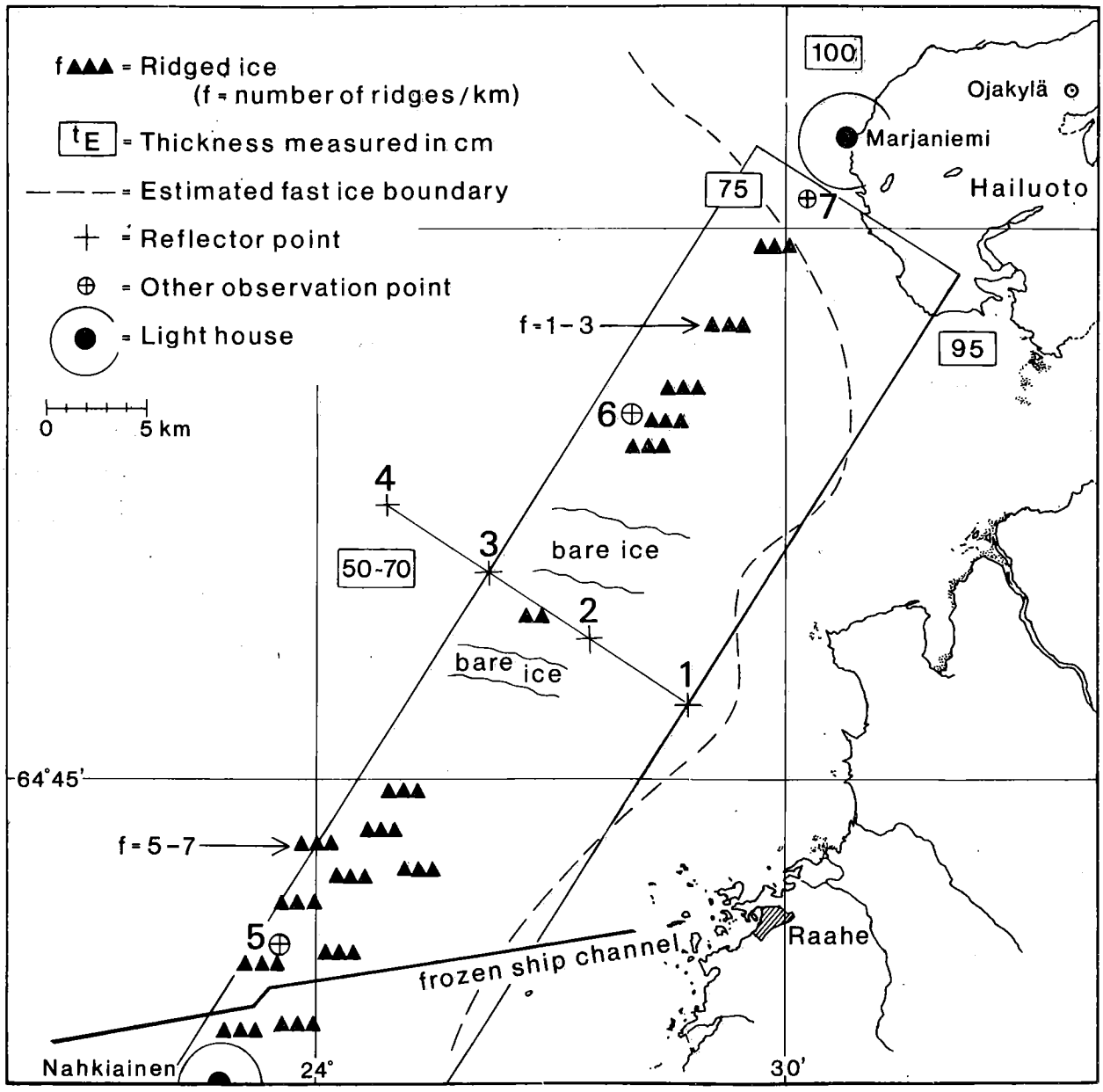

Figure 1. Ice conditions and the observation points in the study area I on the 1st and 2nd of April 1987.

Weather

Meteorological observations at three stations in the neighborhood of area I are shown in Table 1. These stations belong to the standard net of the Finnish Meteorological Institute. The station Hailuoto is closest to our area. The weather was sunny and clear during the SAR-flight. Visibility was good and varied from 25 km to 50 km. Temperature varied from -5°...-2°C in the morning to +7°...+8°C in the late afternoon. The wind blew from south or southeast and wind speed varied from 2 m/s to 5 m/s in the Bay of Bothnia during the SAR-flight day (Table 1).

Table 1. Meteorological observations in the neighborhood of study area I on the 2nd Abril 1987 (Finnish Meteorological Institute, 1987).

Time EET = UTC + 3 hrs	Air temp. °C	Relat. humid. %	Wind dir. deg.	Wind speed m/s	Cloudiness *)	Visib. km
	MÄSSKÄR 63°44'N 22°35'E					
9	-2.5	92	100	3	AB	25
12	3.9	64	100	4	HC	20
15	7.1	68	100	3	HC	25
18	7.5	51	110	4	AC	25
	HAILUOTO 65°02'N 24°48'E					
9	-2.2	84	190	2	AB	25
12	3.8	64	180	3	BB	30
15	5.4	65	100	3	AB	30
18	6.6	52	110	2	AB	30
	OULU AIRPORT 65°01'N 25°29'E					
9	-1.7	82	150	3	AB	50
12	3.0	60	130	4	BB	50
15	6.8	50	130	5	BB	50
18	7.4	38	130	4	AB	50

*) CC = cloudy, AC = almost cloudy, HC = half cloudy, AB = almost bright, BB = bright

3. FIELD MEASUREMENTS

Observations of ice properties were made at seven points in the study area I. The sampling locations are shown in Fig. 1. In this section the following ice properties are described: structure and salinity. At each point also the air temperature, the temperature of surface water and salinity of surface water were measured at the time of sampling. These results are also presented in this section. The salinity sample was sawed vertically into about 10 cm thick pieces in the field, and these pieces were then melted in plastic boxes. The salinity of the melt water was measured in Helsinki after the experiment. The results of the ice salinity measurements are shown in sections 3.1 - 3.7. The ice salinity value was usually a little above or below one per mille. On average this is roughly one-fifth of the salinity of surface water in the region.

The thickness of snow varied from 0 to 24 cm. High thickness values were observed at ice ridges. Everywhere at study area I before the noon on the 2nd of April the snow was dry (e.g. it was not possible to make a snowball).

Symbols S_w, T_w, T_{si}, T_s and T_a mean in sections 3.1 - 3.7 the salinity of water, the temperature of water, the temperature of snow-ice, the temperature of snow and the temperature of air (respectively).

3.1 Reflector-point 1.

Location: (Decca/geographic) G14.5 red / 24°23.6'E
H34.2 green / 64°47.0'N

Time: 1st of April, hrs 12.00

Depth (cm)	S (^{o}/oo)	Depth (cm)	S (^{o}/oo)
0 - 4	0.71	24 - 34	0.77
4 - 14	0.91	34 - 44	0.53
14 - 24	1.01	44 - 54	0.38
		54 - 64	0.23
S_w = 2.13 ^{o}/oo	T_w = +0.0°C	T_a = +2.3°C	

The reflector situated on snow-covered ice near the fast ice boundary. The thickness of ice was 64 cm and there was 24 cm snow on the ice. There were a few ridges and some patches of high ridges which were likely grounded.

3.2 Reflector-point 2.

Location: (Decca/geographic) G10.5 red / 24°17.5'E
H36.1 green / 64°48.8'N

Time: 1st of April, hrs 11.30

Depth (cm)	S (^{o}/oo)	Depth (cm)	S (^{o}/oo)
0 - 6	0.45	26 - 33	0.76
6 - 16	0.75	36 - 46	0.82
16 - 26	0.39	46 - 56	0.57
S_w = 3.38 ^{o}/oo T_w = -0.1°C T_a = +1.7°C T_s = -0.0°C			

The reflector situated on snow-covered ice, which was 56 cm thick. The thickness of snow-cover was 3 cm. The reflector could be expected to be discerned in the SAR-image (reflector could be seen in SAR-quick-look image). There were some low ridges around the reflector.

3.3 Reflector-point 3.

Location: (Decca/geographic) G05.5 red / 24°11.0'E
H38.1 green / 64°50.6'N

Time: 1st of April, hrs 11.00

Depth (cm)	S (^{o}/oo)	Depth (cm)	S (^{o}/oo)
0 - 7	0.67	27 - 37	0.94
7 - 17	0.40	37 - 47	0.85
17 - 27	0.74	47 - 57	0.53
S_w = 3.80 ^{o}/oo T_w = +0.0°C T_a = +1.4°C			

The reflector situated on bare ice, which was 57 cm thick. The reflector could be expected to be discerned in SAR-image. There were some low ridges.

3.4 Reflector-point 4.

Location: (Decca/geographic) G00.2 red / 24°04.6'E
H40.4 green / 64°52.4'N

Time: 1st of April, hrs 10.30

Depth (cm)	S (^{o}/oo)	Depth (cm)	S (^{o}/oo)
0 - 7	0.58	27 - 37	0.43
7 - 17	0.76	37 - 47	0.70
17 - 27	0.65	47 - 57	0.80
		57 - 67	0.66

S_w = 3.64 ^{o}/oo T_w = -0.1°C T_a = +1.0°C
T_s^w = +0.0°C T_{si}^w = +0.0°C

The reflector situated on snow-covered ice and was surrounded by ridges. The thickness of ice was 67 cm and the snow-cover was 10 cm thick.

3.5 Point 5.

Location: (Decca/geographic) G11.3 red / 23°58.0'E
H38.8 green / 64°40.8'N

Time: 2nd of April, hrs 10.10

Depth (cm)	S (^{o}/oo)	Depth (cm)	S (^{o}/oo)
0 - 10	0.16	30 - 40	0.35
10 - 20	0.40	40 - 52	0.55
20 - 30	0.43	52 - (125)	no data

The point was on the ridged ice zone. Heights of the ridges varied between 0.5 and 3.5 metres. Most of the ridges were about

2 m high. The ice thickness was more than 1.25 m (the ice sample broke 52 cm from surface). The thickness of snow was 10 cm and the snow was dry.

3.6 Point 6.

Location: (Decca/geographic) G04.9 red / 24°20.1'E
H45.3 green / 64°54.7'N

Time: 2nd of April, hrs 10.30

Depth (cm)	S (°/oo)	Depth (cm)	S (°/oo)
0 - 10	0.77	30 - 40	0.71
10 - 20	1.02	40 - 50	1.11
20 - 30	0.91	50 - 60	1.21
		60 - (125)	no data

The point was on ridged ice, where the ridges were lower than one meter. The ice was thicker than 1.25 m. Ice field was mainly snow-covered (thickness 5 cm and the snow was dry), but some snowless patches existed.

3.7 Point 7.

Location: (Decca/geographic) G03.3 red / 24°31.4'E
I36.5 green / 65°00.8'N

Time: 2nd of April, hrs 10.50

Depth (cm)	S (°/oo)	Depth (cm)	S (°/oo)
0 - 10	0.60	37 - 48	slush
10 - 20	1.06	48 - 60	0.44
20 - 37	0.77	60 - 72	no data

The point was situated on snow-covered fast ice. The thickness of ice was 72 cm and the thickness of snow was 8 cm and it was dry.

4. ACKNOWLEDGEMENTS

I wish to thank Mr. Jari Haapala and Mr. Henry Söderman who greatly helped me in carrying through the measurements. I also wish to thank our pilot Mr. Jouko Hartikainen from Helikopteripalvelu Oy for safe and competent flights.

5. REFERENCES

Finnish Meteorological Institute, 1987: Meteorological observations on 2 April 1987. - Archives.

In: BEPERS Pilot Study. Data Report. Styrelsen för Vintersjöfartsforskning/Winter Navigation Research Board, Rep. No 45, p. 41-68. Helsinki 1988.

IV ICE AND SNOW GEOPHYSICS IN AREA II

By Matti Leppäranta[1)], Terhikki Manninen[1)], Pekka Kosloff[1)] and Erkki Palosuo[2)]

1) Finnish Institute of Marine Research
P.O. Box 33, SF-00931 Helsinki, Finland

2) University of Helsinki, Department of Geophysics,
Fabianinkatu 24 A, SF-00100 Helsinki, Finland

ABSTRACT

The data of ice and snow geophysics program in study area II in BEPERS Pilot Study is described. The observations were made both in the fast ice field and in the pack ice field. The ice thickness was 20-70 cm and the ice was either bare or covered with wet snow. In the pack ice area there were a lot of ice ridges; the sail height was typically 0.5-1.0 m and the number of ridges 2-4 per km. The salinity of the ice ranged usually from 0.5 to 1.0 per mille. Crystal structure analyses indicate that, as a rough estimate, on average one quarter of the ice was granular and three quarters columnar-grained.

1. INTRODUCTION

Study area II was located in the northern part of the Sea of Bothnia. The base was R/V Aranda. She was moored to fast ice at the boundary of fast ice and pack ice in Vaasa archipelago close to the island of Norrskär (Fig. 1). Aranda was the main ground data base and also the coordination centre of the experiment.

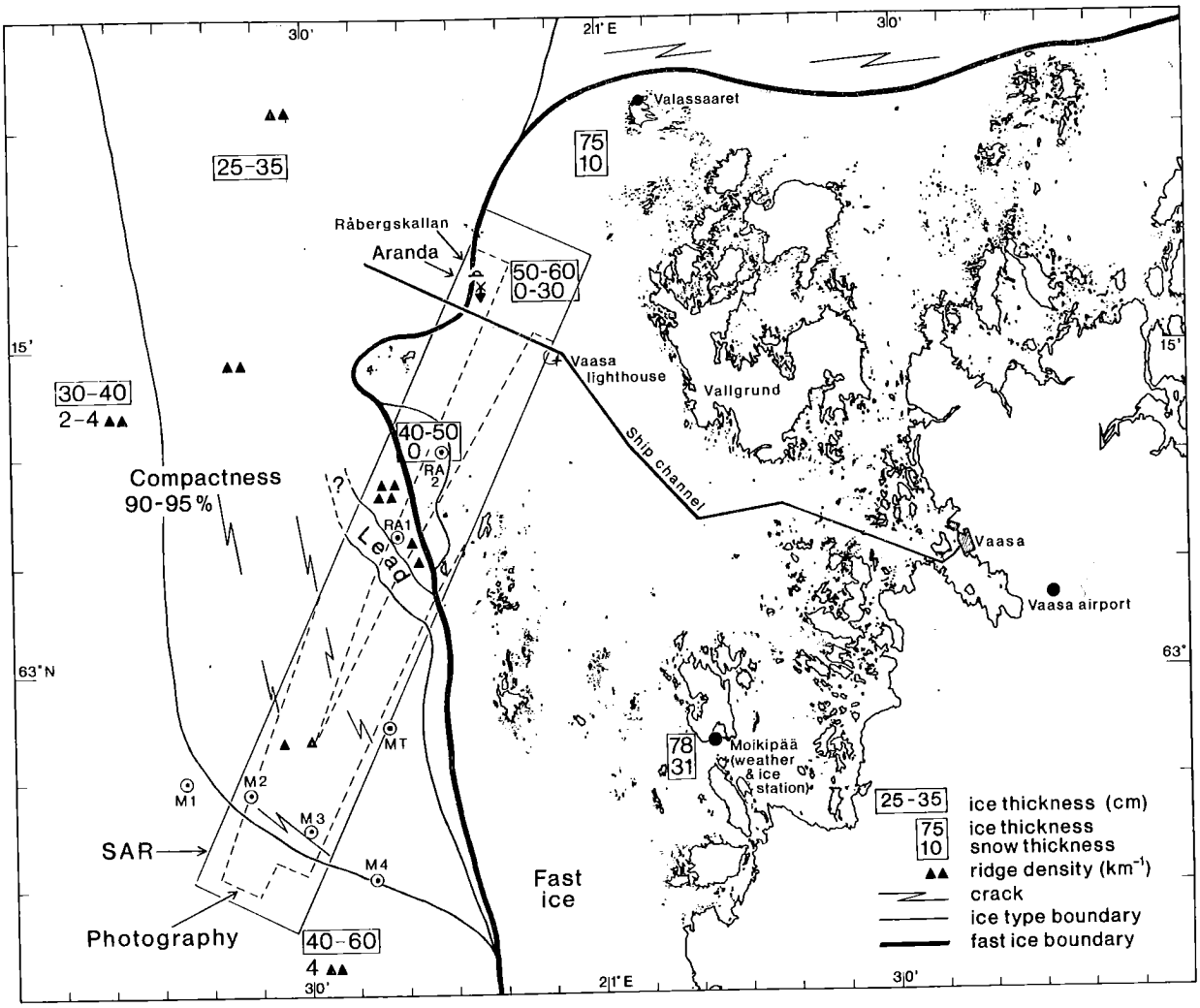

Figure 1. Ice chart of the northeastern part of the Sea of Bothnia, 2 April 1987. The locations of the SAR strip and observation stations are also shown.

This article presents the work and data of the ice and snow geophysics observation programme in the study area II. This programme consists of the following elements: 1) General ice conditions, 2) Ice crystal structure and impurities in ice, 3) Ice temperature, and 4) The grain size and free water content of

snow. Observations were made in the fast ice area close to Aranda and in a few patches in the pack ice area southwest of Aranda.

The measurement period was 31 March - 3 April. The position of Aranda was 63°17.8'N 20°48.1'E and her heading exactly south (180.0 deg). An aerial photograph of Aranda and her surroundings is shown in Fig. 2.

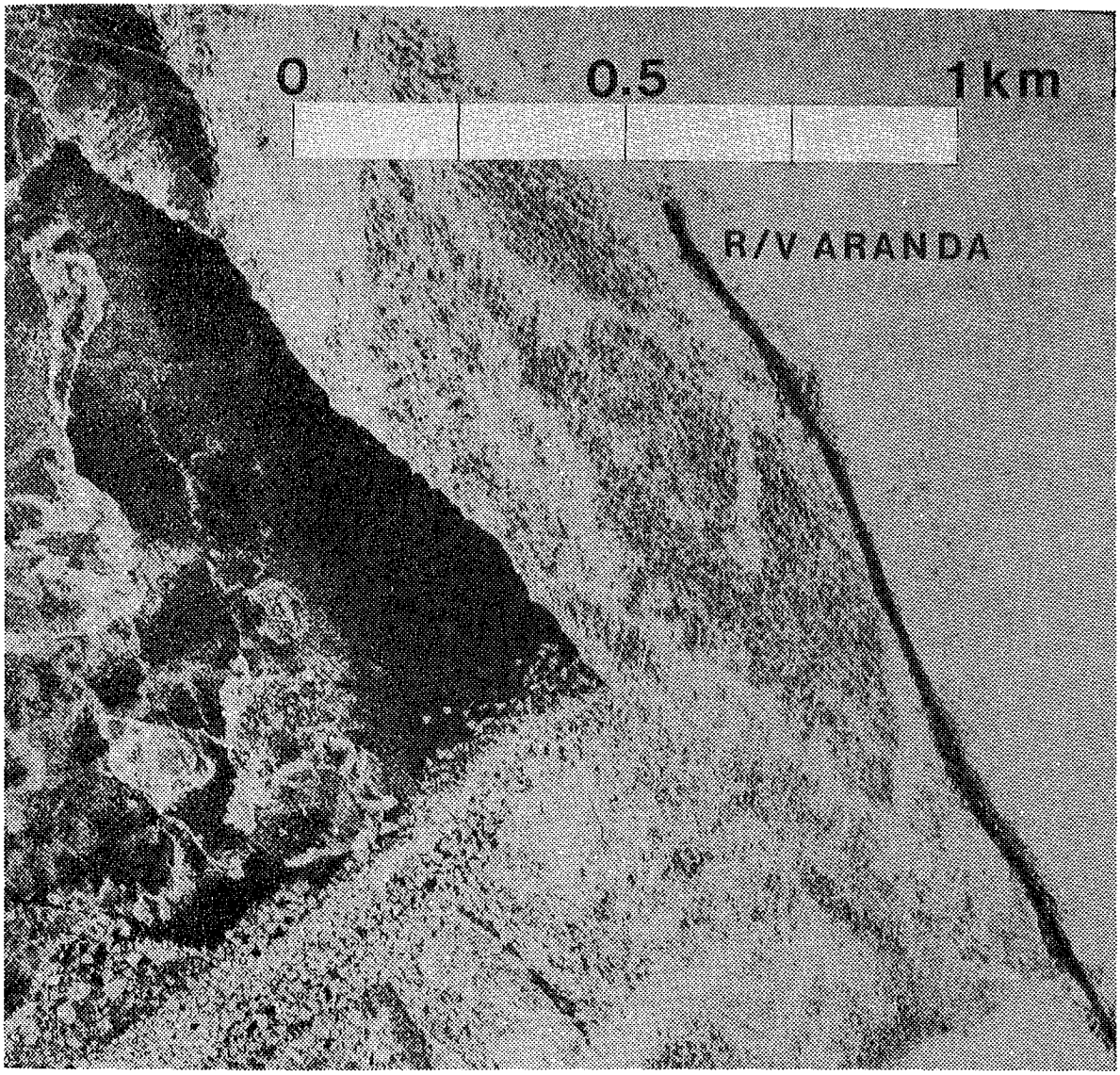

Figure 2. Aerial photograph of R/V Aranda and her surroundings (National Board of Survey).

2. ICE AND WEATHER CONDITIONS

Weather

The weather was very good through the period of the experiment. The air temperature was above zero in the afternoons and a little below zero at other times. In the mornings the air was foggy but by nine o'clock the conditions were good enough for the helicopter to fly. The wind was first southerly with a speed of 7-11 m/s but during the night before 2 April it turned northeast and decreased to 5 m/s. By the next night the wind slowly subsided.

Meteorological observations at three stations in the neighbourhood of area II are shown in Table 1. These stations belong to the standard net of the Finnish Meteorological Institute. The station Valassaaret is closest to Aranda and located on an island at a considerable distance from the continent, and thus provides the most relevant data for the area around Aranda. Table 1 indicates that the air temperature rose above zero between 9 and 12 hrs at Vaasa airport and Moikipää and between 12 and 15 hrs at Valassaaret. This caused a significant change to the character of the snow cover. The wind was northeasterly and weak. The sky was half or almost cloudy but fortunately the clouds were located so high that aerial photography was possible from the altitude of 2 750 m. In Valassaaret there was fog during the night and early morning until 9 hrs.

Meteorological observations made at R/V Aranda with her standard meteorological station are shown in Table 2. The similarity of the data of Aranda and Valassaaret is obvious.

Ice

Ice conditions in the study area II are illustrated in the ice chart in Fig. 1. This chart is based on helicopter

reconnaissance flights during the experiment, aerial photography and routine ice data of the Finnish Ice Service. The Ice Service has observation stations in Valassaaret and Moikipää. The SAR strip covers partly the fast ice field and partly the pack ice field.

Most of the fast ice originated in late December. It was 50-80 cm thick with a 0-30 cm snow cover. South of Norrskär at the fast ice boundary there was an up to 2 km wide zone of a little younger fast ice. This ice was 40-50 cm thick, bare and level.

The fast ice region extended to the outer edge of Vaasa archipelago. Aranda was situated about 2 km from the fast ice boundary. South of Norrskär in the SAR strip the boundary was directed along SSE-NNW.

Table 1. Meteorological observations in the neighborhood of study area II on 2 April 1987 (Finnish Meteorological Institute, 1987).

Time EET = UTC + 3 hrs	Air temp. °C	Relat. humid. %	Wind dir. deg.	Wind speed m/s	Cloudiness*)	Visib. km
	VAASA AIRPORT 63°03'N 21°46'E					
9	-1.4	87	100	3	AC	20
12	2.8	74	80	4	AC	20
15	6.9	60	110	4	AC	20
18	5.9	65	110	3	AC	25
	VALASSAARET 63°25'N 21°04'E					
9	-4.4	96	50	4	CC	0.1
12	-2.4	96	50	5	CC	13
15	1.2	84	40	5	AC	13
18	1.0	88	30	4	AC	13
	MOIKIPÄÄ 62°56'N 21°06'E					
9	-3.6	93	70	3	HC	15
12	1.1	79	60	5	AC	15
15	4.1	71	100	6	HC	18
18	4.3	70	140	5	CC	20
*) CC = cloudy, AC = almost cloudy, HC = half cloudy						

Table 2. Meteorological observations at R/V Aranda on 2 April 1987; "-" alone stands for no data.

Time EET	Air temp. °C	Wind dir. deg.	Wind speed m/s	Cloudiness	Visib. km
6	-3.7	90	2	8/8	0.2
9	-4.5	60	3	5/8	>10
11	-2.9	60	5	-	-
12	-1.8	60	5	7/8	>10
13.30	+0.9	40	4	-	-
14.15	+3.4	40	5	-	-
15	+1.9	50	5	6/8	>10
18	+0.9	50	4	8/8	10-15
24	+2.5	110	4	7/8	>10

In the pack ice field close to the fast ice boundary there was first a heavily ridged zone (1-4 km wide) and then a zone of thin pack ice which slowly became mixed with thicker pack ice farther offshore. In places there was a snow cover up to 15 cm thick. Ice compactness was 90-95 %. South of Norrskär there was a lead between the ridged zone and thin pack ice.

The heavily ridged zone was about 2.5 months old. Some of the ridges were grounded as e.g. close to Aranda at Råbergskallan where the depth of the sea is less than ten meters. The ridges were generally formed of 10-20 cm thick ice. South of Norrskär the broken ice pieces in this ridged zone were typically 0.5 - 1.5 m long. In places there were patches of broken ice pieces.

South of Norrskär there was a 1-2 km wide lead next to the heavily ridged zone. Some small ice floes and ice cakes were found at the western edge of the lead, transported there by the wind. Very few ice pieces were observed farther away from the edges in the lead. This lead had opened just at the beginning of the experiment and was slowly expanding during it. The speed was less than 200 meters per hour; on 2 April it was about 150 m/h between 11 and 17 hrs.

The thin ice zone originated in late February. An example of aerial photographs of this zone is shown in Fig. 3. The ice field consisted of small ice floes frozen together, and the thickness of ice was 25-40 cm. Ice ridges numbered to 2-6 per km. The surface was covered with snow only at ice ridges. In places fractures occurred.

The thick pack ice field was located at 15-30 km from the fast ice boundary in the northeastern corner of the Sea of Bothnia. The thickness of this ice was 30-70 cm, and ridges numbered to 4-8 per km. Near ridges the surface was snow-covered. Both bare and snow-covered level patches occurred. Fractures were more frequent than in the thin ice field, and one long (at least 10 km) fracture parallel to the lead was observed at the distance of 15 km from the lead. A few remnants of old (straight) ship channels existed, and some of them had changed into ridges.

The mark line M1-M4 crossed the boundary of the thin and thick ice fields. At the mark spots it was noted that there was no slush layer at the ice-snow interface. At M3 ridge sails were examined. The ice pieces were of two different types: thin ice pieces which were 20 cm thick and less than 1 m long and thick ice pieces which were 40 cm thick and up to 3 m long.

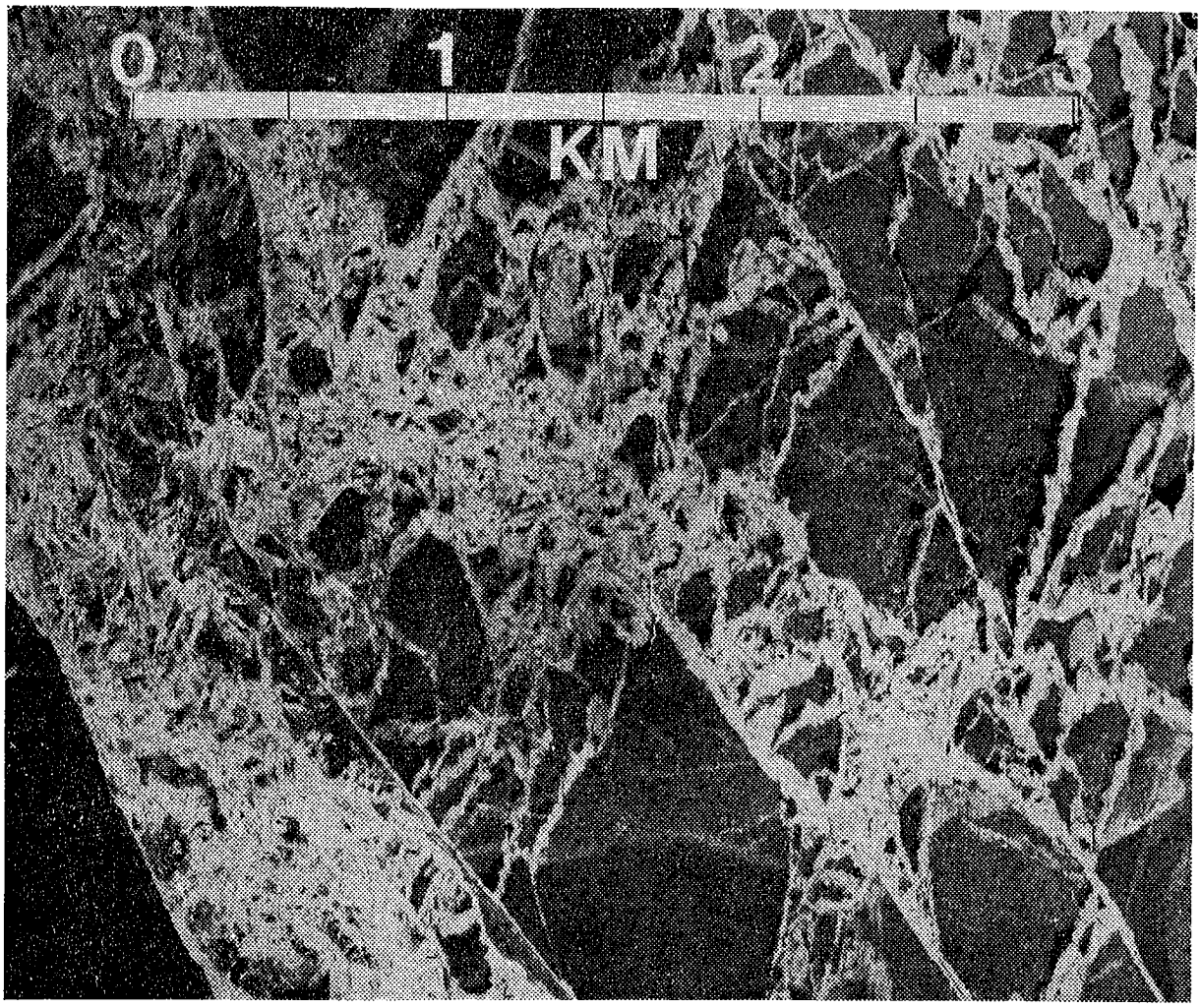

Figure 3. An example of aerial photographs about pack ice in the SAR imaging area. (National Board of Survey, Finland).

3. ICE PROPERTIES

Observations of ice properties were made in the vicinity of Aranda and at several patches in the SAR imaging area. The sampling locations are shown in Fig. 1. Structure, salinity and air bubble content of ice are described in this section. The results of the vertical temperature profile measurements are presented in section 5. In addition, the dielectric properties of ice were studied by the group from the Helsinki University of Technology, and their work is presented in the article by Hallikainen, Toikka and Hyyppä in this report.

3.1 Sampling technique

Ice samples were taken for structural observations and for measurements of salinity and dielectric properties. One large piece of ice was taken with a drill and ice saw. The horizontal cross-section of this piece was rectangular and of size 10 cm x 40 cm, and vertically it extended through the whole thickness of ice. This technique is easy and relatively rapid compared with common type ice core drills since the thickness of our ice was less than one meter. Another advantage is that all samples for further study are taken from the same ice block. The large piece was sawed vertically to three samples which had the horizontal cross-sections of 10 cm x 15 cm (two samples) and 10 cm x 10 cm (one sample). The small one was for the dielectric measurements and the other two for the ice structure and salinity study.

The ice structure sample was transported to Aranda in a plastic bag and stored in a freezer for analysis in a cold room after the experiment. The salinity sample was without delay sawed into pieces about 10 cm thick in the vertical direction, and these pieces were then melted in plastic boxes. The salinity of the melt water was measured in Helsinki after the experiment.

The whole sampling procedure in the field takes 30-60 minutes depending on the thickness of ice. Thus it is rather expensive work in the pack ice field, where a helicopter has to wait while the work is being done. Also the amount of time needed in taking one sample restricts severely the number of samples. This restriction is a major difficulty since the local variations of ice properties can be quite large.

3.2 Ice structure

The ice structure investigations were made by analyzing the crystal structure of some samples through the whole sheet of ice. Together nine samples were taken, three in the fast ice and

six in the pack ice region. Additionally, the surface layer (top 10 cm) features were studied with photographic methods.

Aranda observations

On the top there was a 1-8 cm thick snow ice layer. Next there was typically a 10-30 cm thick obscure layer, and below that only transparent ice. In places there were consecutive layers of obscure and transparent ice. This structure has been produced either by ice rafting or by frazil ice production in leads.

As usual, the air bubble content was by far greatest in the snow ice layer. The diameter of the bubbles was usually 0.3-3 mm, with a maximum of about 8 mm. In one sample a void of 3 cm in diameter was found.

Figure 4. Vertical cross section of the snow ice layer. Tic mark spacing 1 mm.

The snow ice part consisted of two sub-layers, a roughly one centimeter thick top layer and a bottom layer (Fig. 4). Large differences were seen in the air bubble content of the top of the ice beneath snow. The ice in the top layer was weak and porous with a grain size of 1-2 mm. Adhesion between this part and the bottom layer was extremely poor, e.g. the top layer sometimes got loose while sawing. The bottom layer of snow ice was much more transparent than the top layer. The number and size of air bubbles slightly increased downwards. Small brine pockets could be distinguished lower in the bottom layer. Their horizontal diameter was less than 0.5 mm and height 2-4 mm.

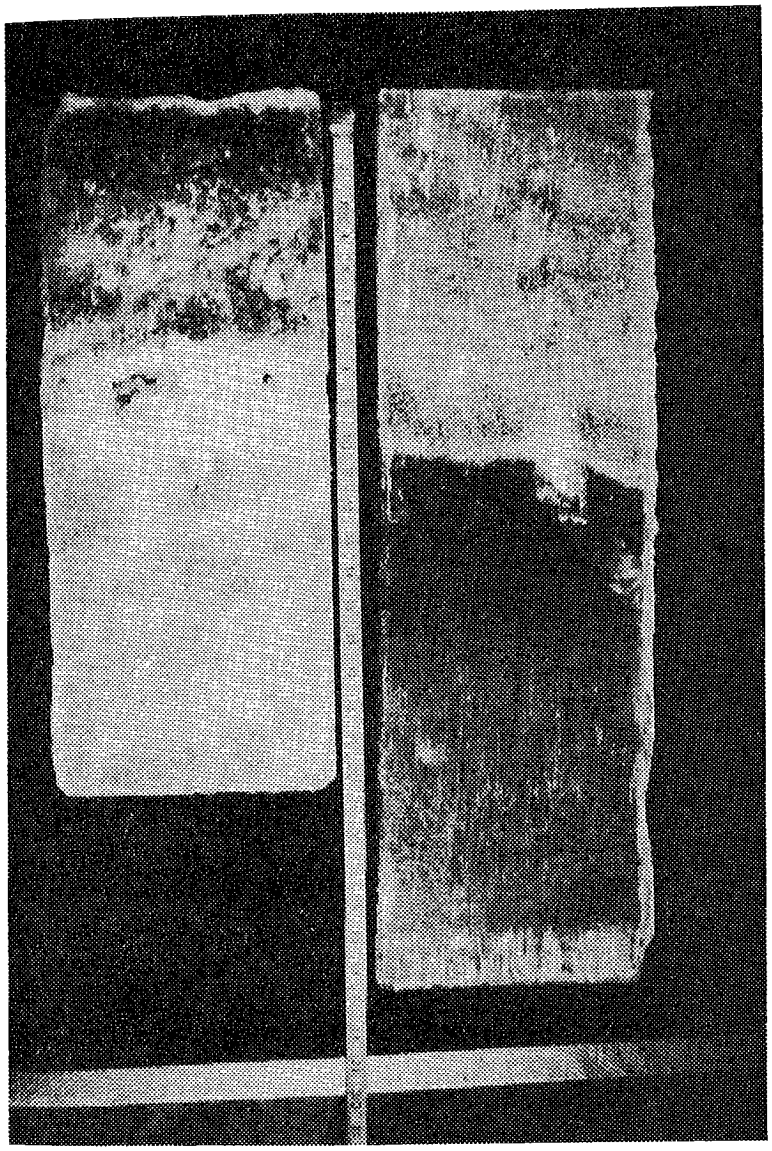

Figure 5. Ice sample A1 at Aranda in normal light.

The ice sample A1 taken at Aranda is shown in Fig. 5 in normal light. The total ice thickness was 47 cm. As a coarse classification there are two main layers: an obscure upper layer from the top to the depth of 32 cm and then a clear lower layer to the bottom. In the upper layer there are three sub-layers: 1) 0 to 3 cm, clear ice without large air bubbles, 2) 3 to 16 cm, very obscure ice with large air bubbles and inclusions (maximum diameter 3 cm), and 3) 16 to 32 cm, obscure ice with many air bubbles and brine pockets. The transition from the obscure upper layer to the clear lower layer is rapid.

The vertical cross-section of the crystal structure is shown in Fig. 6. The obscure upper layer consists of small grains with

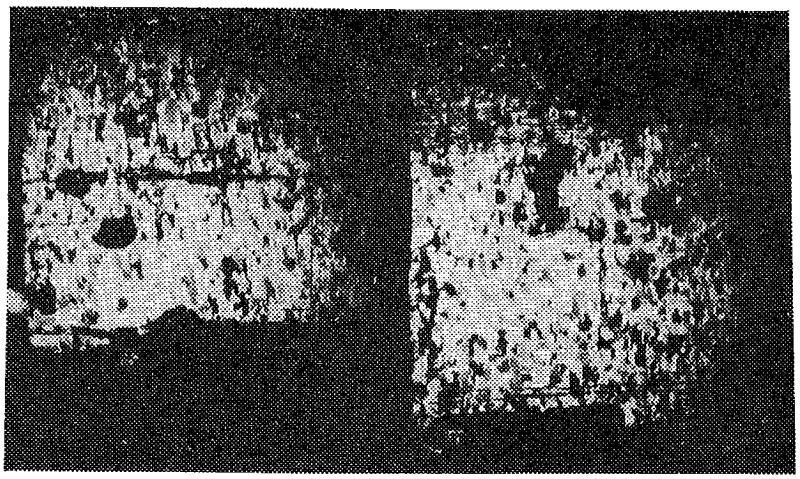

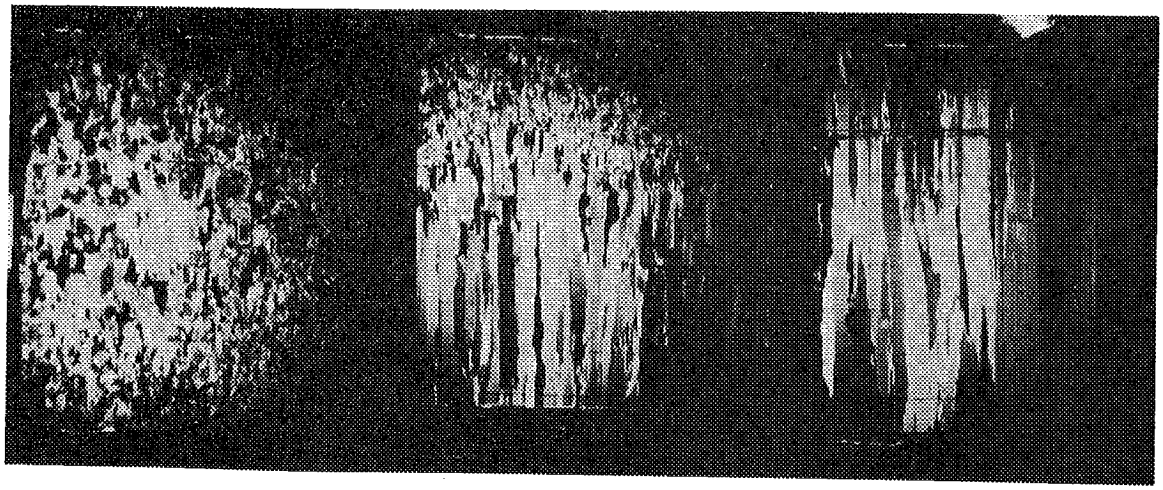

Figure 6. Vertical cross-section of the crystal structure of ice sample A1 at Aranda.

the minimum size occuring in the bottom 5 cm (diameter 1-3 mm). In the top 2-cm layer the grains were also small; here at the depth of 2 cm the c-axes were horizontal with a slight orientation maximum close to SE-NW. The lower clear layer is columnar grained ice with horizontal c-axes. In this layer there is a slight indication of a preference orientation of NEE-SWW in the horizontal c-axis direction.

Fast ice field

Most of the fast ice region in area II was as at Aranda. However, there was an up to 2 km wide zone of bare fast ice south of Norrskär.

In the bare fast ice zone the ice surface was quite rough on a centimeter scale (Fig. 7). There were large air bubbles and some of these even reached the top of the ice. The surface of this zone was completely dry.

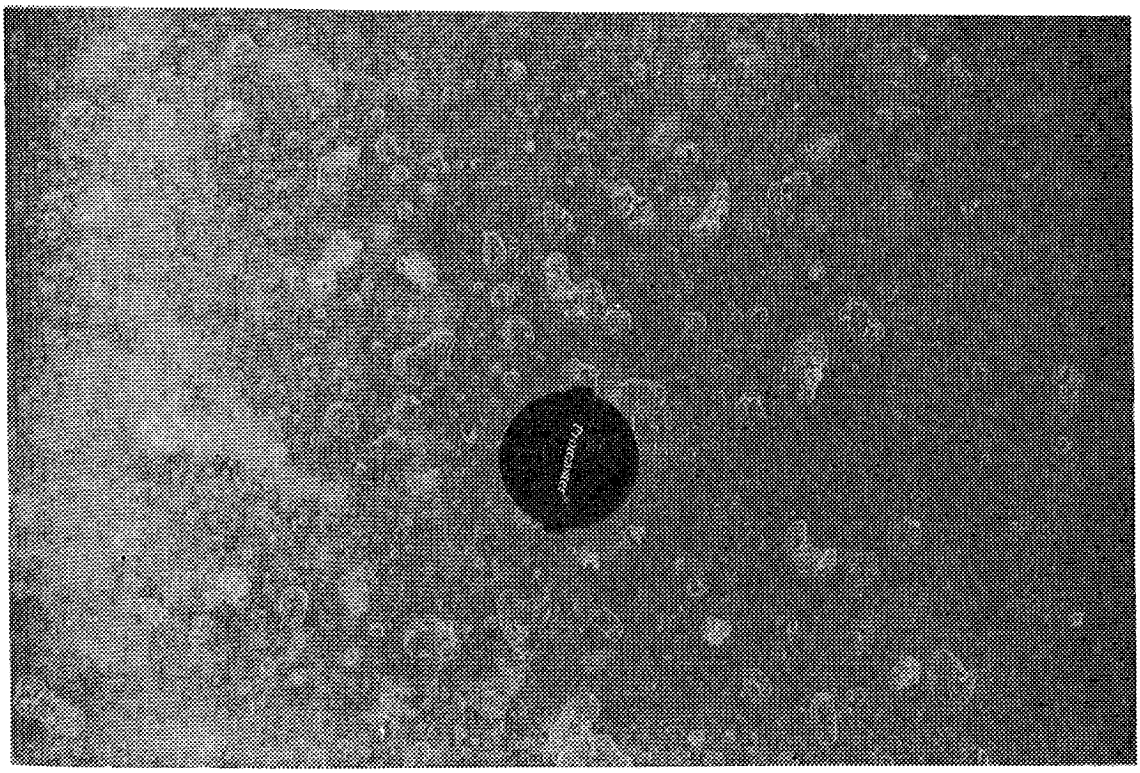

Figure 7. Photograph of the surface of the bare fast ice. Diameter of the scale circle 60 mm.

Pack ice field

The thickness of pack ice in area II was 20-70 cm. This variation is due to the dynamics of the ice which has created ice sheets of different time origin and thermal history. Here the ice thickness tended to increase with distance from the fast ice boundary (see Fig. 1).

Consequently, there were large variations in the structure of the ice sheets. At point M2 in Fig. 1 there was rather young pack ice with the thickness of 36 cm. The top 3 cm was fine-grained (diameter less than 5 mm) ice and the rest of the ice was just one zone of columnar grained ice. The ice at the point M3 was quite different from M2 and had a complicated structure as will be shown below.

The ice at M3 was 58 cm thick representing likely the oldest pack ice in the region. Looking at the sample in normal light reveals several clear and obscure layers (Fig. 8). The obscure appearance is caused by air bubbles and empty brine pockets. The vertical cross-section of the crystal structure shows that the distinct obscure layers are granular ice and clear layers columnar-grained ice (Fig. 9). The top 7-cm layer is fine-grained ice with the grain diameter of 2-5 mm. Next layer, 7-11 cm, is columnar grained, and then there is a 6 cm thick coarse-grained (diameter 1 cm) layer. This way layers alternate down to the bottom. The maximum layer thickness is 10 cm, and the maximum grain diameter in granular layers is 1.5 cm. At the bottom there is a small portion of very fine-grained ice in Fig. 9; this portion is not natural and was created by the sampling process and it originates from the snow on the ice.

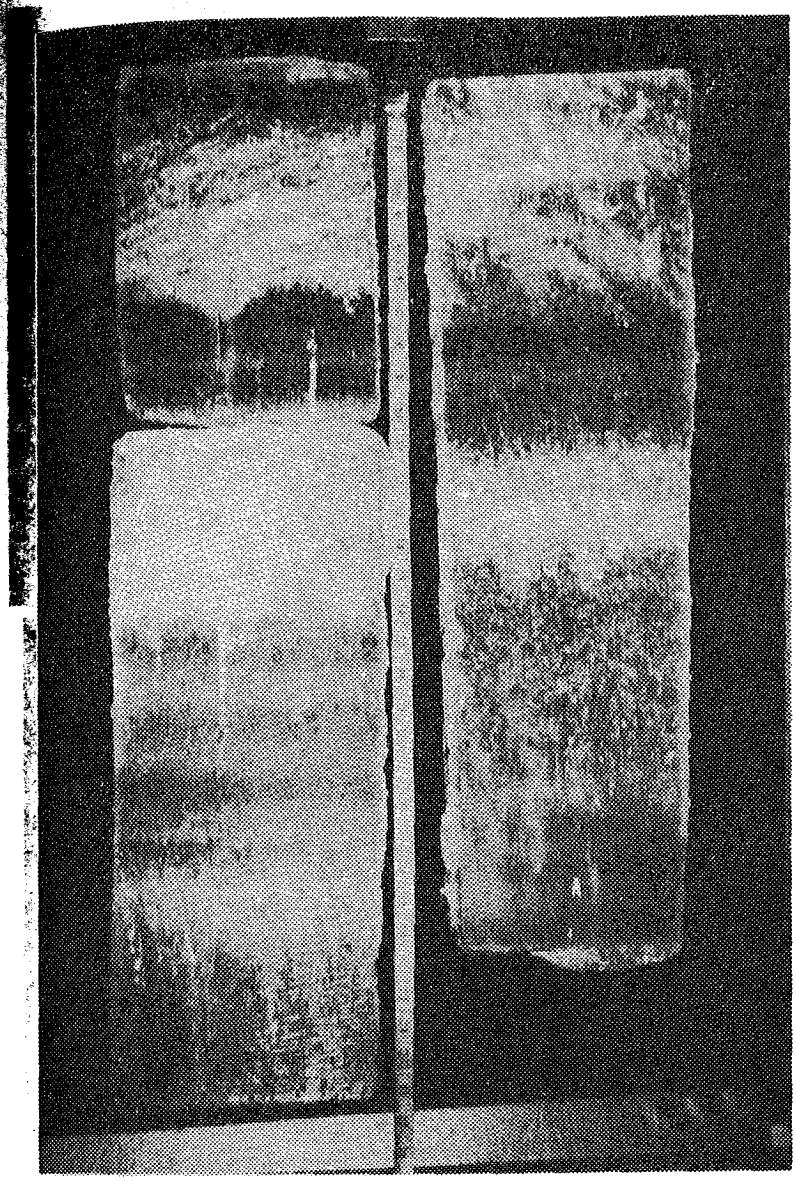

Figure 8. The ice sample M3 in normal light

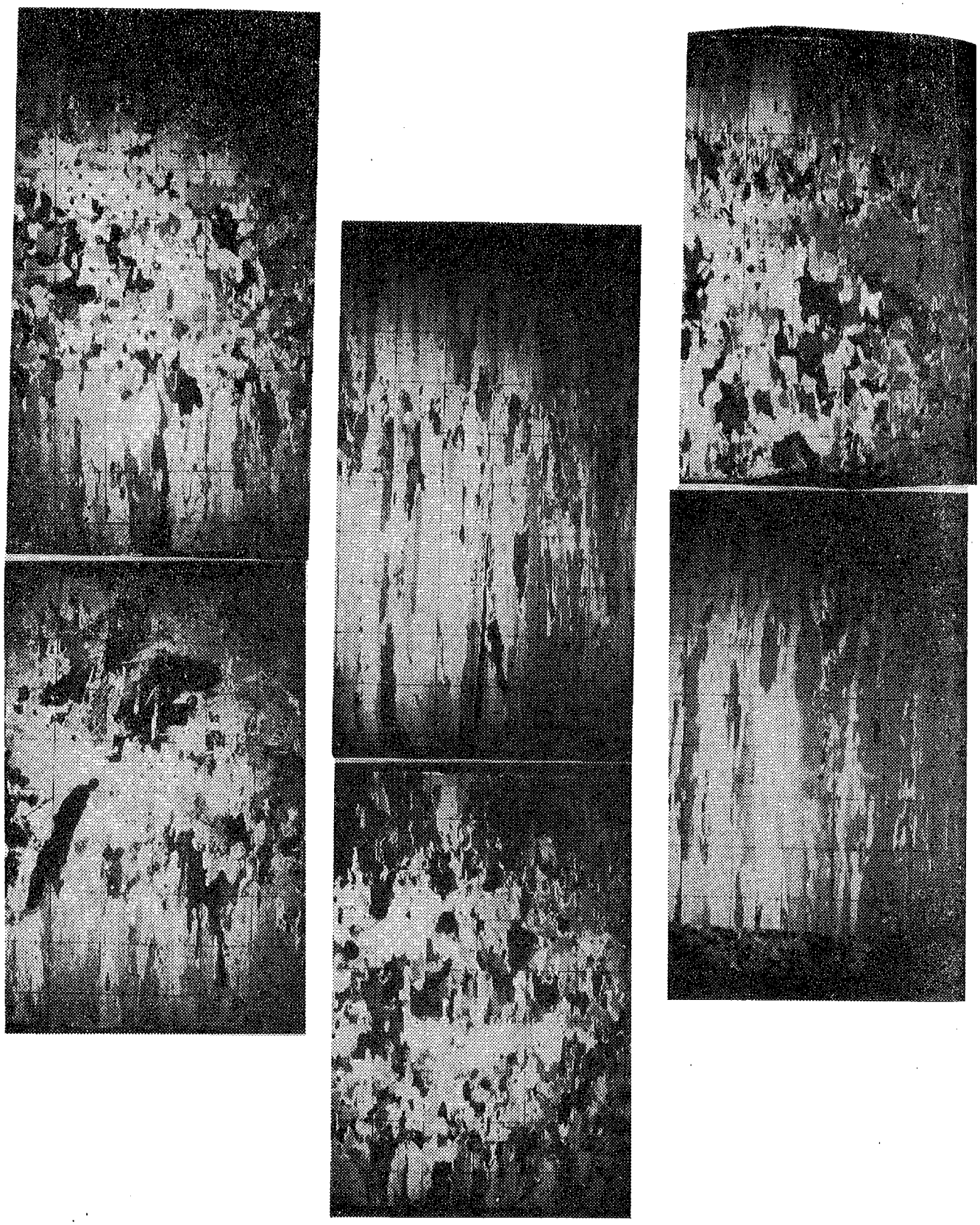

Figure 9. Vertical cross-section of the crystal structure of ice at site M3.

3.3 Ice salinity

The results of the ice salinity measurements are shown in Table 3. The salinity value was usually a little above or below one per mille. On an average this is roughly one fifth of the salinity of surface water and one-half of the salinity of ice in mid-winter in that region.

In the ten topmost centimeters the salinity ranged from 0.3 to 1.0 per mille. Lowest values were measured in the fast ice field around Aranda.

Table 3. Ice salinity.

Location: 63°17'N 20°48'E, 500 m NW from Aranda
Time: 31 March, 17 hours
Type: Frozen layer of an ice ridge at the fast ice boundary

Depth (cm)	S (°/₀₀)	Depth (cm)	S (°/₀₀)
0 - 7	0.42	47 - 55	1.57
7 - 15	0.86	55 - 61	0.99
15 - 23	1.30	61 - 67	1.06
23 - 31	1.20	67 - 97	0.65
31 - 39	0.95	97 - 127	0.51
39 - 47	1.00		

Location: 63°17.8'N 20°48.3'E, at Aranda
Time: 1 April, 15 hrs
Type: Fast ice, 2 samples

1st sample (A1)		2nd sample (A5)	
Depth (cm)	S (°/₀₀)	Depth (cm)	S (°/₀₀)
0 - 8	0.59	0 - 11	0.34
8 - 18	0.71	11 - 22	0.74
18 - 30	0.57	22 - 33	1.03
30 - 38	0.34	33 - 42	0.61
38 - 46	0.39	42 - 53	1.27
		53 - 62	0.26

Location: 62°55.2'N 20°17.8'E (Point M1)
Time: 2 April, 14 hrs
Type: Pack ice

Depth (cm)	S (°/₀₀)	Depth (cm)	S (°/₀₀)
0 - 10	0.79	40 - 50	0.92
10 - 20	1.01	50 - 60	0.85
20 - 30	1.14	60 - 67	0.75
30 - 40	1.13		

Location: 62°55.0'N 20°24.0'E (Point M2)
Time: 2 April, 12 hrs
Type: Pack ice

Depth (cm)	S (°/₀₀)	Depth (cm)	S (°/₀₀)
0 - 10	1.03	19 - 29	1.04
10 - 19	1.16	29 - 36	0.81

Location: 62°53.3'N 20°31.0'E (Point M3)
Time: 1 April, 18 hrs
Type: Pack ice

Depth (cm)	S (°/₀₀)	Depth (cm)	S (°/₀₀)
0 - 10	0.80	30 - 40	1.33
10 - 20	1.12	40 - 50	1.23
20 - 30	1.21	50 - 58	0.68

Location: 62°57.4'N 20°38.6'E (Point MT)
Time: 2 April, 16 hrs
Type: Pack ice

Depth (cm)	S (°/₀₀)	Depth (cm)	S (°/₀₀)
0 - 10	0.75	20 - 30	0.79
10 - 20	1.16	30 - 33.5	0.79

Location: 63°05.1'N 20°39.0'E (Point RA1)
Time: 3 April, 11 hrs
Type: Pack ice

Depth (cm)	S (°/₀₀)	Depth (cm)	S (°/₀₀)
0 - 9	0.69	15 - 22	0.63
9 - 15	0.75		

Location: 63°09.9'N 20°44.0'E (Point RA2)
Time: 3 April, 11 hrs
Type: Bare fast ice area

Depth (cm)	S (°/₀₀)	Depth (cm)	S (°/₀₀)
0 - 8	0.33	24 - 33	1.24
8 - 16	0.89	33 - 40	0.93
16 - 24	1.01	40 - 45	0.70

4. SNOW PROPERTIES

The thickness of snow was 0 to 30 cm in study area II. High values were naturally observed in the fast ice field and at ice ridges.

Around Aranda the thickness of snow also ranged from 0 to 30 cm with an average of about 10 cm. The density of snow varied between 0.30 and 0.35 g cm^{-3}.

The layer structure of the snow cover was studied along a line of 40 m at one meter intervals close to Aranda during 14 to 17 hrs on 2 April. The air temperature was above zero. Fig. 10 shows the large spatial variability of the properties of the snow cover. The thickness of snow ranged from 3 to 22.5 cm. The structure of thick snow is illustrated in Fig. 11. An ice lense was situated in the depth of 1 to 10 cm from the top. Close to the ice-snow interface there was a thin layer of water and an up to 4 cm thick slush layer. The water layer was in places covered with ice (about 1 cm thick). The values of the salinity of snow and slush are also shown in Fig. 11. The high salinity of the slush layer indicates that it was a mixture of snow and sea water. Even in the lower snow layer the salinity was as high as 0.11 °/₀₀.

Observations of the grain size of snow were made at Aranda. Both fine (1 mm) and coarse (2-3 mm) grains occurred. Fig. 12 shows a sample from the surface layer. Snow cover grains were often frozen together, which is typical of spring time. In such clumps there was only weak adhesion between individual grains, and the clumps easily broke into pieces when samples for photography were taken.

The variability of the snow cover features was also studied on a larger scale. Observations were made in the fast ice region using snow mobile for transportation. Lines of a few kilometers were studied south and northeast of Aranda. Typically the snow cover was 10-15 cm thick with the bottom 2-4 cm being slush. Ice lenses turned out to be rare. The density ranged from 0.27 to 0.43 g cm^{-3}.

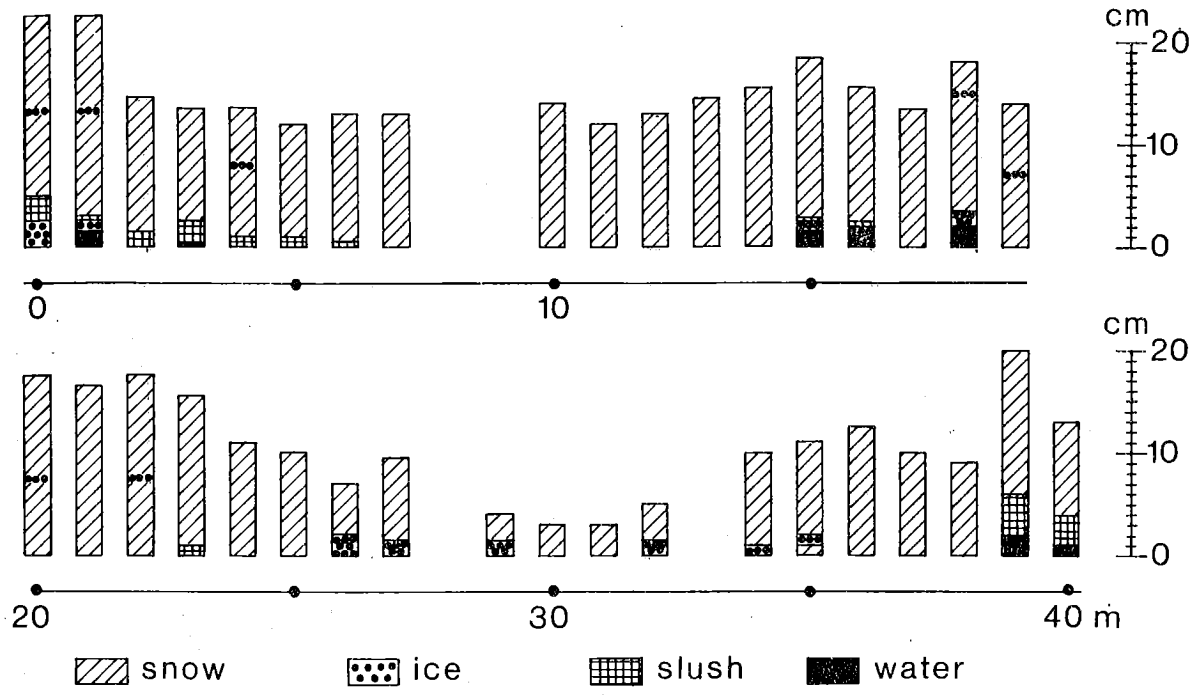

Figure 10. Spatial observation series of the snow cover at Aranda. The horizontal axis shows the distance from the first measurement point in meters.

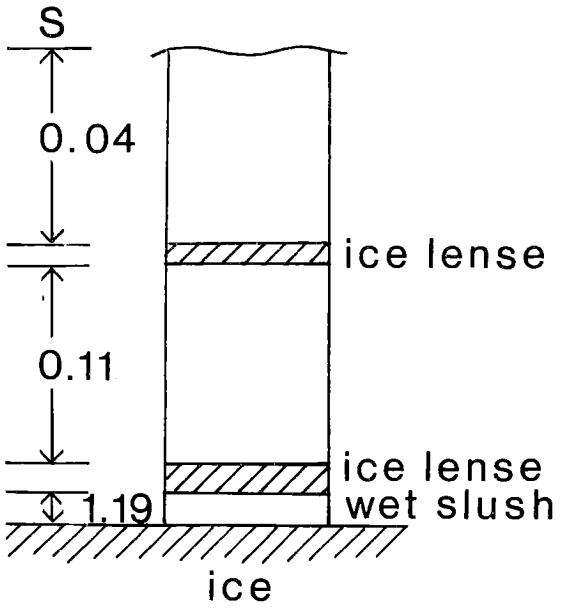

Figure 11. Layer structure of thick snow around Aranda. Salinity is given in per mille on the left.

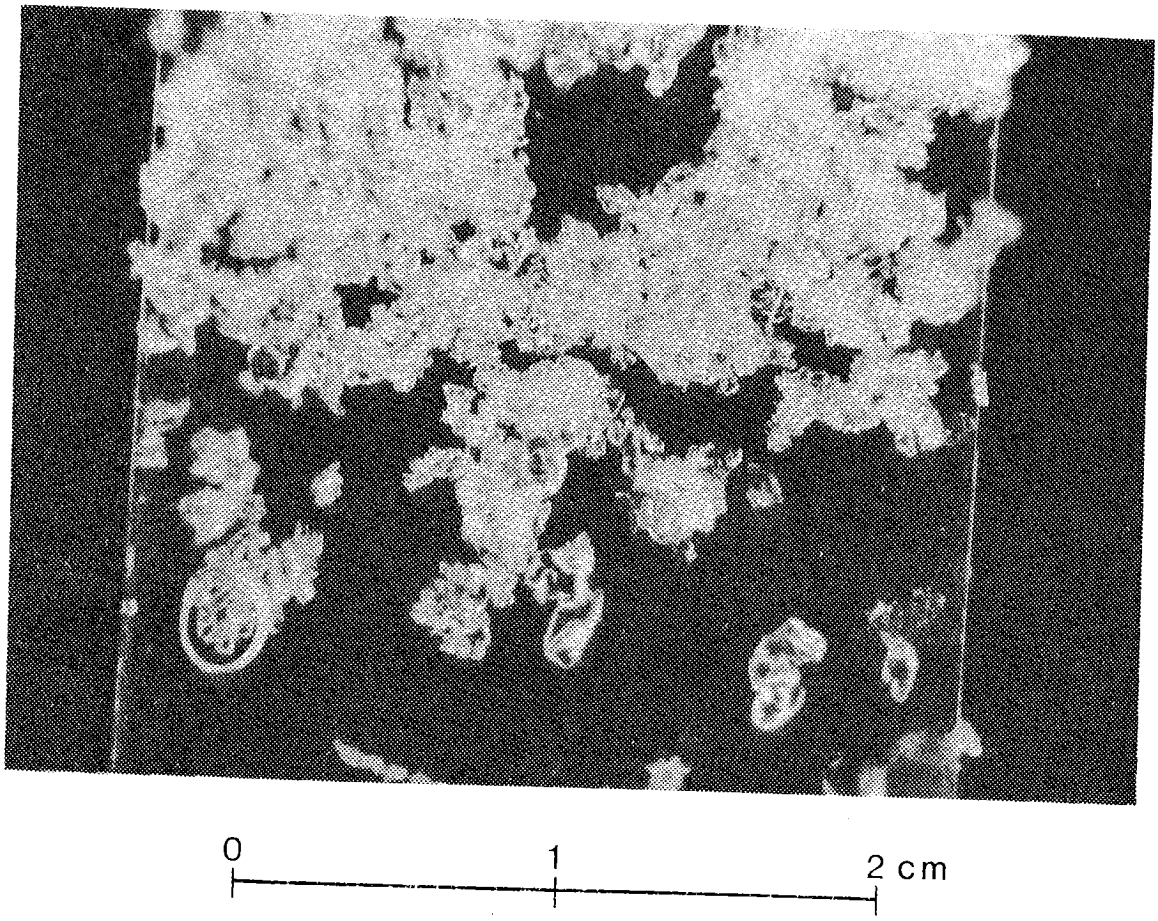

Figure 12. Snow grains close to the surface at Aranda. Large clumps are only weakly frozen together.

The moisture content of the snow was by a rough estimate in the range 5-30 % in the fast ice region. It was easy to make a snow ball. Attempts were made to measure the moisture content with a simple calorimetric method using a 3/4-liter thermos bottle. The results seemed to be too noisy and hence were not satisfactory.

5. TEMPERATURE MEASUREMENTS

Method

Temperature measurements were made with a Tastotherm D700 contact thermometer, which is based on NiCr - NiAl thermo couple. Its measurement range covers the temperature interval -50 to +200 °C, absolute accuracy being 0.5 °C and resolution 0.1 °C. The time constant of the measurement head used (T1202) is 5 seconds.

Only one reference point, the melting temperature of fresh water ice, was available. The thermometer reading at this point was 0.0 °C. The stability of the instrument was not tested. The behaviour of the ice temperature with time could not be followed because of the lack of a portable plotter. Consequently all the temperature values are instantaneous.

The vertical ice temperature profile was measured from the samples used for the analysis of salinity, crystal structure and dielectric properties. The detaching process of the large piece of ice disturbs the vertical surface too much for relevant temperature measurements. Therefore, measurements were made from the surfaces uncovered when the piece was sawed into smaller samples.

The vertical temperature profile can be measured either from one vertical cut or from several horizontal cuts. Vertically cut surfaces provide better spatial resolution, but biases arise, because all the profile points are not equally long in contact with air before the measurements. With horizontally cut surfaces these biases can be avoided, because each profile point corresponds to one sawing. On the other hand the spatial resolution is then poorer.

Results

The air temperature did not differ much from zero, and naturally the temperature of the surface water was also close to zero. Thus the vertical variation of the ice temperature was slight, and the differences were close to the resolution of the thermometer.

Fig. 13 shows the results of the temperature measurements on 1 and 2 April. The largest temperature gradient occurred naturally in the snow layer. The gradient in the ice decreased downwards. The snow layer was only 1-2 cm thick in these samples.

Only the results from the horizontally cut samples at location M1 have a noticeable scatter. This may be due to the fact that then the measurement unit had been the longest time at the low outdoor temperature (-1.5 °C), and the minimum operating temperature of the device is 0.0 °C.

Remarks

The ice and snow temperature measurements have the following basic problems: 1) Difficulty in making a good thermal contact between the sensor and measurement surface, 2) The effect of the method of sampling to the temperature, and 3) The amount of work needed to make the measurements.

There are two different kinds of surface temperature measurement systems available to our problem. One is based on a thermocouple and the other on the electric resistance of a platinum wire. The advantage of thermocouple systems is fast response while platinum resistance systems are more accurate. It seems that the fast response is more importance in practice, especially when the air-ice temperature difference is large.

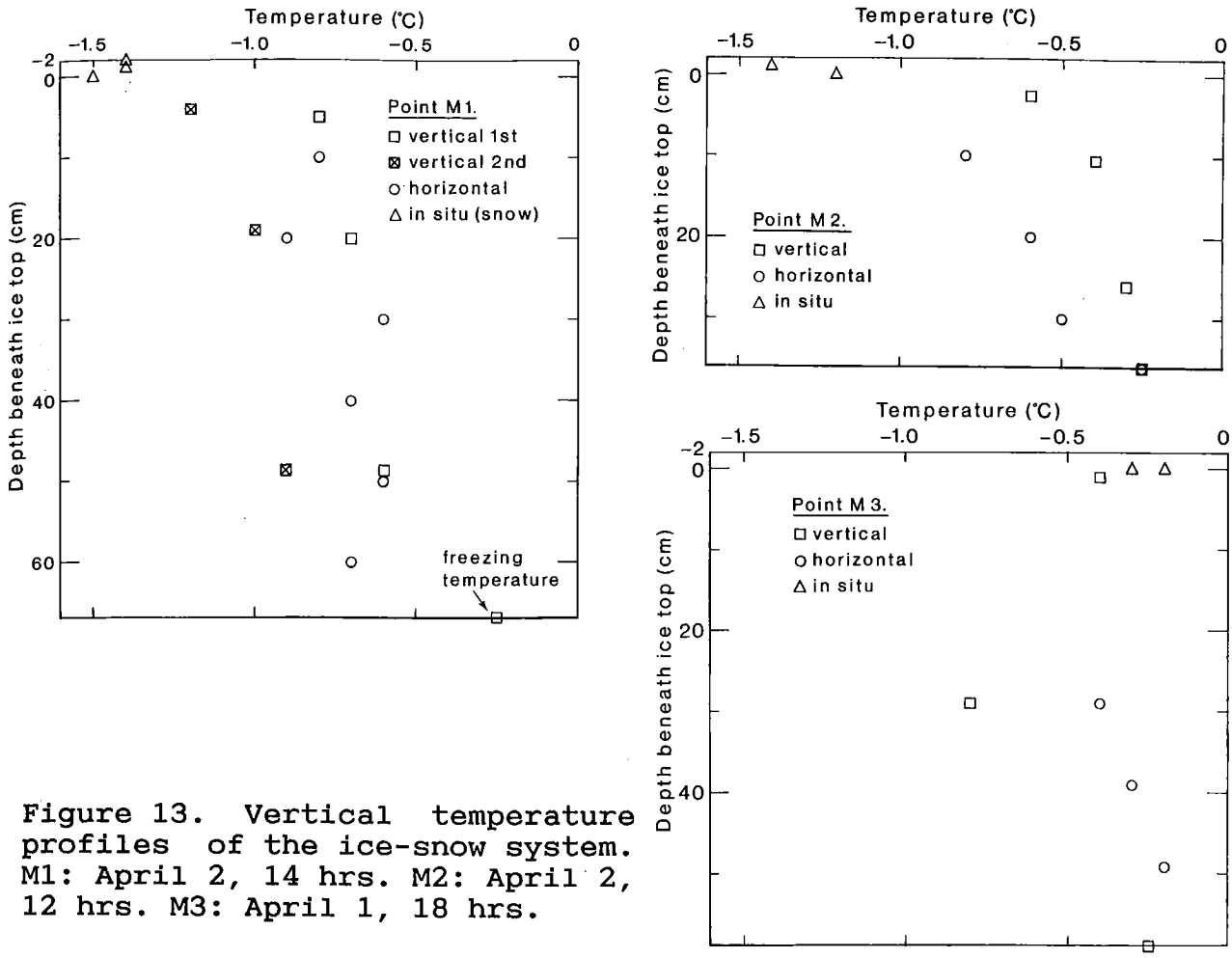

Figure 13. Vertical temperature profiles of the ice-snow system. M1: April 2, 14 hrs. M2: April 2, 12 hrs. M3: April 1, 18 hrs.

When preparing a sample one necessarily disturbs the surface to be measured. Moreover, during the measurements the surface is exposed to air, which tends to bring about another bias to the results. These effects should be studied more in the future.

In this kind of ice temperature measurements one always operates close to the melting temperatures, because the ice-water interface is involved. In this temperature regime small differences are very significant, because the brine volume depends highly nonlinearly on the temperature (e.g., Weeks and Ackley, 1982). Hence the resolution and stability of the measurement system are very important. More consideration should be given to calibration in the future.

6. CONCLUSIONS

The data of ice and snow geophysics program in study area II in BEPERS Pilot Study, have been described. Observations were made during 30 March - 3 April 1987 in the Quark and northern part of the Sea of Bothnia. A large part of the research was carried out in the vicinity of R/V Aranda which was located at the fast ice boundary. The ice pack far from Aranda was mapped with aerial reconnaissance and sampling at seven sites. The study area was located both in the fast ice and in the pack ice field.

The ground observation program consisted of the following elements:

1. General ice conditions;
2. Crystal structure of the ice;
3. Ice salinity;
4. Snow properties;
5. Ice and snow temperature.

The program could be carried out successfully. However, since the ice sampling is quite time consuming only seven sites could be taken for ice structure and salinity studies far from Aranda. The snow properties part was performed only in the vicinity of Aranda.

The thickness of ice was 40-70 cm in the fast ice area. Most of the fast ice was covered with 5-15 cm thick wet snow.

In the pack ice area the ice thickness varied through 20 to 70 cm. Close to the fast ice boundary where the pack ice was thinnest there was snow only on ridges, and the level areas between ridges were bare.

The ice was brackish water ice with the salinity typically in the range 0.5 to 1.5 per mille. Both in the fast ice area and in

the pack ice area alternating granular and columnar-grained layers were found in the ice sheet. As a rough estimate, on average three quarters of the ice was columnar and one quarter granular. Large grains in granular layers were typically of around 1-cm diameter.

During afternoons the snow surface was in the stage of melting and hence must have had the temperature of 0°C. In the night-time the surface temperature went down to around -2°C. According to a few measurements of snow-covered ice, during the afternoons the temperature of the whole ice sheet was less than -1°C with maximum of at least -0.2°C.

This project BEPERS Pilot Study, has given us much practical experience to carry out the ground programme of a remote sensing experiment. To improve the interpretation of remotely sensed data, the following two points need to be deeply considered in following field studies:

1) The spatial variation of ice and snow properties need to be deeply investigated to understand the pixel-size averaged values of remote sensing instruments.

2) The temporal variation of ice and snow properties need to be followed to know them exactly at the time of the remote sensing measurements.

Acknowledgements

Our work has been supported by the Finnish Board of Navigation and Technology Development Centre which is greatly acknowledged. Thanks are also due to Mr. Juhani Rapo for technical assistance in the field, and due to the helicopter pilot Dick Lindholm and R/V Aranda's captain Jukka Kyröhonka for fruitful cooperation.

7. REFERENCES

Finnish Meteorological Institute, 1987: Meteorological observations on 2 April 1987. - Archives.

Weeks, W. F. and S. F. Ackley, 1982: The growth, structure and properties of sea ice. - CRREL Monograph 82-1, 130 p. U.S. Army Cold Reg. Res. Eng. Lab., Hanover, N.H.

In: BEPERS Pilot Study. Data Report. Styrelsen för Vintersjöfartsforskning/Winter Navigation Research Board, Rep. No 45, p. 69-83. Helsinki 1988.

V MICROWAVE MEASUREMENTS OF ICE AND SNOW

By Martti Hallikainen, Martti Toikka and Juha Hyyppä

Helsinki University of Technology, Radio Laboratory
Otakaari 5 A, 02150 Espoo, Finland

ABSTRACT

Microwave instruments were used to measure the dielectric properties of sea ice, the liquid water content and density of snow cover, and the thickness of sea ice in Area II. Due to air temperatures above 0°C, both the snow cover and the sea ice layer were wet, resulting in high attenuation. Consequently, the main sources of SAR backscattering are the snow cover and the topmost sea ice layers.

1. INTRODUCTION

In order to investigate the relation between the backscattering coefficient and the sea ice and snow properties, the physical and electrical parameters of the two media have to be measured simultaneously with the SAR over pass.

The ground truth instruments developed at the Helsinki University of Technology include an FM-CW radar (operates at 1-2 GHz; measures the thickness of sea ice), a snow fork (operates at 500 - 1000 MHz; measures the liquid water content and density profiles of snow), and the dielectric measurement system (operates at 10 GHz; measures the complex dielectric constant of sea ice). During the Sea Ice 87 campaign, these instruments were used to collect ground truth data in Area II.

2. DIELECTRIC MEASUREMENTS OF ICE

2.1 Measurement System

The dielectric properties of numerous sea ice samples were measured at 10 GHz. The samples were collected both near R/V Aranda and (by helicopter) from other interesting sites. The block diagram of the dielectric measurement system is depicted in Fig. 1.

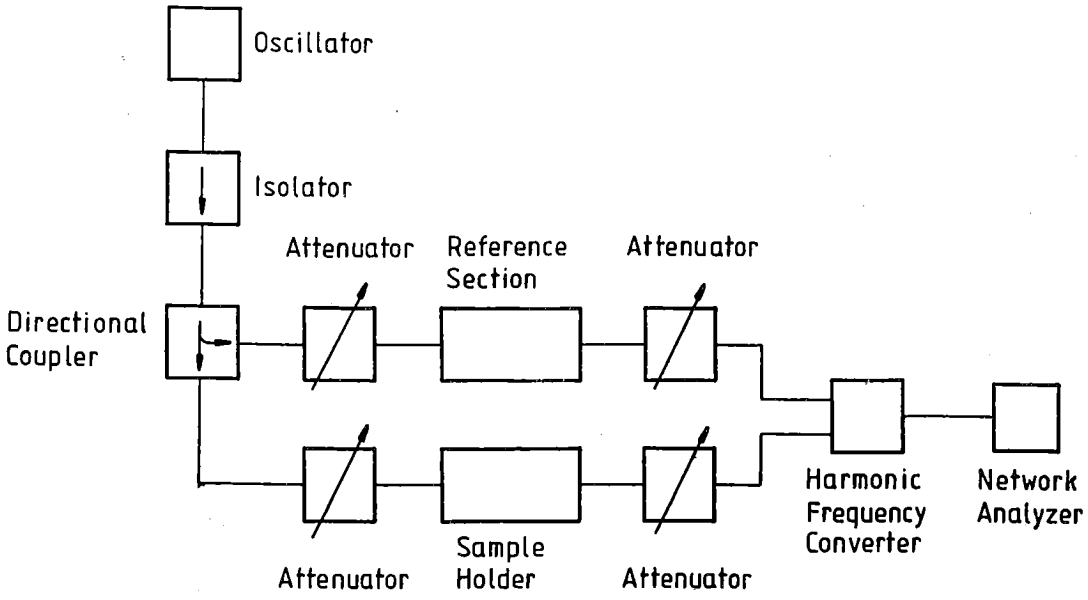

Figure. 1. Block diagram of the dielectric measurement system.

The cross section of the ice sample is rectangular with dimensions of 10 mm by 23 mm in order to fit to the waveguide used as a sample holder. The maximum length of the sample is 14 cm. Usually, sample lengths of the order of 10 to 12 cm are used.

The loss and the phase shift due to the insertion of the sample into the waveguide are measured with a network analyzer. From the measured loss and the phase shift, the attenuation coefficient (α) and the phase coefficient (β) are calculated. The real and the imaginary part of the complex dielectric constant, denoted

$$\epsilon = \epsilon' - j\,\epsilon'' \qquad (1)$$

are computed from α and β using the following equations (Hallikainen et al. 1985),

$$\epsilon' = \left(\frac{\lambda_o}{2\pi}\right)^2 \left(\frac{2\pi}{\lambda_c}\right)^2 - (\alpha^2 - \beta^2) \qquad (2)$$

$$\epsilon'' = \left(\frac{\lambda_o}{2\pi}\right)^2 2\alpha\beta \qquad (3)$$

where λ_o = wavelength of electromagnetic wave in free space
L_c = cut-off wavelength in rectangular waveguide.

In remote sensing of sea ice, two additional parameters are of interest, namely the absorption coefficient (K) and the penetration depth (δ). The absorption coefficient gives the electromagnetic loss per one meter of sea ice,

$$K = 2\,\alpha\,. \qquad (4)$$

The penetration depth gives the maximum depth that contributes to the measured backscattering coefficient,

$$\delta = 1/K \ . \qquad (5)$$

If the penetration depth is smaller than the ice thickness, the bottom layers of the ice do not contribute to the backscattering coefficient. For sea ice, this is usually the case. The main contribution to the absorption coefficient of sea ice comes from the entrapped salt in the ice matrix.

The temperature of each sample was measured with an electronic thermometer both before and after the dielectric measurement. The salinity of each sample was determined by the Marine Research Institute after the measurement campaign.

The salinity range of the samples was 0.02 to 0.94 °/₀₀, and the temperature range was -5.9 to -0.3°C. Temperatures below -1°C were due to storing some samples in the freezer; consequently, they were not at the original ice temperature during the dielectric measurement. The density of the samples was not measured because of the small sample size. The orientation of the ice samples during the dielectric measurement corresponds to a case where the electromagnetic wave propagates vertically in the sea ice layer.

The temperature of the sample holder must be of the same order as that of the sample in order to eliminate any temperature changes. Due to the warm weather during the campaign ($T_{air} \approx$ 0°C), the dielectric measurement system was placed in a freezer to keep its temperature slightly below 0°C.

2.2 Results

A total of 44 ice samples were measured from March 31 through April 3, 1987. Most of the samples were at a temperature very

close to 0°C. Consequently, extreme care was taken when processing and handling the samples. In some cases, the sample surface got wet during the measurement; consequently, the results were deleted.

In order to compare all measured values, the results are shown as a function of the relative brine volume (Stogryn and Desargant 1985). The brine volume fraction increases with increasing temperature and increasing salinity.

Figs. 2 and 3 show the real and the imaginary part of the complex dielectric constant. The real part increases with increasing brine volume fraction. The value for pure ice is $\epsilon' \approx 3.15$. Air bubbles tend to decrease this value down to $\epsilon' \approx 2.5$, as shown in Fig. 2. The dielectric constant of brine liquid is much higher than that of pure ice (Stogryn and Desargant 1985); consequently, the real part increases with increasing brine volume fraction.

The values shown in Fig. 2 are slightly lower than those measured previously at 600 MHz and 900 MHz (Hallikainen 1983). Since the salinity of Arctic first-year sea ice may be up to 10 °/₀₀, the results in Fig. 2 are also lower than those reported for Arctic areas (Vant 1976).

Figs. 4 and 5 show the experimental absorption coefficient and the penetration depth for the ice samples. The absorption coefficient depends strongly on the brine volume fraction. The penetration depth is in most cases less than 10 cm. This means that the SAR can "see" only the upmost ice layer. Table 1 shows a review of the experimental data for samples taken from the ice surface.

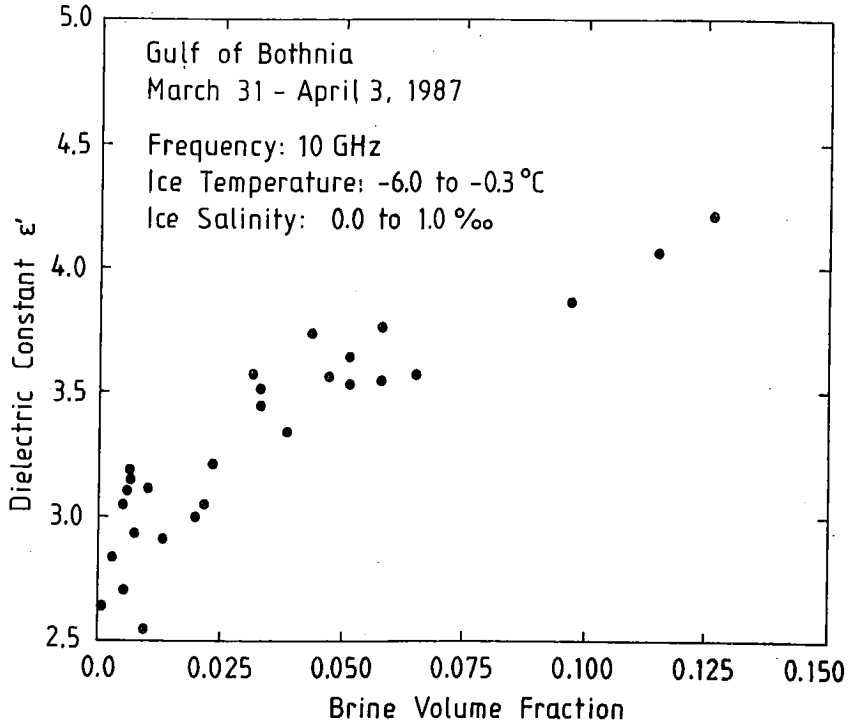

Figure 2. Experimental real part of the dielectric constant of sea ice at 10 GHz.

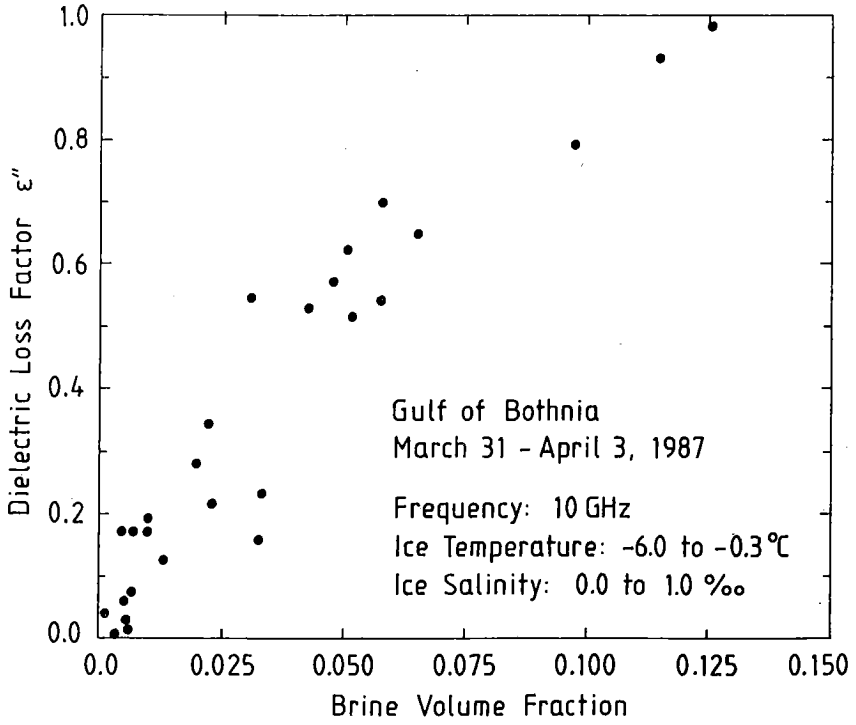

Figure 3. Experimental imaginary part of the dielectric constant of sea ice at 10 GHz.

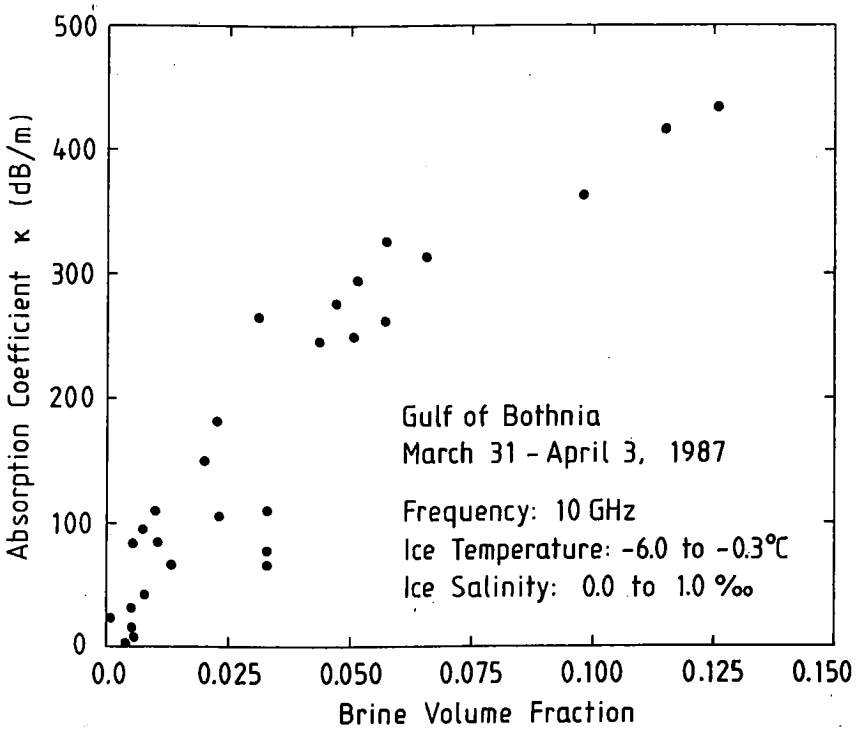

Figure 4. Experimental absorption coefficient of sea ice at 10 GHz.

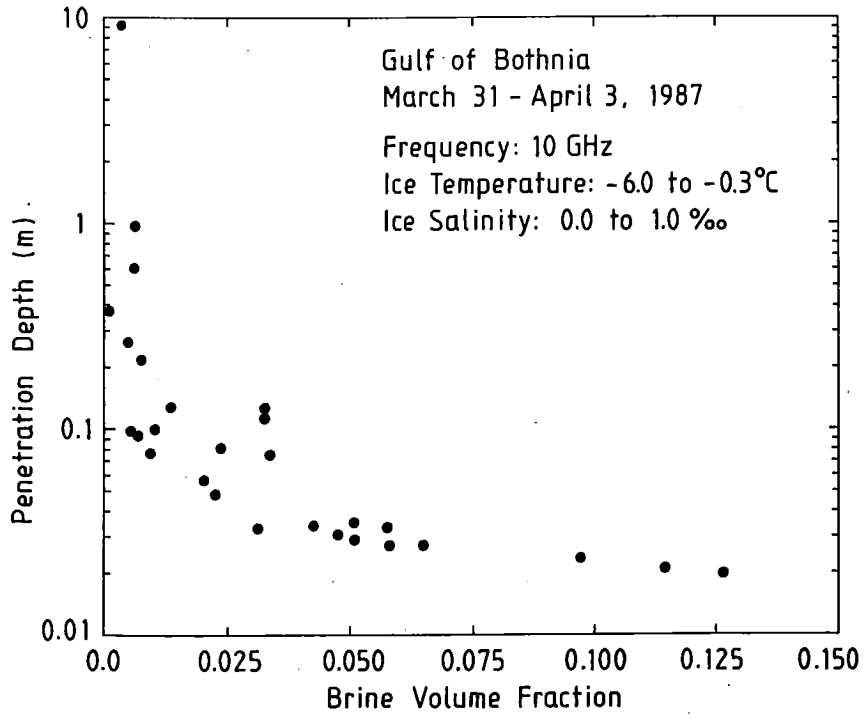

Figure 5. Experimental penetration depth in sea ice at 10 GHz.

Table 1. Experimental data for ice samples taken from the ice surface.

Date	Time (hours)	Area	Depth (cm)	T (°C)	Sal-inity (°/₀₀)	ε'	ε"	δ (cm)	Comments
April									
1	09	Aranda/1	2-10	-0.9	0.38	3.01	0.29	5.7	
1	10	Aranda/2	2-10	-1.5	0.31	2.55	0.19	7.9	air bubbles
1	18	62°53'N 20°31'E (point M3)	2-12	-0.9	0.45	3.21	0.21	8.2	
2	10	Aranda/ice ridge	1-11	-1.5	0.19	2.17	0.03	60.0	Surface of ice ridge
2	12	62°55'N 20°24'E (point M2)	1-12	-0.5	0.61	3.76	0.70	2.7	
2	14	62°55'N 20°18'E (point M1)	1-12	-0.3	0.35	3.55	0.54	3.3	
2	16	62°57'N 20°39°E (point MT)	0-10	-0.4	0.42	3.66	0.62	3.0	
3	11	63°05'N 20°39'E (point RA1)	0-10	-0.5	0.51	3.34	0.83	2.1	
3	11	63°10'N 20°44'E (point RA2)	0-10	-0.4	0.21	-	-	-	

3. MEASUREMENTS OF SNOW PROPERTIES

A radiowave sensor called snow fork, was used to determine the density and the wetness profile of snow cover upon the sea ice. The snow fork measures the dielectric constant (real and imaginary part) of snow around 1 GHz (Sihvola and Tiuri 1986). From the dielectric constant, the density and the liquid water content of snow can be calculated, Fig. 6.

The snow sensor is a parallel-wire transmission-line resonator. It has two parallel spikes, the length of each is 60 mm. The distance between the spikes is 18 mm. When the sensor is pushed into the snow, the microprocessor automatically measures the dielectric constant and stores the results in the memory. The data can be printed out or the results can be transmitted into a computer.

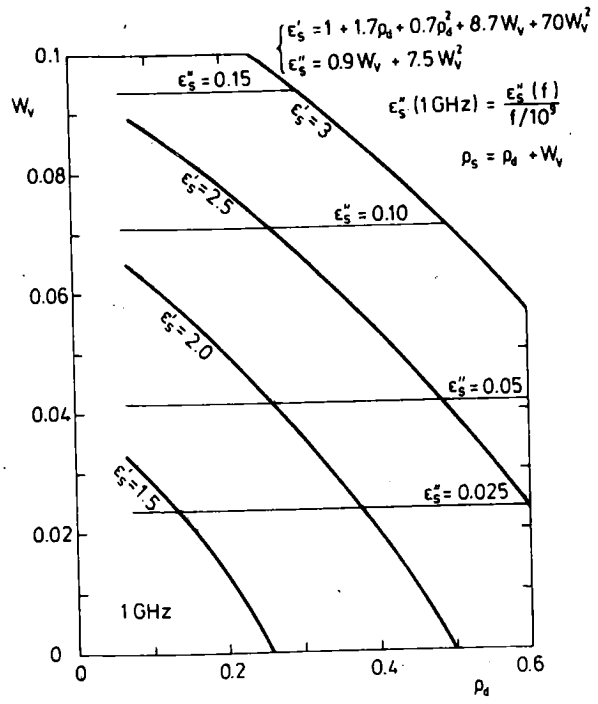

Figure 6. Nomogram to obtain the liquid water content and density of snow from the complex dielectric constant.

During the measurement campaign the snow properties were measured in areas near R/V Aranda. Several daily measurements were made from 31 March to 3 April. Fig. 7 shows an example of the measured density and wetness profile. The measurement was made on 1 April at 21.00. The air temperature was -1°C and the snow was drying. The measurement was made twice in locations about 0.5 m from each other. The average density of snow was about 0.3 g/cm^3 as illustrated in Fig. 8.

The liquid water content varied substantially, depending on the snow depth, air temperature, and cloudiness. Fig. 9 shows the diurnal variation of the liquid water content at various depths of the snowpack. Close to the ice-snow interface was a wet slush layer. The diurnal thickness variation of slush was substantial.

Some measurements showed large variation in the snow density values. This can be attributed to the salinity of snow. Fig. 10 shows the error in density measurement for saline snow. The salinity in Fig. 10 is the total salinity of snow. It is assumed that the salt is dissolved in liquid water. The error increases

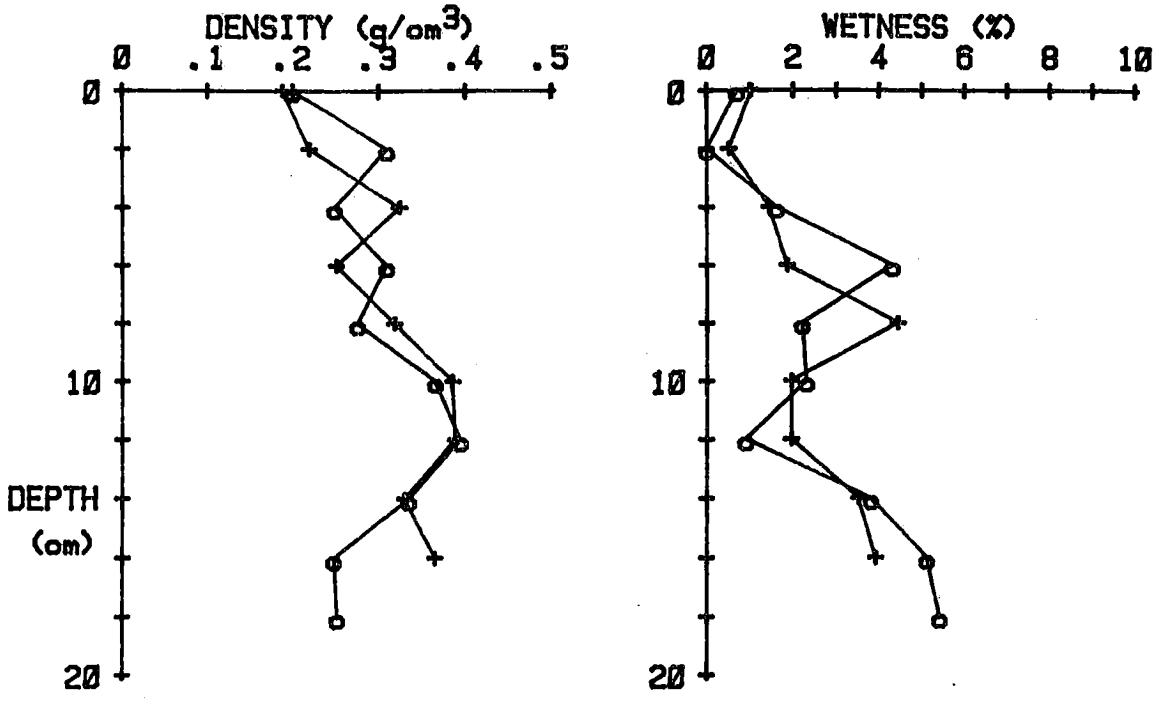

Figure 7. Measured snow density and wetness profile near R/V Aranda. The measurement was made twice in 2 cm intervals. First measurement: 0, second: +.

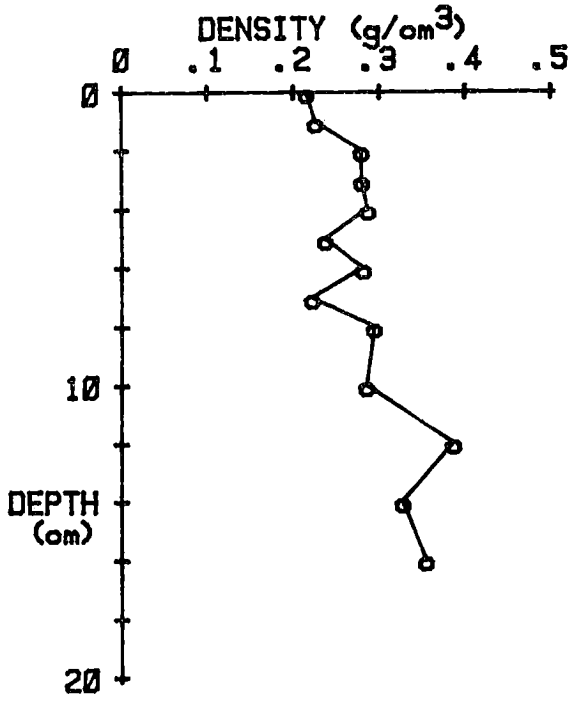

Figure 8. Average snow density profile near R/V Aranda. Ten measurements are averaged.

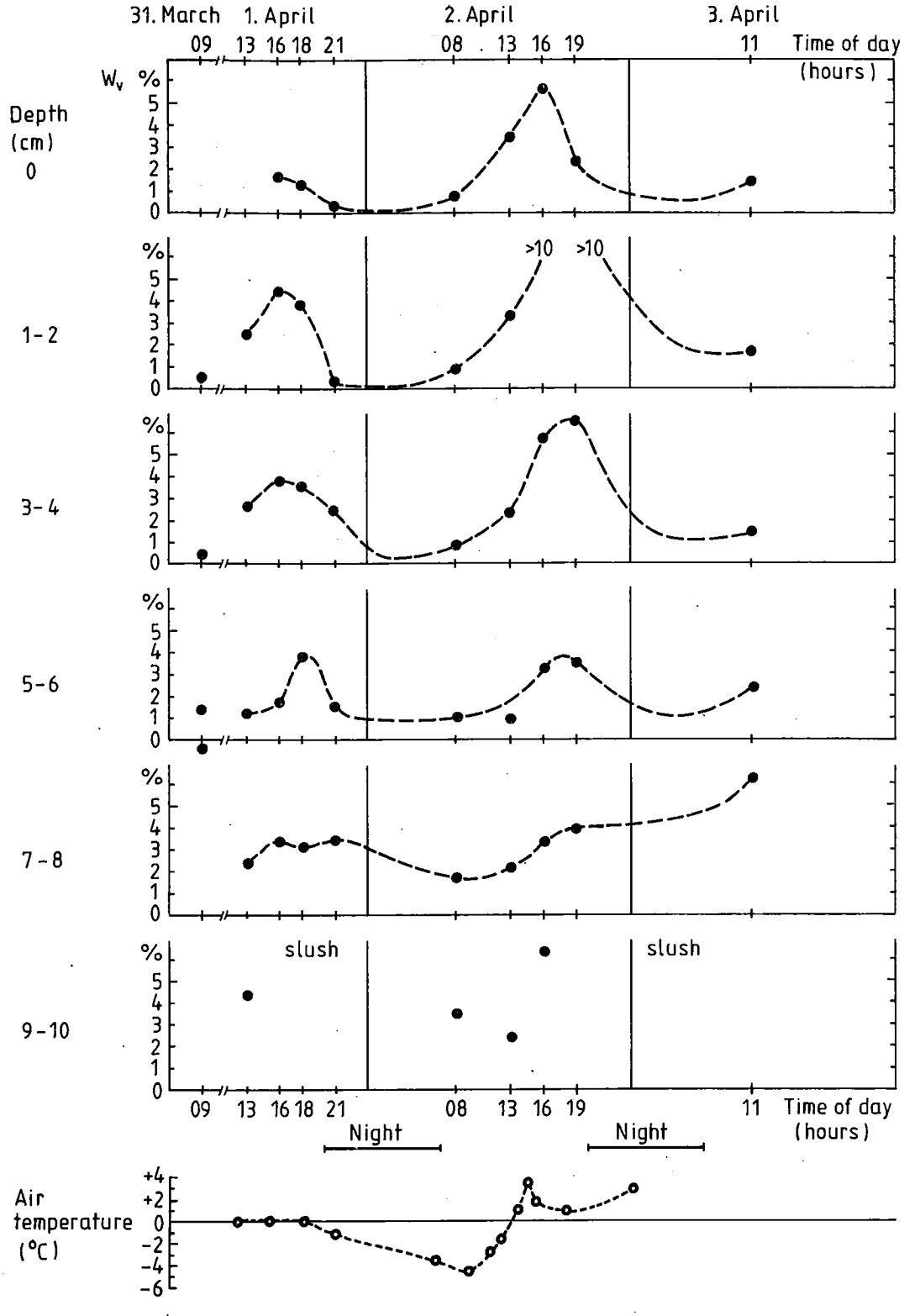

Figure 9. Measured diurnal variation of the liquid water content at various depths of the snowpack.

rapidly with increasing salinity and increasing water content. In the lower part of the snow layer, a salinity of 0.11 °/₀₀ was reported. If the water content is assumed to be 5 %, the measured density will be about 0.03 g/cm^3 too low. This can be seen in some density profiles, where the density decreases in the lower snow layers. In the upper part of the snowpack the salinity was 0.04 °/₀₀. In that case, the density error may be large if the wetness is high. Large variations in density values were observed when the snow was melting of drying. This suggests that the liquid water and salt are not uniformly distributed in the snow. Fig. 11 shows the effect of salinity to the wetness measurement. The effect is not as strong as it is to the density. If a salinity of 0.11 °/₀₀ and a wetness of 5 % are assumed, the error in wetness value is 0.004. Consequently, the correct value is 4.6 % instead of 5 %.

4. MEASUREMENT OF ICE THICKNESS

An FM-CW radar was used to measure the ice thickness (Jakkula et al. 1980). The center frequency of the radar is 1.5 GHz and the frequency sweep is 1 GHz. The IF signal is between 1 kHz and 2.5 kHz. It is fed to a filter bank consisting of 32 channels. The bandwidth of each channel is 50 Hz which corresponds to a resolution of 5 cm in the ice. The radar was installed on a sledge and a snow-mobile was used for towing the sledge. The results were recorded on a tape and later plotted with an intensity-plotter. Fig. 12 shows a profile that was measured near R/V Aranda. It is not possible to interpret the ice thickness from this profile.

The first echo returns from the snow-ice interface. This echo is strong and the depth varies according to snow thickness 0-20 cm. Additional echoes can be observed at different depths in the ice. The interface between ice and water should be at 60 to 80 cm, but there are only few very weak echoes.

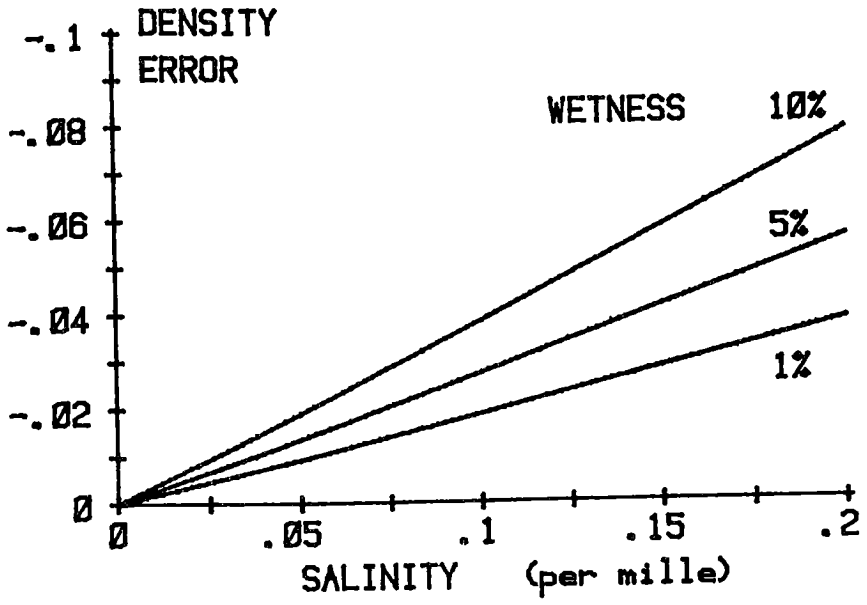

Figure 10. Error in density measurement as a function of snow salinity. Snow density of 0.3 g/cm^3 is assumed.

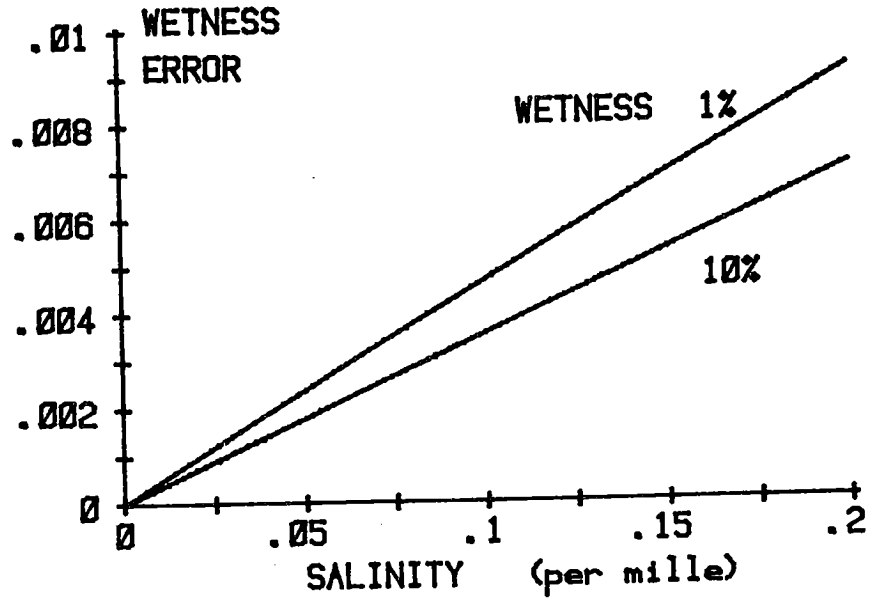

Figure 11. Error in wetness measurement as a function of snow salinity. Snow density of 0.3 g/cm^3 is assumed.

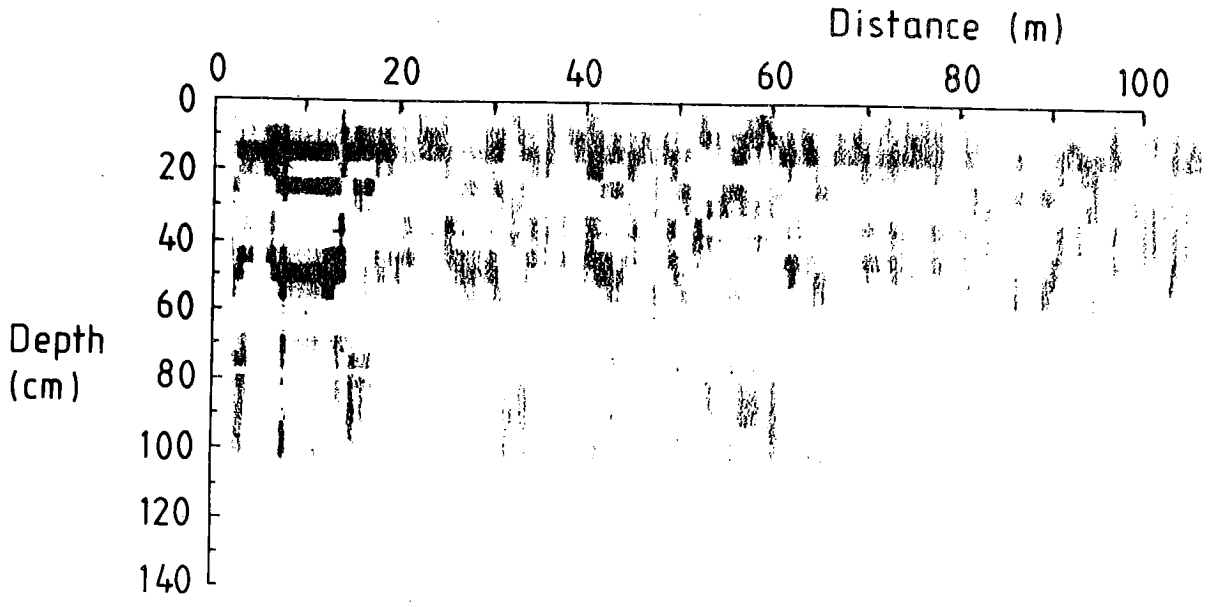

Figure 12. A sea ice thickness profile measured with the FM-CW radar.

The reason for this is the melting process of ice which had already started. The absorption coefficients measured for sea ice at 10 GHz (Fig. 4) suggest that the absorption is very high at the 1-2 GHz range as well. Additionally, the ice bottom was rough and water was penetrating into the ice. Rough interface is a good absorber resulting in small reflections. The echoes inside the ice may be interfaces between different ice layers.

REFERENCES

Hallikainen, M., 1983: A new low-salinity sea-ice model for UHF radiometry. International Journal of Remote Sensing, Vol. 4, No. 3, pp. 655-681.

Hallikainen, M., F.T. Ulaby, M.C. Dobson and M. El-Rayes, 1985: Microwave dielectric behavior of wet soil - Part I: Empirical models and experimental observations. IEEE Transactions on Geoscience and Remote Sensing, Vol. GE-23, No. 1, pp. 25-34.

Jakkula, P., P. Ylinen and M. Tiuri, 1980: Measurement of ice and frost thickness with an FM-CW radar. Proceedings 10th European Microwave Conference, Warszawa, Poland, pp. 584-587.

Sihvola, A. and M. Tiuri, 1986: Snow fork for field determination of the density and wetness profiles of a snow pack. IEEE Transactions on Geoscience and Remote Sensing, Vol GE-24, No. 5, pp. 717-721.

Stogryn, A. and G. Desargant, 1985: The dielectric properties of brine in sea ice at microwave frequencies. IEEE Transactions on Antennas and Propagation, Vol. AP-33, No. 5, pp. 523-532.

Vant, M., 1976: A combined empirical and theoretical study of the dielectric properties of sea ice over the frequency range 100 MHz to 40 GHz. Carleton University, Ph.D. Thesis, Ottawa, Ontario.

In: BEPERS Pilot Study. Data Report. Styrelsen för Vintersjöfartsforskning/Winter Navigation Research Board, Rep. No 45, p. 85-101. Helsinki 1988.

VI GROUND TRUTH MEASUREMENTS FOR SAR-DATA INTERPRETATION AT STUDY AREA III / SMHI

By Bertil Håkansson and Thomas Thompson

Swedish Meteorological and Hydrological Institute
S-601 76 Norrköping, Sweden

ABSTRACT

Ground truth data from an ice station located 40 km east of the Swedish coast in the Bothnian Sea are presented. The weather conditions during the investigation are characterized as warm with air temperatures around zero. This weather situation has large impacts on ice and snow properties. Hence, it was found that the sea ice porosity was estimated to approximately 28 %. The ice surface and the snow, which mainly covered the ice ridges, were crusted. The ice ridges occurred with a mean density of 4 to 6 ridges/km.

1. INTRODUCTION

On March 31 a ground station was established on the ice approximately 42 km offshore Hornslandet on the Swedish east coast. The station was evacuated in the morning of April 3.

The station could only be reached by helicopter from the landbase at Hölick, Hornslandet (see Fig. 1), which limited the field program to a certain extent since transportation of staff and equipment became time consuming. However, the station was visited every day during the field program.

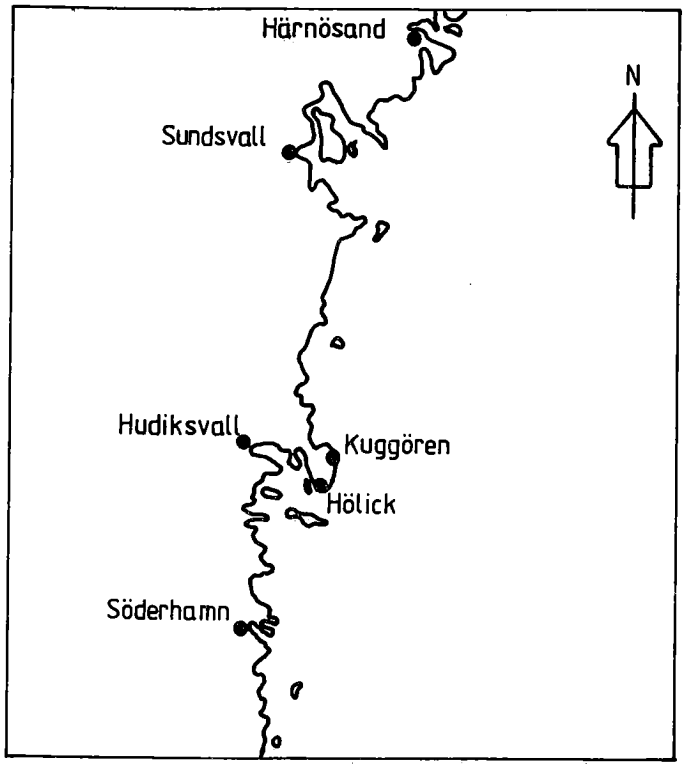

Figure 1. The location of the landbase at Hölick and the weather station at Kuggören.

At these occasions the ice station was geographically located with the Decca navigation system onboard the helicopter. From these data the mean ice drift of the station was found to be almost 18 km in a northward direction during March 31 to April 3 (see Fig. 2). Despite of this ice drift the station was always found without difficulty by the helicopter, since the ice drift could be succesfully forecasted from the wind information in the area.

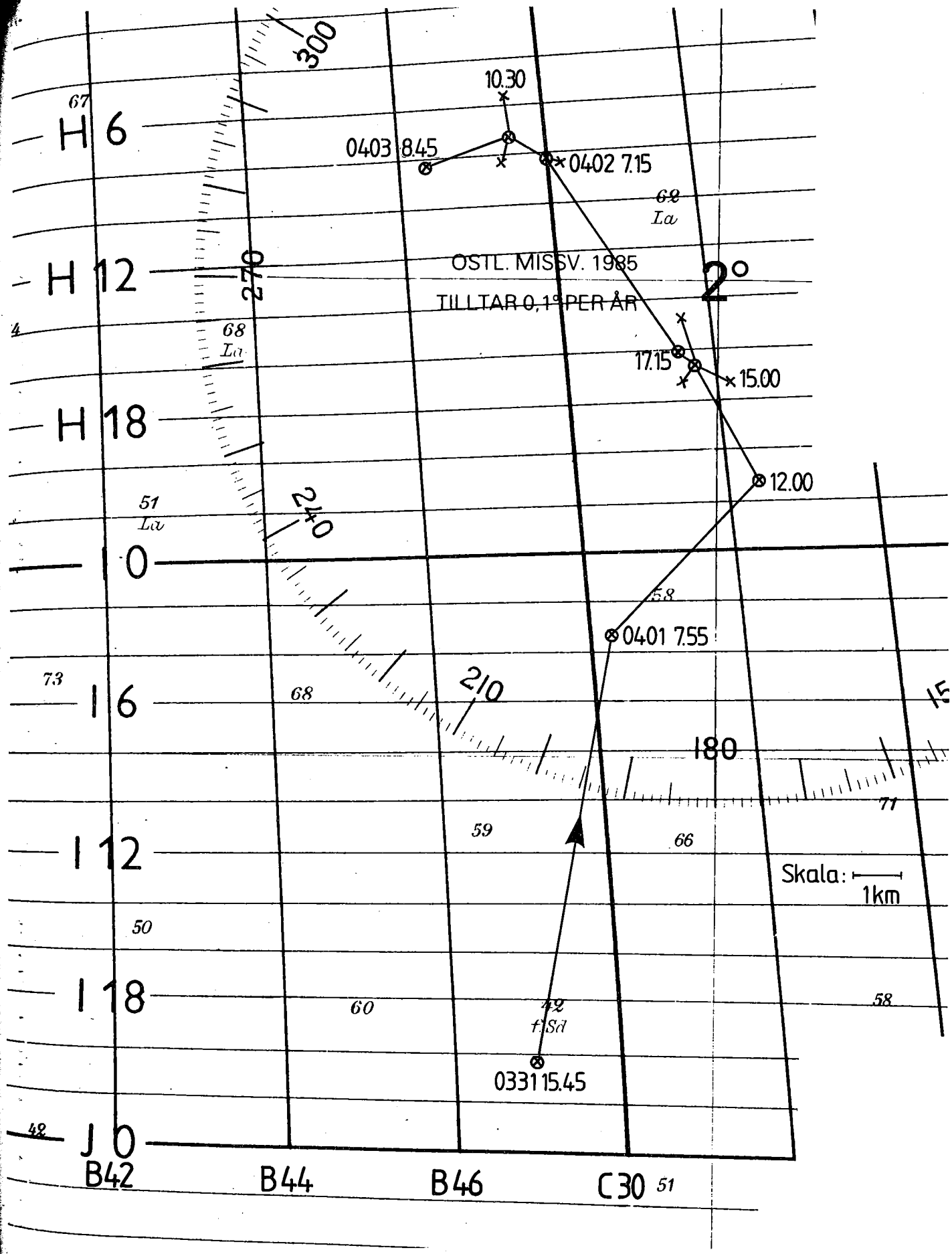

Figure 2. Ice drift of station III between March 31 to April 3.

Four radar reflectors were mounted on the ice in a triangular fashion as shown in Fig. (3) in which also the coordinates of the reflectors on the day of the SAR flight are noted. These coordinates are correct

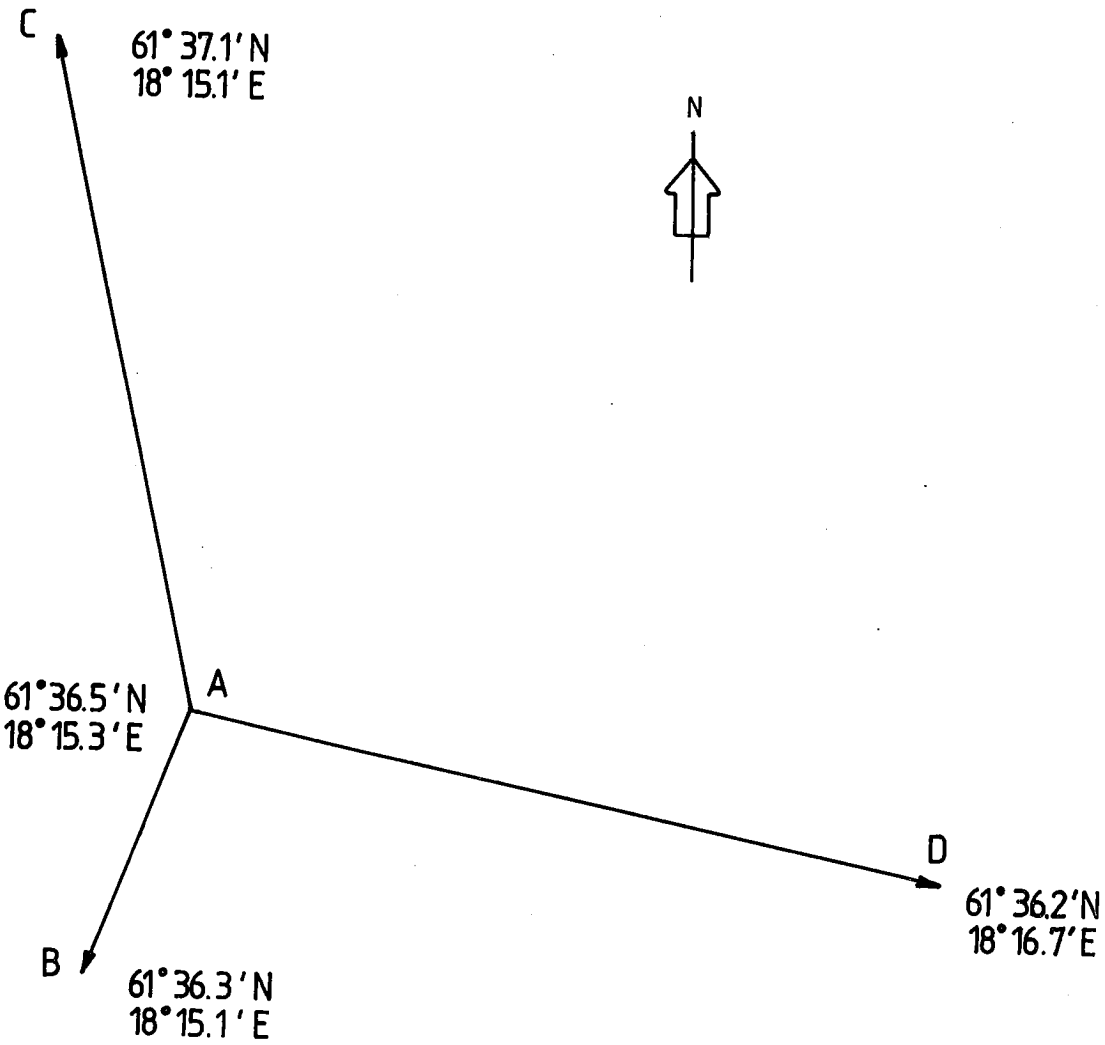

Figure 3. The location of radar reflectors at 1030 local time Arpil 2. The scale is 1:10 000.

within 50 to 100 meters, which is the resolution of the Decca navigation system.

The weather was favourable for ground measurements during the whole experiment. The winds varied between 2 and 7 m/s with directions from south and east. Daily mean temperatures were around zero degree the whole week before the SAR flight took place. Only occasionally did the night temperatures decrease below zero. Standard meteorological data are taken from the coast station Kuggören at Hornslandet shown in Fig. 1 and these are presented in Table 1.

Table 1. Data from the weather station Kuggören at Hornslandet, the wind data represent daily mean values.

Date	Windspeed (m/s)	Direction	Temperature (degr. Celsius) at 0000	Temperature at 1200
23/3	4.0	140	-6.7	-2.1
24	3.0	180	-1.2	-3.1
25	3.0	180	-4.3	-2.9
26	7.0	180	-2.7	-2.4
27	4.0	160	-1.1	1.2
28	6.0	180	0.8	1.4
29	3.0	180	0.9	1.1
30	6.0	320	1.2	5.9
31	6.0	180	-2.0	3.5
01/4	7.0	180	2.1	2.7
02	4.0	050	-2.3	1.1
03	2.0	050	-0.8	1.4
04	3.0	180	-1.7	2.1

The field program carried out at the station was conformed to aspects important for SAR-data interpretation. Note, however, that the parameters involved in the program might be considered necessary by far from sufficient, to determine the reflectivity conditions for SAR. The parameters together with short comments are shown in Table 2.

Table 2. Physical parameters either measured or estimated from observations during the pre-Bepers study at station three offshore Hornslandet.

PARAMETERS	COMMENTS
Standard meteorological observations	data taken from the coast station Kuggören
important features in the area (ridges, openings)	observed visually
photography	vertically taken from helicopter over part of the station area
ridge counting	two perpendicular lines
water temperature	two profiles
ice thickness	three lines
snow thickness and density	observations taken on level ice at Hornslandet
ice cores	three samples
temperature profile	measured
salinity profile	measured
ice density	calculated
gas volume content	calculated
brine volume content	calculated

In the present study some of the data have been further developed. Hence, in section two the ice core measurements are described and used for estimation of gas and brine volume. Ridge density and distribution are commented upon in section three, while surface features are shortly discussed in section four. The last section is devoted to concluding remarks.

2. ICE CORE PARAMETERS

Temperature

In all, three ice cores were drilled at the ice station. The ice core temperature profile was measured at once after the core had been removed from the ice. The measurements were done by first drilling holes into the center of the core with five centimeters interval in the vertical, whereafter the temperature probe was inserted. The measurements were made with a Pentronic 82100 digital thermometer to which a PT100 probe were mounted. The resolution of the digital thermometer is $\pm$ 0.1 degrees

Celsius. It turned out to be insufficiently low for ice temperature measurements at the prevailing weather conditions. Only a rough indication of the temperature gradient was obtained. Furthermore, the registred ice temperatures were found to be positive throughout the whole profile in all three cores. This bias is believed to be caused by the ambient air temperature and the released frictional heat when drilling the holes.

For air and water temperature measurements an instrument with a resolution of $\pm$ 0.01 degrees Celsius was used which well resolved the vertical temperature gradient in the water below the ice. In Fig. 4 the whole temperature profile is shown, beginning in the air (T_a) through the ice (θ) and into the water (T_w). The positive gradient of T_w indicates that the water is warmed from above.

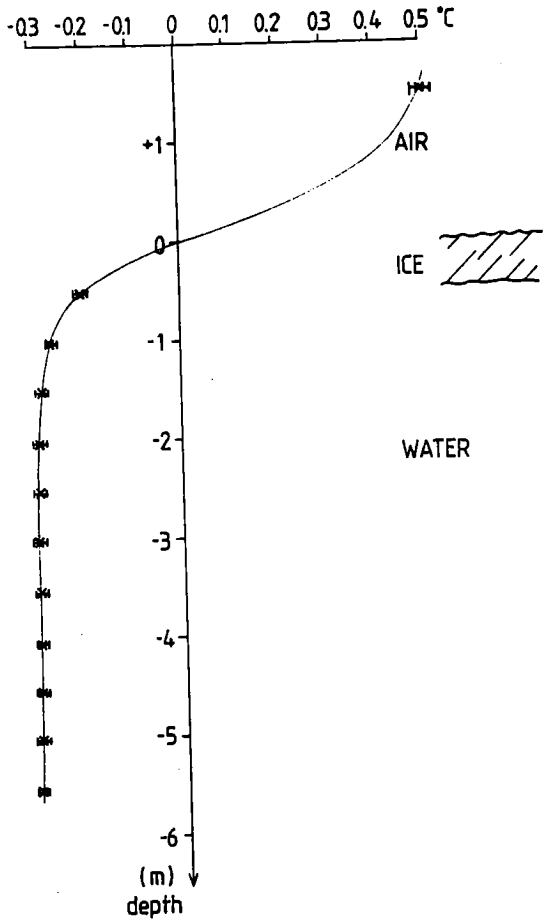

Figure 4. Temperature profile through air, ice and water taken at 0830 local time April 2.

Note, that the ice temperature profile shown in Fig. 4 is not based on the measured temperatures, since these turned out to be unreliable. Instead it has been assumed that the ice temperature profile is linear with a bottom temperature equal to the water temperature, while the surface ice temperature is zero due to the warm weather. Hence, the vertical mean ice temperature can be estimated to be -0.1 degrees Celsius

Salinity

After the temperature measurements the ice core was packed into a box for transportation to the onshore located camp at Hölick, Hornslandet. Within five hours after the sample was taken the volume and weight of the ice core were measured whereafter the core was sawed into five centimeter thick pieces in the vertical for salinity measurements. As previously mentioned, the air temperature was only slightly above ice temperature. Hence, brine may have been removed because of the high air temperature during the storage and transportation.

The ice core salinities are shown in Table 3. Typical features are that the surface part of the cores have lost almost all salinity, while a maximum is found slightly above the bottom. The mean salinity was found to be 0.46 °/₀₀ when data from all three cores were used.

Unfortunately, the very limited number of ice samples taken during the experiment does not permit any definit conclusion to be made whether this low ice salinity is typical or not for the sea ice of the western part of Bothnian Sea. But, taking into account the result of Omstedt (1985) it appears possible to conclude that the observed mean ice salinity is typical for the area. The arguments behind this conclusion is outlined in the following part of this section.

Table 3. Measured salinity at ground station three. The ice cores were taken within a radii of 100 meters from point A. The two profiles from April 1 were taken of level ice while the profile from April 2 was taken in a small snowcovered ridge.

Date 1/4-87 depth (cm)	salinity (°/₀₀)	depth (cm)	salinity (°/₀₀)
0-5	0.15	25-30	0.69
5-10	0.28	30-35	0.66
10-15	0.30	35-40	0.64
15-20	0.40		
20-25	0.64		

Date 1/4-87 depth (cm)	salinity (°/₀₀)	depth (cm)	salinity (°/₀₀)
0-5	0.14	25-30	0.43
5-10	0.55	30-35	0.34
10-15	0.51	35-40	0.37
15-20	0.46	40-45	0.36
20-25	0.59	45-50	0.41

Date 2/4-87 depth (cm)	salinity (°/₀₀)	depth (cm)	salinity (°/₀₀)
0-5	0.09	25-30	0.67
5-10	0.22	30-35	0.64
10-15	0.31	35-40	0.65
15-20	0.33	40-45	0.72
20-25	0.52	45-50	0.54

Omstedt (1985) investigated the ice salinity in the Bay of Bothnia during the growth season. He found that the mean ice salinity varied between 0.37 to 0.75 °/₀₀, which are about 4 to 8 times as low as the underlying water salinity. This relation suggests that mean ice salinity in the Bothnian Sea might be 0.8 to 1.6 °/₀₀ during the growth season. However, in the present study the mean ice salinity was found to vary between 0.42 to 0.47 °/₀₀ which indeed is lower than the above mentioned expected value. This suggests that warm ice conditions prevails in the western part of the Bothnian Sea, and that the brine is moving out of the ice. Also the past warm weather, the salinity profile and the ice temperature indicate warm ice conditions.

Density

The density of the ice cores are shown in Table 4. They were calculated from measurements of the ice core volume and weight. The core with largest density was taken in a small ridge which was covered with snow of approximately 10 cm depth, while the other two cores were taken on level snowfree ice.

Table 4. The mean density, salinity and temperature of the ice cores.

	ρ (kg m^{-3})	S (‰)	θ (°C)
core 1	800 ± 30	0.47	-0.1
core 2	810 ± 30	0.42	-0.1
core 3	880 ± 30	0.47	-0.1

Sea ice porosities

The porosity is determined from the content of gas and brine in the ice. These parameters are difficult to measure, but can be theoretically estimated from ice density, salinity and temperature. A recent study devoted to this subject is that of Cox and Weeks (1983). Their equations, however, are valid in the temperature range from -2 to -30 degrees Celsius, while in the present investigation ice temperatures were closed to zero degrees, which invalidates the usefulness of their results. Instead the results of Schwerdtfeger (1963) are used, since he considers sea ice between the melting point and -8.2 degrees Celsius. In this temperature range essentially all salts trapped within the ice are in solution. This condition simplifies the theoretical framework, but does not change the results substantially from Cox and Weeks study for warm ice, as noted by these authors. Schwerdtfegers work is here shortly reviewed.

By definition the bulk ice salinity (S_i) and brine salinity (s) are:

$$S_i = m_s/M \quad (1)$$

$$s = m_s/m_w \quad (2)$$

Here are m_s, M and m_w the mass of salt, bulk ice and pure water in brine respectively. Hence, the mass of brine becomes:

$$m_b = m_s + m_w,$$

or

$$m_b = S_i \, M \, (1+ 1/s), \tag{3}$$

while the mass of pure ice is given by:

$$m_i = M(1-S_i \, (1 + 1/s) \tag{4}$$

Note, that in this equation the mass of gas is assumed to be negligible. The corresponding volumes of brine and pure ice in units of ice mass are:

$$V_b = \varrho \, S_i(1+s)/\varrho_b \cdot s \tag{5}$$

$$V_i = \varrho \, (1-S_i(1 + 1/s))/\varrho_i \tag{6}$$

By reconsidering equation (3) it may be shown that the brine density becomes:

$$\varrho_b = \varrho_w(1+s) \tag{7}$$

Using this expression in equation (5), yields:

$$V_b = \varrho \, S_i/\varrho_w \cdot s \tag{8}$$

Here are ϱ, ϱ_i and ϱ_w the densities of sea ice, fresh ice and water respectively. The relative content of gas volume may now be obtained by summing up the different parts giving the total volume of ice, hence:

$$V_a = 1 - \frac{\varrho}{\varrho_w} \left[\frac{\varrho_w}{\varrho_i} (1-S_i) + (1-\varrho_w/\varrho_i) \frac{S_i}{s} \right] \tag{9}$$

Still, however, the brine salinity (s) has to be related to a measurable bulk parameter. A linear relationship between s and

ice temperature was stated by Assur (1960), based upon phase equilibrium. Hence, as long as the salts remain in solution the brine salt content becomes $s = \alpha\theta$ where θ is the temperature and $\alpha^{-1} = -55$ °C. Using this relationship and standard values of $\varrho_w = 0.999$ g cm and $\varrho_i = 0.917$ g cm, the present results may be summarized to:

$$V_b = -55.1\ \varrho\ S_i/\theta \tag{10}$$

$$V_a = 1 - \varrho/\varrho_w \left[\frac{\varrho_w}{\varrho_i} (1-S_i) + 4.9\ S_i/\theta \right] \tag{11}$$

The ice porosity constitute the sum of these relative volumes.

At the prevailing temperatures the relative brine volume content is indeed sensitive to θ. Nevertheless, in Fig. 5 the vertical profile of brine and gas volume is shown. The volumes are calculated by using the assumed linear temperature profile which was previously found to be T_w (z/h). Here is z the vertical coordinated and h the total ice core depth. Furthermore the mean ice density is used.

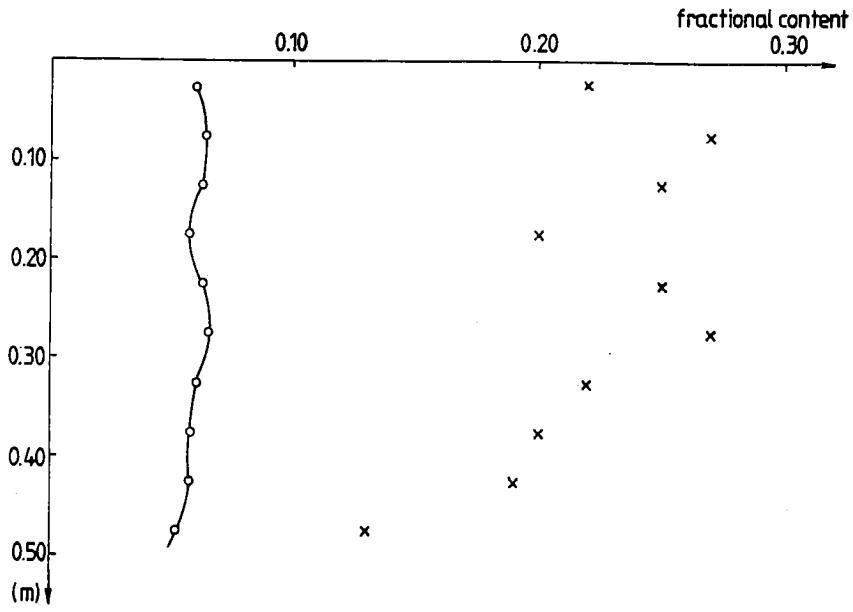

Figure 5. Brine (x) and gas (o) volume profiles estimated from the ice core taken during April 2.

The result indicates that the porosity is indeed large especially due to the large content of brine volume. However, this state of affairs is not inconsistent with estimates from other areas (i.e. Golden and Ackley (1981) found brine volumes of the same order as in the present study close to the bottom of the ice where the ice and water temperature reaches the freezing point).

3. RIDGE STATISTICS AND ICE THICKNESS

The large scale roughness in the area consists of the ice ridges. These were visually counted from helicopter along two perpendicular lines, oriented in an east-west and north-south direction with a length of 17 and 23 km, respectively. Both lines passed over the area of intensive studies. The mean ridge density (μ) was found to be 6 km^{-1} in the east-west and 4 km^{-1} in the north-south line.

By counting the ridges at every 1 km along the lines, it is possible to estimate the distribution of ridge spacing. It was suggested by Hibler et al. (1972) that ridge spacing has a simple statistical distribution, yielding:

$$Pdx = \mu e^{-\mu x} dx \qquad (12)$$

Here is Pdx the probability of two ridges being separated by x and x+dx. The ridge spacing might therefore be used as a suitable test for estimation of spatial ridge distribution. Equation 12, in particular, is derived from the assumption that the number of ridges per given length has a Poisson distribution.

In order to test the validity of equation 12 the present data has been used in such a way that the number of ridges (N_j) as function of the distance between the ridges (x) is obtained. The

probability Pdx may then be estimated with N_j/N, where N is the total number of counted ridges in the line. These estimates are plotted against the nondimensional distance μx in Fig. 6. The method of least squares is used to find the best fit to a linear relationship (the broken line in Fig. 6), as suggested from the logarithm of equation 12. The analysis yields

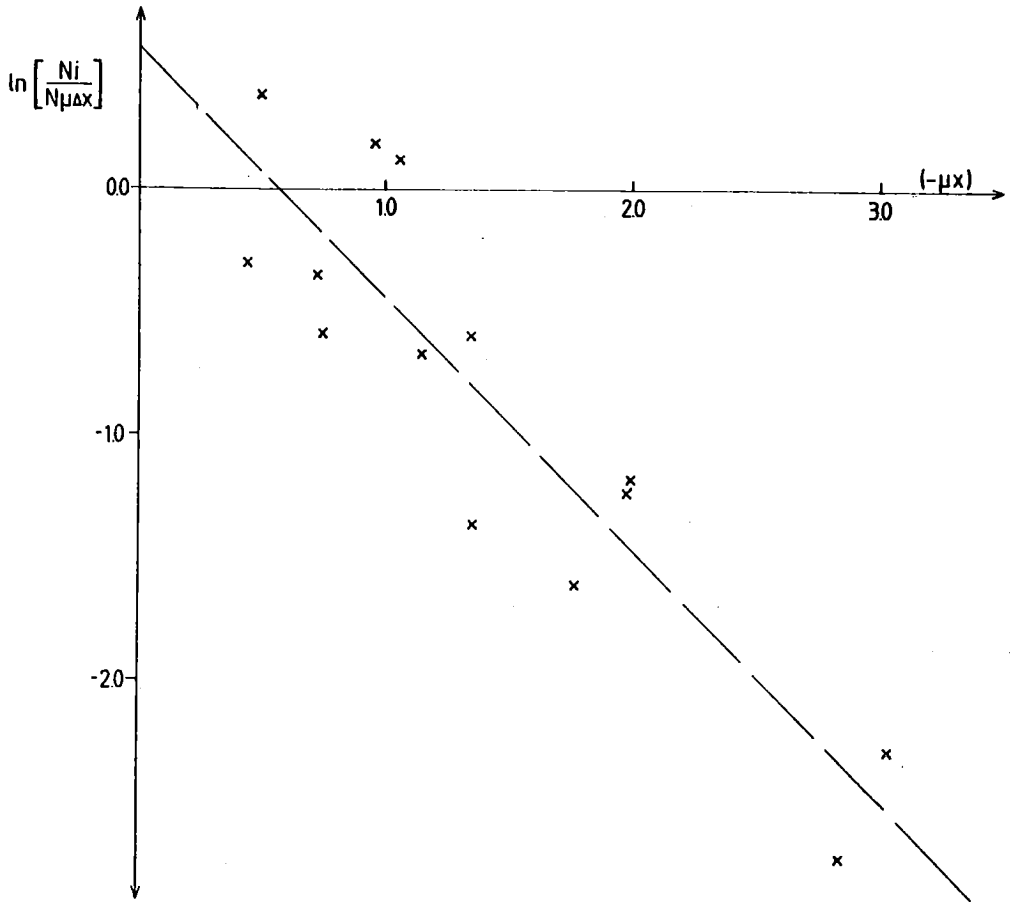

Figure 6. The dependence of nondimensional probability of ridge spacing on nondimensional spacing. The broken line is obtained from linear regression.

a correlation coefficient of 0.90 and a slope close to what is predicted by the exponential distribution. This ridge distribution is also in agreement with results indeed obtained by Leppäranta (1981).

Ice thickness along three lines were observed. The thickness was measured by a ruler in drilled holes twenty meters apart in a radii of 300 m from point A, and with an interval of 40 m beyond this radii. The mean thickness and variance were found to be 42 and ± 10 cm, 51 and ± 18 and 46 and ± 4 in line A to B, line A to C and line A to D, respectively.

4. SURFACE FEATURES

Air protography partly covering the study area was taken from helicopter of which Fig. 7 is an example. The position of the radar reflectors A, B and C are shown. They are located in the photography by visual means using information from mapped areas around points A and B. The positions are located within an estimated accuracy of ± 100 m.

Fig. 7 indicates that level ice is almost snowfree while ridges are generally snowcovered with a measured thickness of 5 to 15 cm. It is also recognized from the photography that level ice appears with a texture indicating refrozen icefloes. However, the main feature is the ice ridge at which point B is located. The ridge runs in an east-west direction perpendicular to the line between A and B. The highest point of the ridge was measured to be 2 m, while the mean height appeared to be around 1 m. Open water occurs frequently at the southern part of the ridge.

The small scale surface features with a lenghtscale of a few centimeter on level ice was visually observed. It consisted of crust ice and beneath it a thin layer of air and sometimes water covered the underlying sea ice. Air bubbles were frequently observed where the crust was absent. The bubble size was estimated to vary between 0.001 to 0.01 m in diameter.

Figure 7. Aerial photography covering the reflector points A, B, C and D at the study area three.

5. REMARKS

During the field program rodamin B was used for colouring of snow and ice at places which were to be used as identification points for aerial photography. The method was not successful since the colour soon after release became to diluted and faded away. For the BEPERS experiment it is of vital importance to found out suitable ways to mark identification points for all remote sensing techniques.

Note, also that the ground measurements in the area of intensive studies should be done to such an extent, that a statistical analysis is possible. This is one way in which the sea ice observations can be of value for the remotely sensed data.

REFERENCES

Assur, A. 1960: Composition of sea ice and its tensile strenght. U.S. Snow, Ice and Permafrost Research Establishment.

Cox, N. and W. Weeks, 1983: Equations for determining the gas and brine volumes in sea ice samples. J. Glaciology, vol. 29, No. 102.

Hibler, W.D. III, Weeks, W.F. and Mock, S.J. 1972: Statistical aspects of sea ice ridge distributions. - J. Geophysical Res., Vol. 77.

Holden, K.M. and Ackley, S.F. 1981: Modeling of anisotropic electromagnetic reflections from sea ice. - J. Geophysical Res., Vol. 86, No. C9.

Leppäranta, M. 1981: Statistical features of sea ice ridging in the Gulf of Bothnia. - Res. Rep. No. 32, Winter Navigation Research Board, Helsinki, Finland.

Omstedt, A. 1985: An investigation of the crystal structure of sea ice in the Bothnian Bay. - SMHI Reports, RHO 40.

Schwerdtfeger, P. 1963: The thermal properties of sea ice. J. Glaciology, Vol. 4, No 36.

In: BEPERS Pilot Study. Data Report. Styrelsen för Vintersjöfartsforskning/Winter Navigation Research Board, Rep. No 45, p. 103-106. Helsinki 1988.

VII GROUND DATA FOR AREA IV

By Matti Leppäranta

Finnish Institute of Marine Research
P.O. Box 33, SF-00931 Helsinki, Finland

ABSTRACT

Area IV in BEPERS Pilot Study located at the ice edge in the Northern Baltic Sea Proper. No ground truth base was set up here. Basic features of the ice could be obtained from the routine data of the Finnish Ice Information Service. There was compact pack ice of thickness 10-40 cm and some rigdes. The surface was in the stage of melting and bare or covered with a thin snow layer.

1. INTRODUCTION

Study area IV was located in the Northern Baltic Proper in the vicinity of the Finnish light-house of Bogskär (Fig. 1). There

was no base for this area, and consequently all the ground data are based on routine observation systems.

The reason for including this area in the experiment was to map the ice edge region with SAR. As it is known, the ice floe characteristics show large changes in the ice edge region. In particular due to the wave action from the open sea ice floes break into smaller pieces, and as a result the floe size increases with distance from the ice edge. These changes in the horizontal floe size characteristics are clearly seen in the aerial photographs which are the principal data for SAR verification in this study area.

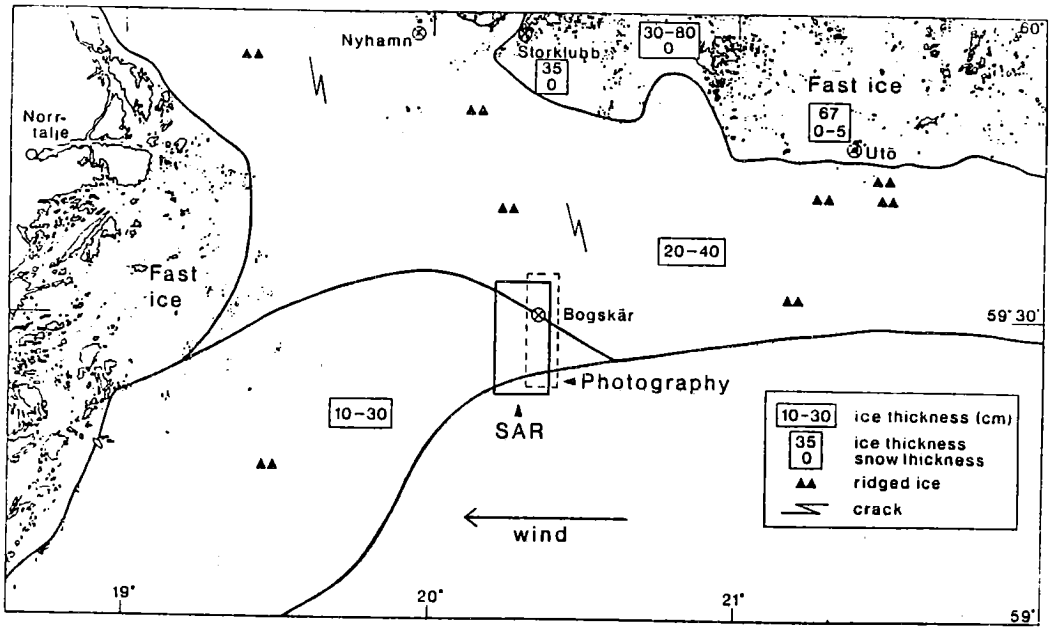

Figure 1. Ice chart of the Northern Baltic Proper, 2 April 1987. The locations of the SAR strip and observation stations are also shown.

2. ICE AND WEATHER CONDITIONS

Weather

The weather was rather good on 2 April although not so good as in the other study areas. The sky was cloudy or almost cloudy but the clouds were also here high. In the nearby weather stations of Nyhamn and Utö the air temperature was positive all the daytime (Table 1).

The wind was easterly with the speed of 6 to 10 m/s. In the SAR imaging area south of Bogskär the wind was about 30 degrees on-ice. East of ice edge in this region there was a fetch of 100-200 km for the wind to blow over open water. Consequently, the significant wave height was likely 1-2 meters (Kahma, 1986). The wave field has been partially reflected from the ice edge and partially absorbed in to the ice pack. The incoming waves have likely caused radiation pressure to the ice edge which has helped the wind to keep the ice edge compact.

Ice

In the Northern Baltic Proper there was fast ice in the Archipelago Sea and Stockholm Archipelago (Fig. 1). In the Archipelago Sea the thickness of ice was 30-80 cm. In the observation station of Storklubb there was 2 cm of snow-ice and no snow on top of the ice whereas in Utö the thicknesses of snow-ice and snow were 25 and 0-5 cm, respectively. It was reported that the surface features indicated that the melting period had begun.

In the open sea there was very close or compact ice with ridges. The thickness of level ice was 10-40 cm.

Table 1. Meteorological observations in the neighborhood of area IV on 2 April 1987 (Finnish Meteorological Institute, 1987).

Time EET = UTC + 3 hrs	Air temp. °C	Relat. humid. %	Wind dir. deg.	Wind speed m/s	Cloudiness*)	Visib. km
	MARIEHAMN AIRPORT				60°07'N 19°54'E	
9	1.1	94	90	3	CC	8
12	2.8	82	100	6	AC	8
15	3.6	78	120	6	CC	8
18	3.9	65	120	6	CC	15
	NYHAMN				59°58'N 19°57'E	
9	0.3	95	80	5	CC	5
12	0.6	91	100	8	CC	5
15	1.0	88	100	8	CC	5
18	1.2	91	90	7	CC	5
	UTÖ				59°47'E 21°23'E	
9	0.4	96	80	7	CC	7
12	1.1	91	90	7	AC	6
15	1.5	86	90	10	AC	7
18	0.7	91	90	8	C	6

*) CC = cloudy, AC = almost cloudy, HC = half cloudy

3. REFERENCES

Finnish Meteorological Institute, 1987: Meteorological observations in Åland area on 2 April 1987. - Archives.

Kahma, K.K., 1986: On prediction of the fetch-limited wave spectrum in a steady wind. - Finnish Mar. Res. 253:52-78.

In: BEPERS Pilot study. Data Report. Styrelsen för Vintersjöfartsforskning/Winter Navigation Research Board, Rep. No 45, p. 107-117. Helsinki 1988.

VIII AERIAL PHOTOGRAPHY IN BEPERS PILOT STUDY

By Hanna Kemppainen[1] and Yrjö Rauste[2]

1) Finnish Institute of Marine Research
P.O. Box 33, SF-00931 Helsinki, Finland

2) Technical Research Centre of Finland VTT,
Vuorimiehentie 5, 02150 Espoo, Finland

ABSTRACT

The purpose of aerial photography in BEPERS Pilot Study is to provide information about the distribution of ice types and snow cover that is needed in interpreting SAR imagery. Small-scale photography covers study areas I, Bay of Bothnia (to the south-west of Hailuoto), II, Nothern Sea of Bothnia (to the west of Raippaluoto) and IV, Nothern Baltic Proper (to the south of Åland) in scales of 1:31 000, 1:18 000 and 1:10 000, respectively. The variation in scale is due to different cloud heights. Large scale photography covers an area of approximately 1000 m by 380 m. The small scale photography was acquired using 20 per cent forward overlap and the large scale photography using 60 per cent to obtain stereo coverage. Image quality in general is good. Some holes in common coverage with SAR images exist especially in area IV.

1. INTRODUCTION

In an airborne SAR remote sensing campaign information about the imaged area is always needed. In sea ice applications this information contains distribution of different ice types, snow cover and physical and electric properties of ice. The three most often used methods for acquiring this information are:

- field observations
- aerial photography, and
- satellite images.

Field observations are always only point observations and consequently they cannot cover the whole study area, which in BEPERS Pilot Study was about 2000 square kilometers. The chances to get high-quality images from Landsat or Spot satellites are rather small due to clouds and a rather long repetition cycle of these satellites (e.g. 16 days for Landsat). Futhermore, the resolution of these satellites is poorer than that of the Varan-S SAR. Aerial photography is less vulnerable to clouds than satellite images because images can be acquired on cloudy days also, by flying under the clouds. Besides the flexibility in selecting the image acquisition time makes aerial photography the most reliable way of acquiring information for large areas.

2. SMALL SCALE PHOTOGRAPHY

The purpose of small scale photography in BEPERS Pilot Study is to show the distribution of different ice types, floe size and snow cover and the locations of ridges and other ice features within the whole study area.

National Board of Survey was contracted to carry out the aerial photography campaign. The camera used was of the type Wild RC10/UAgII with a focal legnth of 150 mm and the film was Double-X.

There was only a limited amount of money available for aerial photography. Therefore a rather small image scale of 1:30 000 was selected to achieve as complete coverage of the study area with as few photo strips as possible. During the SAR image acquisition a moderate wind prevailed. Therefore aerial photographs had to be acquired almost simultaneously with SAR image acquisition to avoid problems with moving ice. So the cloud situation during the SAR image acquisition determined the maximum usable flying height for the aerial photography. Image scale of 1:30 000 requires the flying height of 4.5 km (using 23 cm image format and 150 mm focal length). Area II in the Quark was imaged in scale of 1:18 000 (corresponding to flying height of 2.7 km) and area IV south of Bogskär lighthouse in scale of 1:10 000 (corresponding to flying height of 1.5 km).

The width of image strip in scale 1:30 000 is approximately the same as the swath width of Varan-S SAR (10 km). The bigger image scale in areas II and IV required use of more than one strip to cover the whole SAR swath. Financial reasons limited aerial photography to two image strips per study area. So coverage of the SAR swath is complete in area I only. The navigation of the aircraft was performed with the help of lighthouses and other landmarks and the compass of the aircraft. In area IV there were problems with the compass of the aircraft. This caused navigation error which further restricted coverage of SAR swath. Fig. 1 shows the overlap between SAR images and aerial photographs. In general the coverage can be regarded reasonably good.

Because no stereo models are needed forward overlap of 20 per cent was used. In areas II and IV side overlap of 20 per cent was used to avoid holes in coverage due to navigation errors.

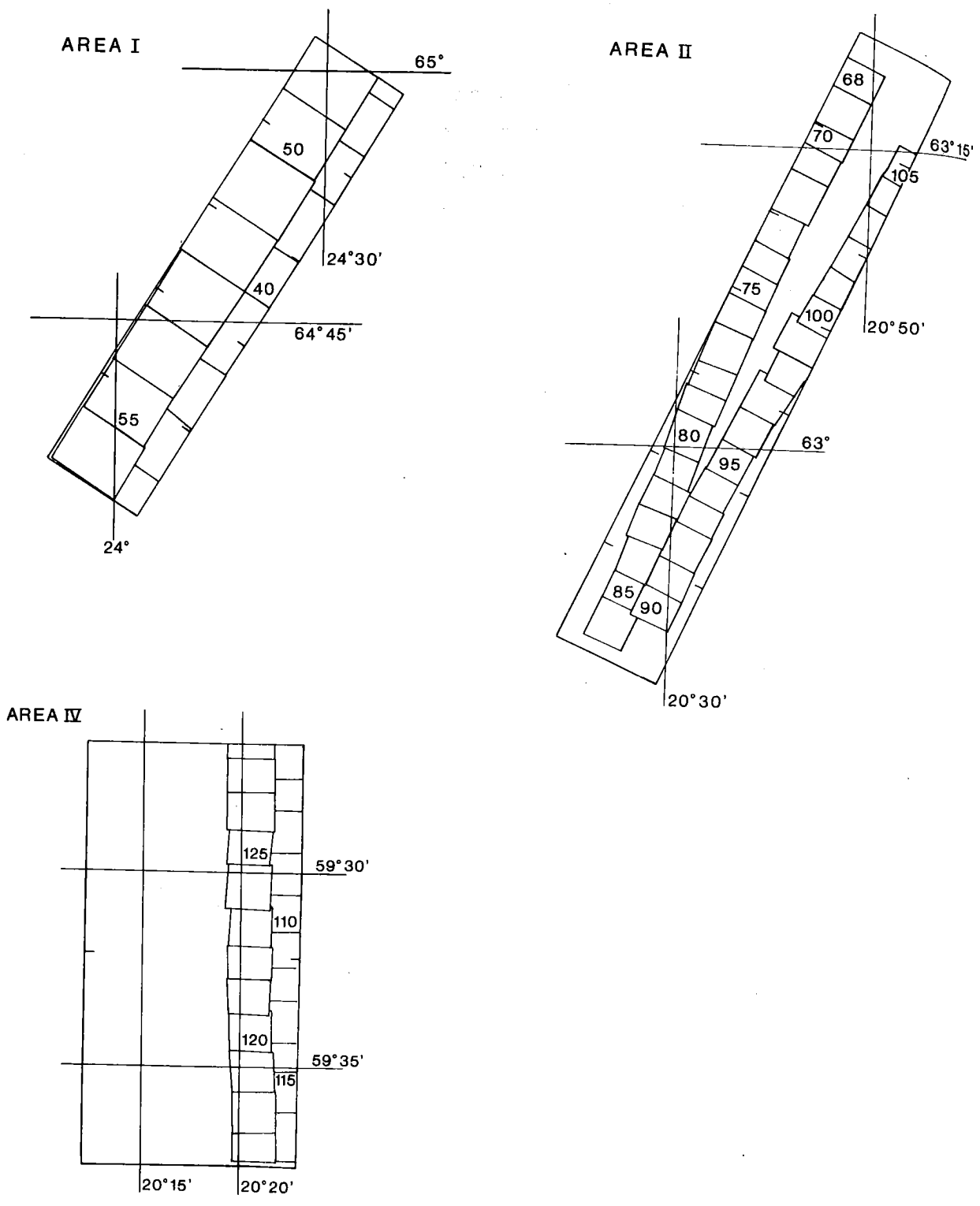

Figure 1. Overlapping coverage between small scale photography and SAR image of areas I, II and IV.

3. LARGE SCALE PHOTOGRAPHY

The purpose of large scale photography in BEPERS Pilot Study is to enable determination of decimeter scale roughness of ice by stereoscopic measurement of elevation profiles and heights of ice features. The area photographed in large scale covers approximately 1000 meters by 380 meters and contains six stereo models (seven photographs). Image scale is approximately 1:1 660 corresponding to flying height of 250 meters. For stereo measurements overlap of 60 per cent was used.

3.1 Control points for large scale photography

The set-up of stereo models requires certain number of control points. The co-ordinates of these points must be known with high accuracy and they must be reliably and accurately identifiable in the photographs. Four planimetric control points (one at each corner of the strip) and 14 vertical control points were used (Fig. 2). The planimetric control points were at the corners of the photogrammetric strips and the vertical control points at the corners of every other stereo model. 50 m margins were used to allow small navigation errors. The control points were located using a tape measure and compass.

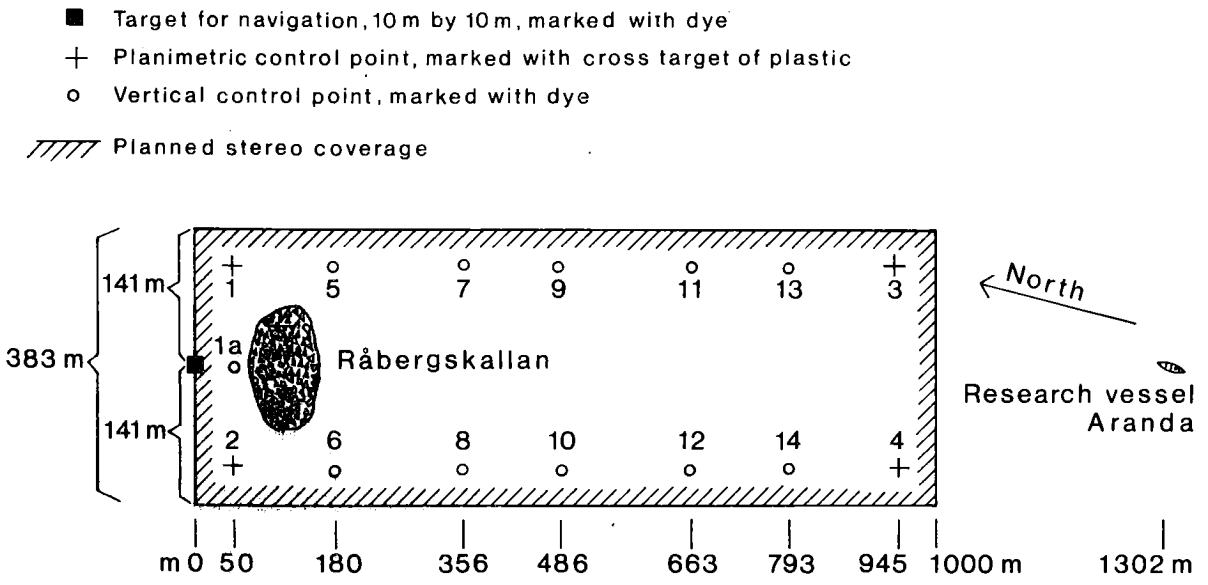

Figure 2. Locations of control points for the large scale photogrammetric strip (as planned).

Vertical control points were marked with dark red dye. A cross with stroke length of 40 cm was dyed by pouring dye from a pot. The marking was done the day before the image acquisition. The dye turned out to spread very irregularly depending on the properties of the underlying ice. For example one target on ice surface spread to a nearly circular spot with a diameter of two meters in 24 hours. On the other hand some crosses on snow retained their shape but became light orange and lost much of their contrast compared to their surrounding snow surface because the dye went through the snow. In one instance the target was on a slightly sloping ice facet. The following day most of the dye had flowed to a horizontal ice surface about two meters apart from the original location.

It was planned that the planimetric control points would be marked with dye also. Irregular spreading of the dye prevented measurement of these points with the required a couple of centimeters accuracy. Therefore the targets for planimetric control points were made of orange plastic. The plastic stuff is the same material as that in flags used by the Institute of Marine Research for marking measuring instruments on ice for easy finding by helicopter. In that application light orange is a good colour. Unfortunately its contrast with white snow or light grey ice on panchromatic photographs is very weak. Therefore the planimetric control points marked with this plastic material are very hard to identify on the photographs.

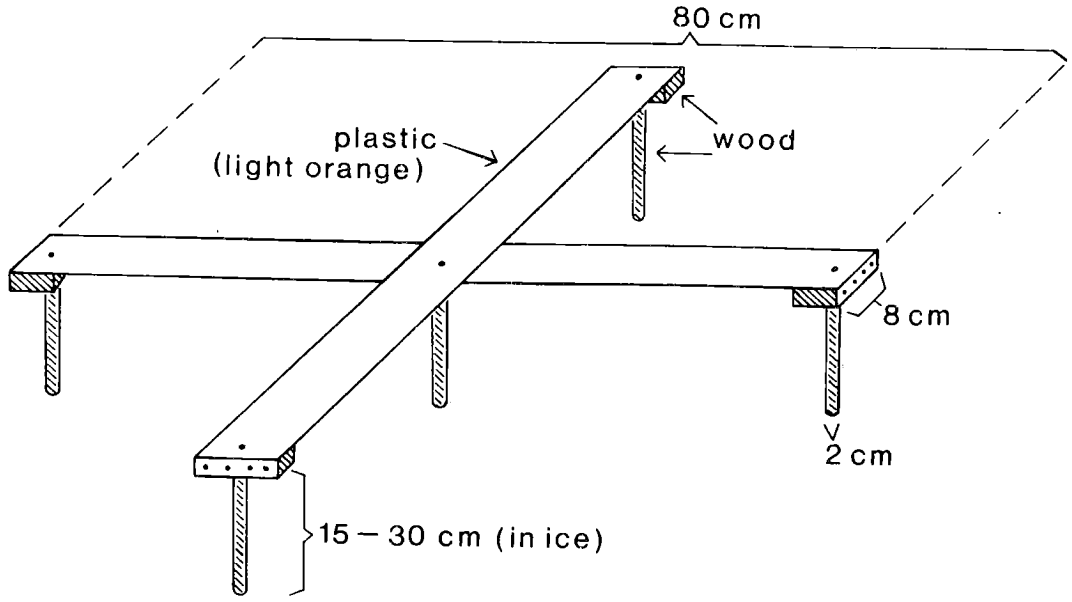

Figure 3. A target for planimetric control points.

Dimension of targets were determined according to instructions for ordinary mapping photogrammetry. For scale 1:1 660 a target was made by crossing two strips of plastic, 8 cm wide and 80 cm long. The strips were nailed to small pieces of wood to keep the plastic material flat. A hole with two-cm diameter and 15 cm deep was made into ice for each end of the strips and one such hole for the crossing point. Small pieces of wood were then wedged to these holes and the ends of the plastic strips were nailed to these pieces of wood. This type of fastening turned out appropriate even during strong wind.

3.2 Determination of co-ordinates for control points

The planimetric co-ordinates of the four control points were measured for set-up of the stereo strip. Consequently there are no requirements for high absolute accuracy and even a separate co-ordinate system could be used. Fortunately the large scale strip was situated so that seven lighthouses were visible. So it was possible to determine the locations of the control points with respect to the national co-ordinate system and not only with respect to each other.

The measurements were carried out in two phases. First the location of a base point near R/V Aranda was determined. Then the locations of ground control points were determined by measuring angles and distances from the base point.

The location of the base point was determined by measuring angles only. The large-scale photogrammetric strip was situated favourably so that eight lighthouses or other known geodetic control points could be seen under good weather conditions. The directions to these control points formed good intersection angles at the base point (Fig. 4).

The observations were made on March 31st. This was the only day when all eight lighthouses could be seen during the ground truth

mission of five days. The observations were made using a theodolite of the type Wild T2. The horizontal angle to each lighthouse was observed three times. The standard deviation of a single observation in preliminary adjustment was 6.3 new seconds (0.0000099 radians). In the adjustment two control points (marked with dashed lines in Fig. 4) were rejected, one due to obvious misidentification of the point and the other due to difficulties to direct the theodolite at the center point of the lighthouse (or errors in co-ordinates used for this particular point). The final adjustment gave the following rectangular basic co-ordinate system co-ordinates for the base point: X = 7 021 677.496 m, Y = 1 490 385.348 with co-ordinate standard deviations 0.09 and 0.06 (9 and 6 cm) in X and Y respectively. The adjustment was carried out by Mr. Seppo Väätäinen in Technical Research Centre of Finland using a pocket calculator of the type HP 41 CV and a program published by Meier (1982).

The planimetric control points for the large scale photogrammetric strip were measured using an electronic distance measuring instrument of the type Wild Distomat Di 3S. The observations were made on the same day as the image acquisition: April, 2nd. Weather reductions were made assuming the temperature to be zero degrees Celcius and the air pressure 760 mm Hg using the equation published in the instruction manual of the distance measuring instrument:
DD = 28.2 - 0.0387 * p/(1 + 0.0037 * t, where t = temperature in Celsius degrees, p = air pressure in mm Hg and DD = the correction to be added to the observed distance in mm per 100 m. The co-ordinates of the control points are shown in Table 1.

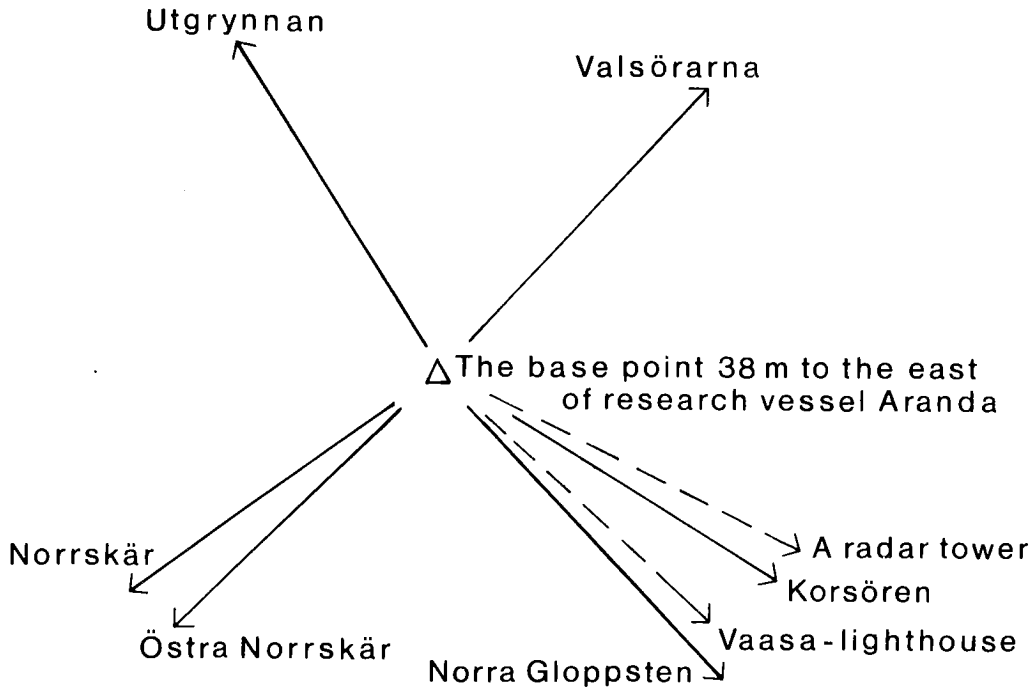

Figure 4. Directions to the geodetic control points used in determining the location of the base point.

Table 1. Ground control points for the large scale photogrammetric strip.

No	Direction from base (grades)	Observed distance (m)	X (m)	Y (m)
1	372.0518	1303.954	7022857.786	1489831.118
2	358.2412	1340.613	7022739.881	1489567.706
3	385.3643	371.095	7022038.824	1490300.785
4	342.3792	453.639	7021957.662	1490028.569

Elevations for control points were determined by drilling a hole through the ice and then measuring the elevation with tape-measure. The elevations are listed in Table 2.

Table 2. Elevations of vertical control points.

No	Elevation (cm)
3	2.5
4	3.5
14	2.0
13	6.0
11	2.5
12	2.0
10	0.5
9	2.5
7	5.0
8	1.5
6	1.5
5	4.0
1	2.0
1a	1.5
2	4.0

Marking ground control points and measuring their co-ordinates was rather time consuming. Locating and marking the 14 points and measuring the elevations took one and a half day with a group of two persons on foot, even though the large scale photogrammetric strip was situated only 300 meters from R/V Aranda which was used as a base during the ground truth mission. Exact measurements with teodolite and distance measuring instrument took more than one day.

4. RECOMMENDATIONS FOR FUTURE ICE REMOTE SENSING CAMPAIGNS

Very small scale aerial photographs cannot usually be acquired on the SAR image acquisition day due to very probable cloud cover. Therefore provisions must be made in the aerial photography planning for larger scale photography in case the clouds are low.

A suitable way for marking planimetric control points for stereo photogrammetric strips is the use of black cross-formed targets made of plywood or other similar rigid materials and painted

black for a good contrast against the surrounding ice or snow surface. Targets can be fastened to ice using wooden sticks wedged to drilled holes in ice. Dye cannot be used if accuracies of the order of one centimeter are required. When dye is used to mark control points the (last) painting must be done on the same day as the image acquisition.

5. REFERENCES

Meier, U. 1982: Ein Taschenrechnerprogram zur Punkteinschaltung und freien Stationierung. Allgemeine Vermessungsnachrichten, vol 89, Heft 4, April 1982, pp. 158-165.

In: BEPERS Pilot Study. Data Report. Styrelsen för Vintersjöfartsforskning/Winter Navigation Research Board, Rep. No 45, p. 119-147. Helsinki 1988.

IX AIRBORNE RADAR OBSERVATIONS

By Roland Johansson, Lars Ulander and Jan Askne

Department of Radio and Space Science
Chalmers University of Technology
S-412 96 Göteborg, Sweden

ABSTRACT

A preliminary analysis has been given of the SLAR and SAR observations from the BEPERS Pilot Study experiment. The theory for electromagnetic scattering from ice and ice ridges has been recaptulated. The results obtained from scattering from radar reflectors, the ocean surface and the ice surface have been compared.

1. INTRODUCTION

This is a preliminary evaluation of the SLAR (Side-Looking Airborne Radar) observations as compared with simultaneous SAR (Synthetic Aperture Radar) observations. Ground truth observations and aerial photography were not available for the analysis in this report. The digital image analysis of the SLAR and SAR registrations is also postponed to the future.

2. RADAR CROSS SECTION THEORY

Since the SLAR and SAR sensors used in BEPERS Pilot Study have different incidence angles we need to know the backscatter from sea ice as a function of incidence angle to be able to explain some of the differences in the SLAR and SAR images. However, the incidence angle behaviour of the backscatter in the Baltic Sea has not yet been measured and because the ice is different as compared with the Arctic Ocean there are no observational results available. Therefore we need models to predict the backscatter coefficient.

Due to the varying ice conditions, for example: smooth and rough ice, dry or wet snow cover, ridges, floes, leads, etc, it is a very hard task to make a complete model. Instead, we have applied existing models to the level ice and snow cover. Furthermore, a model for ice ridges has been used (Johansson and Askne, 1987) and applied to the ridges in the Baltic Sea. We give here a short overview of the models used and some Figs. illustrating the principal features of the backscatter coefficient as a function of incidence angle.

2.1 Level ice

The backscatter from the bare level ice consists at least of two parts, the air-ice surface scattering and the ice volume scattering. Additionally, if the radar wave penetrates through the ice then even the ice-water surface might contribute.

The air-ice surface scattering is calculated according to the well-known Kirchhoff theory (Ulaby et al. 1982). The method is generally applicable if:

$$k\ell > 6$$

$$\ell^2 > 2.76 \cdot \sigma \cdot \lambda \text{ and}$$

rms surface slope < 0.25

where $k=2\pi/\lambda$ and λ is the radar wavelength, σ the surface height standard deviation and ℓ the correlation length. Since no measurements were done of σ and ℓ it is difficult to tell whether the constraints are fulfilled or not. But measurements done in other areas by for example Rott (1984) suggest that they might be. The expression for $\sigma^\circ_{surface}$ according to the Kirchhoff theory is given in Appendix A. Significant parameters are surface roughness σ, correlation length ℓ and dielectric constant ϵ.

The volume scattering is based upon Rayleigh scattering from air bubbles and brine inclusions in the ice (Ulaby et al. 1981). Rayleigh scattering, which is a simplification of the Mie solution, requires that the radius of the inhomogenities are smaller than the incident wavelength (3.2 cm in this case). Some observations were done (see paper IV in this report) and the radius of the air bubbles varied between 0.3 and 3 mm while the brine inclusions had a horizontal radius less than 0.5 mm and a height of 2-4 mm. The expression for σ°_{volume} is given in Appendix B. Significant parameters are salinity, temperature and radius of the inclusions.

The ice water surface scattering σ°_{water} is calculated in the same manner as the air-ice surface scattering. The difference is that the radar wave is attenuated on its way through the ice, which means that the salinity has to be low if the water surface will contribute.

The total backscatter coefficient including all three contributions can be written as:

$$\sigma^\circ_{level\ ice} = \sigma^\circ_{surface} + T^2_{ice}\left(\sigma^\circ_{volume} + \frac{\sigma^\circ_{water}}{L^2_{ice}}\right) \qquad (1)$$

where T_{ice} is the power transmission coefficient from air to ice and L_{ice} is the attenuation in the ice.

Fig. 1 illustrates a typical incidence angle dependence of σ° to be expected in the Baltic Sea. The exponential correlation function is widely used while the gaussian correlation function in some cases have been shown valid. In practice the truth might be somewhere inbetween these two cases.

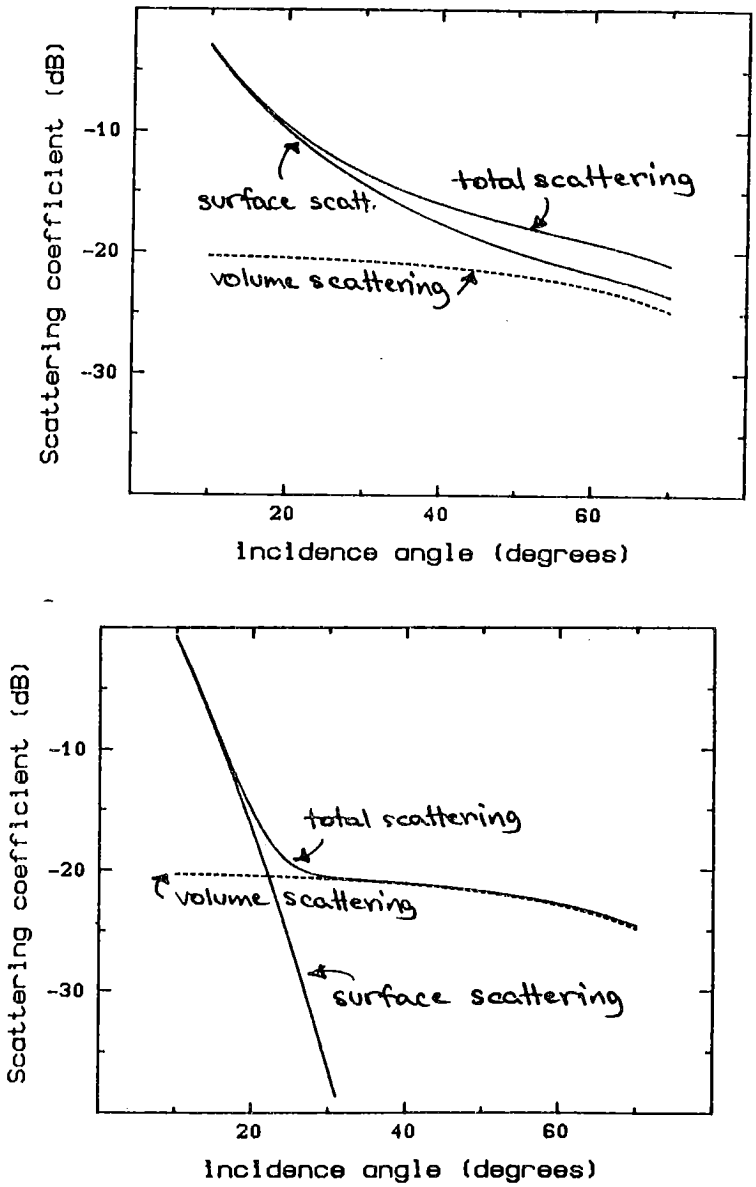

Figure 1. The total backscattering coefficient together with the surface and volume scattering contributions shown as a function of incidence angle. 1a is calculated with an exponential correlation function, 1b with a gaussian. The parameters are:
frequency 9.4 GHz, horizontal polarization, surface roughness 2 mm, corr. length 8.5 cm (exponential) and 7.1 cm (gaussian) resp., temperature -1°, salinity 1.0 °/$_{oo}$, density 0.9 g/cm^3, thickness 0.5 m, air bubble radius 1 mm and brine radius 0.2 mm.

2.2 Ice ridges

Ice ridges always gives a strong contribution to the scattering but little has been done to develop comprehensive models for ridge scattering. Recently, however, a model for the backscattering from ice ridges was suggested in the article by Johansson and Askne (1987). The model includes two different scattering components, one being a specular component due to ice blocks with zero incidence angle and the other being an integrated mean value obtained from distributed ice blocks around a triangular profile. The model does not include the effects of snow, multiple scattering or shadowing. The expression for σ°_{ridge} is given in Appendix C.

If an ice ridge of area A_{ridge} is viewed against a background of area A_{bg} with a backscatter coefficient σ°_{bg} then the total backscatter coefficient will be:

$$\sigma^\circ_{tot} = \sigma^\circ_{bg} \left(\frac{A_{bg} - A_{ridge}}{A_{bd}}\right) + \sigma^\circ_{ridge} \frac{A_{ridge}}{A_{bg}} \qquad (2)$$

An illustration of σ°_{tot} as a function of incidence angle is given in Figs. 2a and 2b for exponential and gaussian correlation function resp.

2.3 Snow

To study the effect of a snow cover it is instructive to look at Fig. 3 showing the penetration depth into snow as a function of snow wetness. If the snow is dry it is almost transparent to the radar wave implying that the snow surface scattering can be neglected. Thus the only important contribution comes from volume scattering. The same expression as for sea ice volume scattering (Appendix B (eq. B1)) can be used provided the snow grains, which act as scatterers, are smaller than the radar

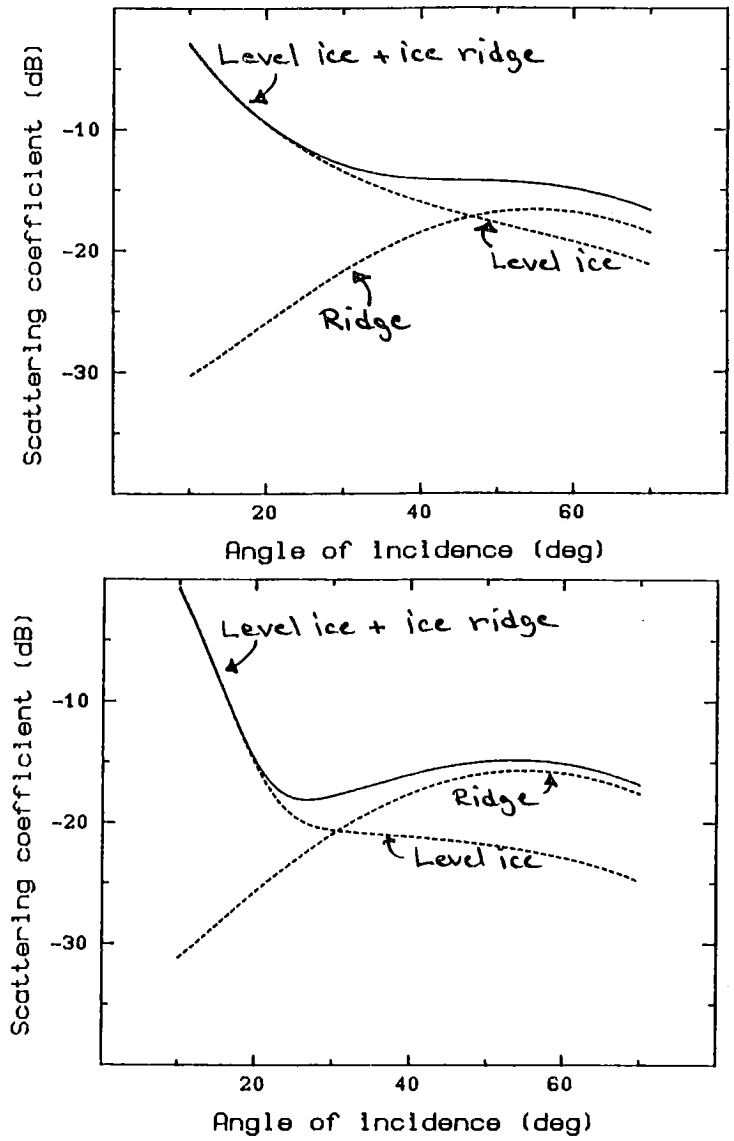

Figure 2. Illustration of the backscattering coefficient from an ice ridge with sail inclination 40° for exponential and gaussian correlation function resp. The parameters for the background are the same as in Fig. 1 whereas the parameters for the ridge are:
surface roughness 2 mm, corr. length 8.5 cm (exponential) and 7.1 cm (gaussian resp., temperature -1°, salinity 0.75 °/₀₀, density 0.9 g/cm^3, thickness 0.35 m, air bubble radius 1 mm and equivalent brine radius 0.1 mm, sail inclination 20°, standard deviation of angular distribution 15°, background area 300*1000 m^2, ice ridge area 5*1000 m^2.

wavelength. Hence the expression for the backscattering coefficient is given by (Kim et al. 1984);

$$\sigma^\circ_{tot} = \sigma^\circ_{snow\ volume} + \frac{\sigma^\circ_{level\ ice}}{L^2_{snow}} \qquad (3)$$

where $\sigma^\circ_{\text{level ice}}$ is calculated according the eq. (1) and L_{snow} is the attenuation in the snow layer.

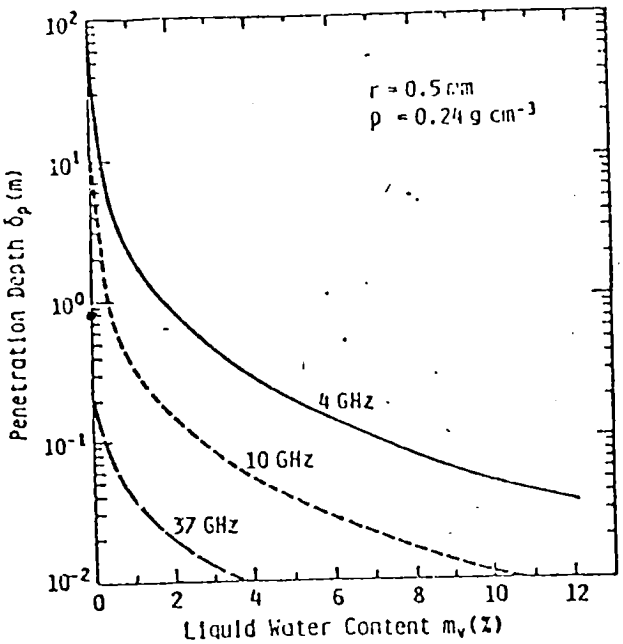

Figure 3. Calculated penetration depth for snow as a function of liquid water content from Hallikainen (1984).

When the snow becomes wet it is no longer valid to neglect the snow surface scattering. As shown in Fig. 3 the penetration depth is only a few millimeters when the moisture content is large and the effect of a snow cover is to reduce or even block the return from the underlaying ice medium. The backscatter coefficient for wet snow is given by (Kim et al. 1984):

$$\sigma^\circ_{\text{tot}} = \sigma^\circ_{\text{snow surface}} + T^2_{\text{snow}} \left(\sigma^\circ_{\text{snow volume}} + \frac{\sigma^\circ_{\text{level ice}}}{L^2_{\text{snow}}}\right) \quad (4)$$

where $\sigma^\circ_{\text{snow surface}}$ is calculated according to the Kirchhoff model, $\sigma^\circ_{\text{snow volume}}$ and $\sigma^\circ_{\text{level ice}}$ as before and T_{snow} is the power transmission coefficient from air to wet snow.

According to calculations made by Kim et al. (1984) 5 cm of dry snow can raise $\sigma^\circ_{\text{tot}}$ by 8 dB at 9 GHz, while $\sigma^\circ_{\text{tot}}$ may increase or decrease due to a wet snow cover depending on the contribution of $\sigma^\circ_{\text{level ice}}$ relative to the other terms in eq. (4).

3. SLAR AND SAR INSTRUMENTS

The SLAR used in the experiment was the ERICSSON SLAR carried on the Swedish Coast Guard aircraft. The characteristics of the SLAR are as follows:

- frequency: 9.4 GHz
- wavelength: 3.2 cm
- pulse repetition frequency: 1.0 kHz
- pulse length: 0.5 μs
- output power: 10 kW
- sampling rate: 2 MHz
- noise factor: 8 dB
- swath: 20 km on both sides of the aircraft
- spatial resolution: the resolution cell varies in both azimuth and range from 11 m by 106 m at 45° incidence angle to 173 m by 75 m at 87° incidence angle (flying altitude 3000 ft)
- polarization: vertical on transmit, vertical on receive
- incidence angle: from 45° to 87° (flying altitude 3000 ft).

For the VARAN-S SAR we refer to paper II section 2 and give here only the most relevant parameters:

- frequency: 9.37 GHz
- wavelength: 3.2 cm
- swath: 10 km on one side of the aircraft
- spatial resolution: single look 3 m x 3 m
  9 looks 9 m x 9 m
- incidence angles: 28° to 66°.

4. CALIBRATION OF SAR IMAGES

During the BEPERS Pilot Study campaign four corner reflectors were deployed at and around the Swedish experiment site in area III (see also paper VI). Primarily they were intended for locating the field site and rectifying the SAR images. Hence, their positions were carefully monitored using a Decca instrument. A second and minor objective was to attempt an absolute calibration of the entire SAR system. Fig. 4 shows the four reflectors (A, B, C and D) at the field site.

The following sections will describe the theoretical RCS (Radar Cross Section) of the reflectors and the results obtained from analyzing the SAR image data. An approach to the calibration problem using area-extended targets as a reference level will also be demonstrated.

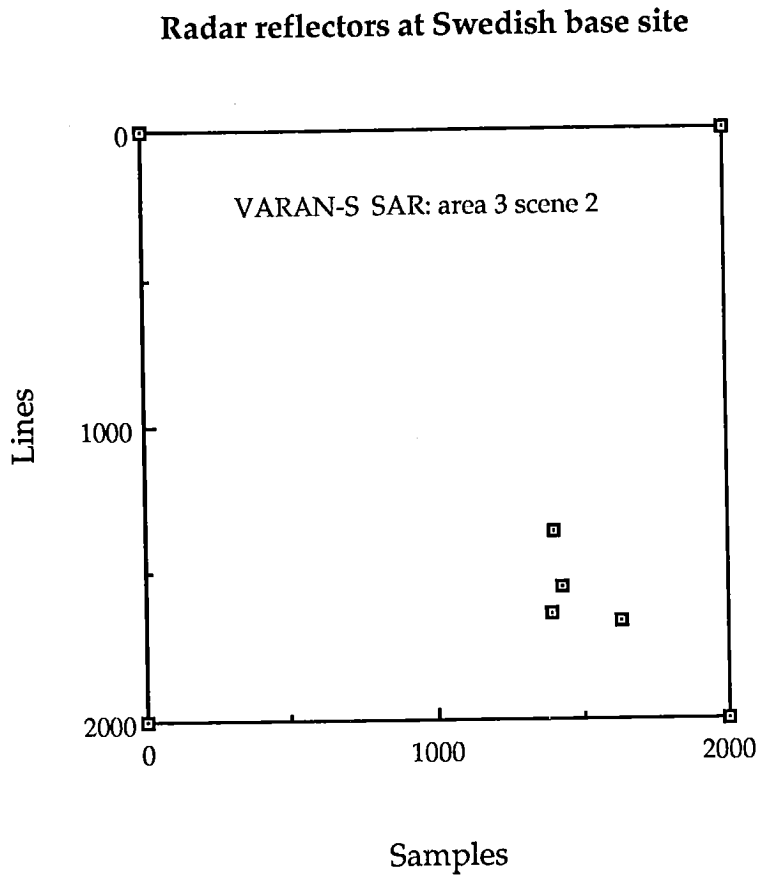

Figure 4. The position of the four reflectors given in line and sample numbers (SAR scene 2 in area II).

4.1 Radar cross section of the corner reflectors

The design of the reflectors is shown in paper II Fig. 6. Note that the trihedral shape has been complemented with a square base. The square base design was used for two reasons: firstly, it provides an efficient shield screening off radar reflections from the surrounding ice into the reflector and secondly, a square base is easier and more stable to deploy in the field by fixing it directly onto the level ice.

The RCS of the trihedral reflector with a square base may be analyzed by the methods described by Robertson (1947). In general, the RCS of a reflector is given by:

$$\sigma = \frac{4\pi}{\lambda^2} A_{eff}^2 \qquad (5)$$

where λ is the wavelength and A_{eff} is the effective area of the reflector. For the trihedral reflector with a square base the maximum effective area may be shown to be:

$$A_{eff} = \frac{4}{3\sqrt{3}} a^2 \qquad (6)$$

where a is the side length of the square base. The RCS is $\sim$ 2.5 dB higher than from an ordinary trihedral reflector and the maximum effective area is obtained at an incidence angle of 54.7°. In the BEPERS Pilot Study experiment the parameters were: a = 1 m and λ = 3.2 cm implying that σ = 7300 m² (of 39 dB/m²). The beamwidth of the reflectors was estimated to $\sim$ 40° according to the data given by Robertson (1947).

4.2 Analysis of the corner reflectors in the SAR imagery

Initially we were unable to locate the reflectors in the SAR images due to the lack of adequate navigational data from the flight track. By identifying ice features in the SLAR and SAR data and utilizing the more accurate Decca system used by the SLAR it was possible to locate the approximate site and find the reflectors.

All of the four reflectors were identified in the image but their response functions were observed to vary. However, all showed signs of saturation in several (4-8) pixels in the range direction and in a few (1-2) pixels in the azimuth. Also, sidelobes were identified in both range and azimuth. In the azimuth direction the response function showed signs of anomalous behaviour in at least two cases, where large and in one case saturated pixels were located symmetrically around the main peak at a distance of $\tilde{}$100 m. The cause of the anomaly is currently not understood.

Fig. 5 shows a cross-section of pixel values in the range and azimuth directions around the corner reflectors. Note the azimuth response of reflector A and B the variety of response functions obtained. Due to the broad and saturated range response the sample numbers are only accurate to a few pixels, while the line numbers are accurate to 1 pixel. To perform rectification of the images the geographical coordinates of the reflectors are required and they are given in paper VI Fig. 2.

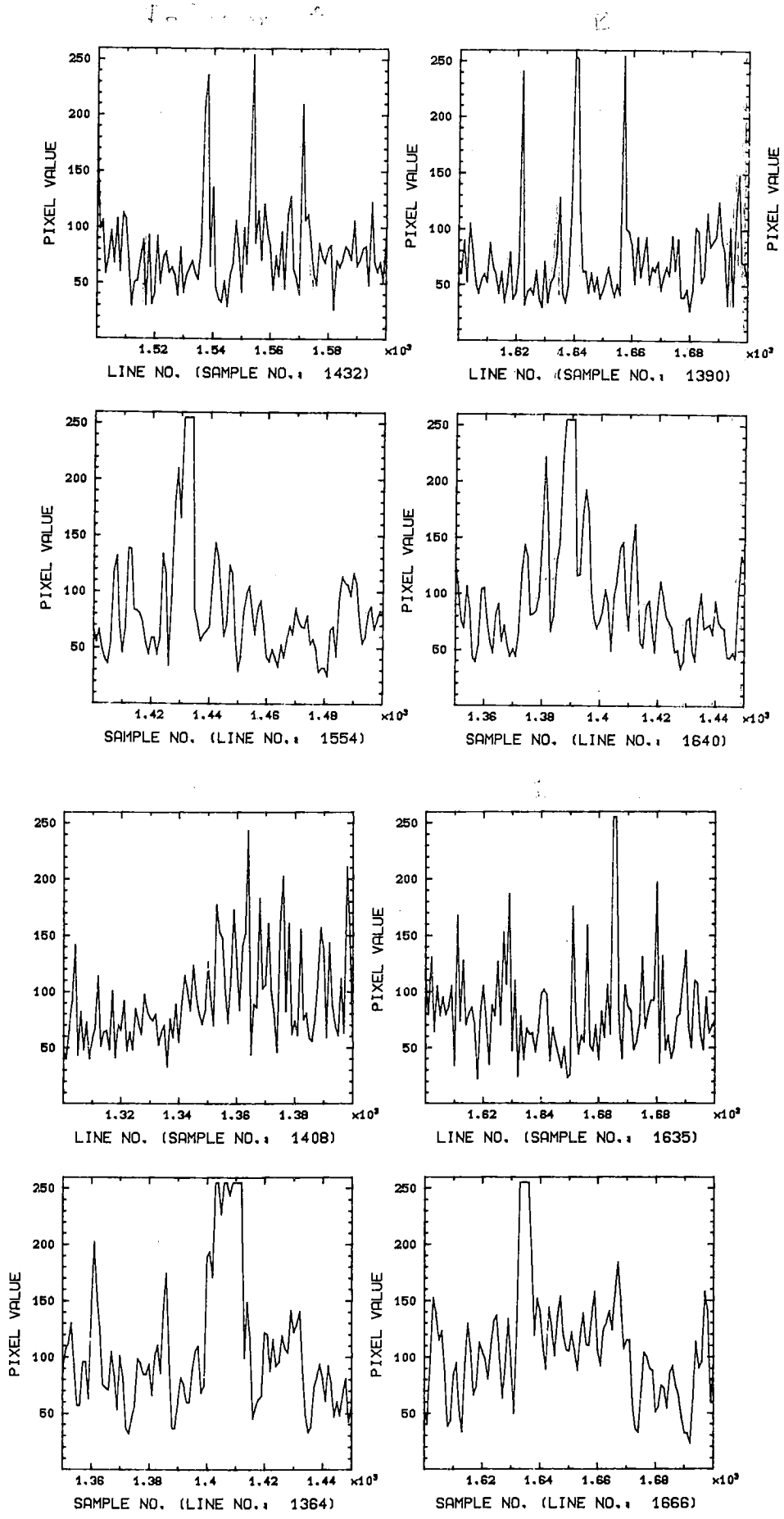

Figure 5. Pixel values given around the reflectors.

4.3 Using area-extended targets for absolute calibration

Due to the saturated responses of the radar reflectors they could not in practice be used for absolute calibration. Instead, an alternative approach which utilizes the ocean surface as a reference level will be described here. The main advantage of using area-extended targets is that the effects of saturation, antenna sidelobes and defocussing of the SAR is eliminated, the disadvantage being that the RCS must be established by other means. In this case we have relied on other measurements which have been made at a similar frequency, and the same polarization, incidence angle, and wind speed.

The technique has been applied to SAR scene 3 in area 4 showing the ice edge and the penetrating swell. As described in chapter II section 3.2 the SAR azimuth lines have been scaled by the inverse of their mean pixel value to obtain an even grey-scale across the imagery. This implies that averaging to reduce fading noise should be performed in the azimuth direction, where the same scale factor has been applied.

Two boxes with a size of 2000 samples by 300 lines (line no. 1001 to 1300 resp. 1701 to 2000) were selected, one over the ice and one over the ocean. First order statistics (mean and standard deviation) for each azimuth line were calculated based on the 300 pixel values. Figs. 6 and 7 show the results obtained for the power-to-mean ratio (standard deviation/mean = σ/μ) over the ice and ocean, respectively. For a linear detector the power-to-mean ratio for pure fading noise (speckle) is given by (Ulaby et al. 1982):

$$\frac{\sigma}{\mu} = \frac{0.523}{\sqrt{N}}$$

where N is the number of independent samples (looks) used in the processing. Over the ocean the fluctuations are expected to be

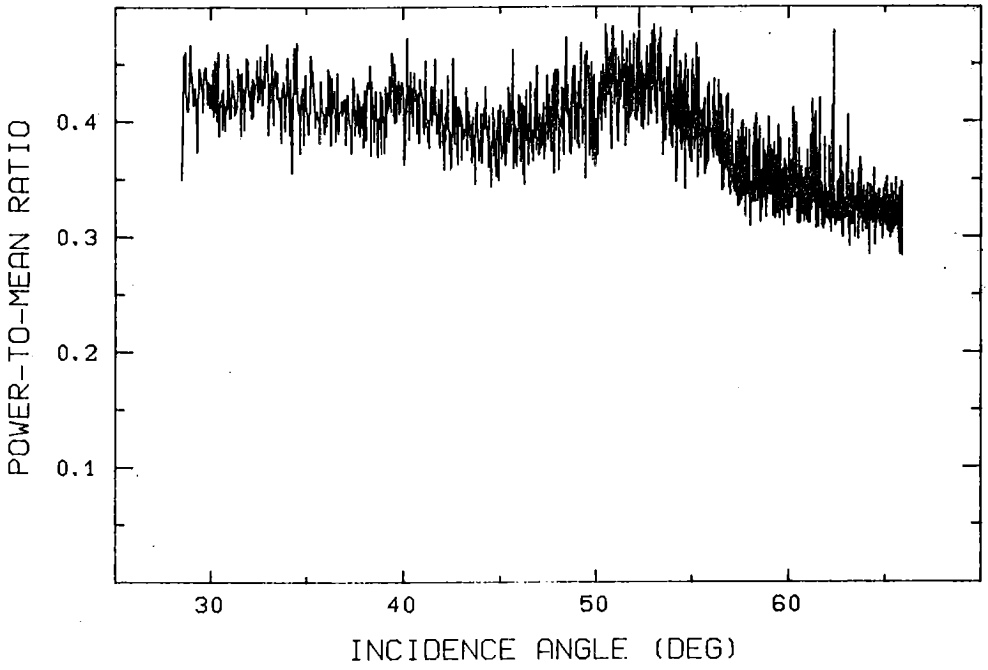

Figure 6. Power to mean ratio over the ice.

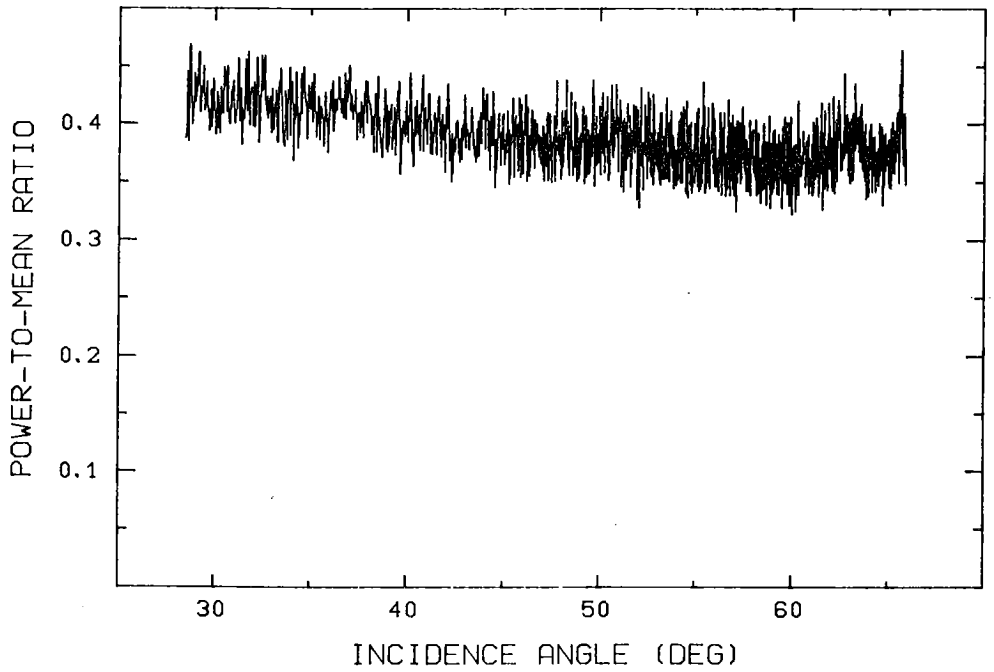

Figure 7. Power to mean ratio over the ocean.

due to pure fading noise, and the observed values in Fig. 7 of the power-to-mean between 0.36 and 0.42 correspond to N $\tilde{-}$ 1.5 - 2.1. These values should to be compered with N = 7, which is the theoretical values obtained with the stated resolution of 8 by 8 m. Full resolution corresponds to a resolution of 3 by 3 m (Massonet, 1987). Further analysis remains in order to understand this discrepancy

By determining the intensity ratio between the ice and ocean as a function of incidence angle we obtain Fig. 8. The contrast is seen to have a low value at 28° of $\tilde{-}$ 2 dB increasing to a peak at 58° of 14 dB.

Ground data in area IV were not collected except for routine meteorological observations. It was however reported that the ice was very close or compact without snow cover but with ice ridges. Observations at the nearby stations at Utö and Nyhamn (see paper VII Table 1) show that the wind was easterly with a

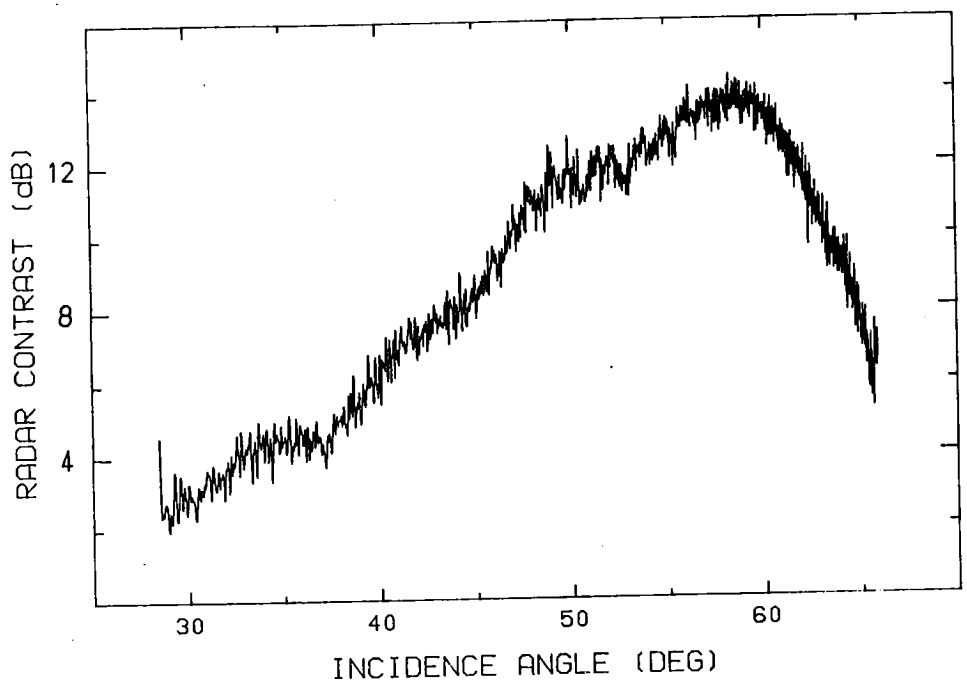

Figure 8. Radar contrast between the ice and ocean in area IV.

speed of 8-10 m/s at the time of the SAR overflight. Hence, since the flight track was southerly the SAR was viewing the ocean waves downwind.

Few airborne observations of the dependence of σ° at X-band and HH polarization on wind speed and direction have been reported (Ulaby et al. 1986). Tower measurements have been reported but a discrepancy with airborne measurements of up to 10 dB depending on incidence angle has been noted. Airborne measurements by the Naval Research Laboratory at P, L, C and X-band have been reported by Daley (1973). The measurements at X-band with HH polarization were unfortunately only reported for upwind conditions. However, measurements with VV polarization at up- and downwind conditions show a small difference of 2-3 dB in the range 20°-70° of incidence angle (Guinard, 1971). Therefore we apply this correction to transform the HH polarization data from upwind to downwind. Fig. 9 shows the estimated σ° for the ocean. Based on the calculated ice/ocean ratio in the SAR image we are also able to estimate absolute values of σ° for the sea ice, which is also included in Fig. 9. The uncertainty of these values, however, is rather large and may be of the order $\pm$ 5 dB owing to the uncertainty in the estimated ocean backscatter.

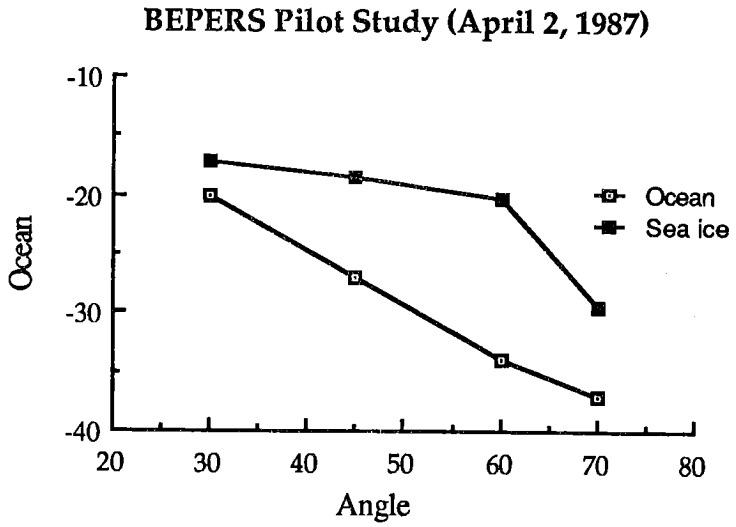

Figure 9. Illustration of estimated σ° values for the ocean surface (wind speed of 10 m/s) and the ice surface at the ice-water edge.

The curve given in Fig. 9 should be compared with the theoretical calculations made in section 2.1, Figs. 1a and 1b. However, in this preliminary analysis it is too early to discuss the similarities or the differences, which might be due to technical problems, backscatter model for the ocean or the quite simple model used for the level ice. A better comparison would be possible if extensive ground truth data were available. Note the better agreement with an exponental correlation function.

5. SLAR - SAR COMPARISON

5.1 Introduction

In order to compare and the SLAR and SAR data interpret the radar signatures two areas were selected with overlapping data. On the Finnish side area II was selected (see paper I, Fig. 1) where also aerial photography, SPOT data and some GEOSAT data exist. On the Swedish side area III was selected with only some overlapping helicopter photography and a small amount GEOSAT data. In Fig. 10a and 10b the two areas are shown with the different sensors indicated as well as the ground measurement sites.

As we can see SLAR and SAR data do not overlap fully in any of the two areas. This was due to a severe error in the SLAR recording equipment which meant that the SLAR data acquisition stopped just before the Swedish ground base in area III. Similarly the research vessel Aranda was not recorded in area II.

In order to compare SLAR and SAR data it is of vital importance to study the incidence angles used. In area II the SLAR flew from SW to NE looking at both sides, however only the nearest 10 km at the right hand side overlaps with the SAR. The SAR on the other hand flew in the opposite direction also looking at the right hand side. Fig. 11a illustrates the geometry together with the corresponding incidence angles. In area III the SLAR flew in the S-N direction while the SAR flew in the N-S. The SLAR looked at the left hand side and the SAR at the right hand side. The geometry and incidence angles are shown in Fig. 11b. The incidence angles are in both cases 54° - 87° for the SLAR and 28° - 66° for the SAR.

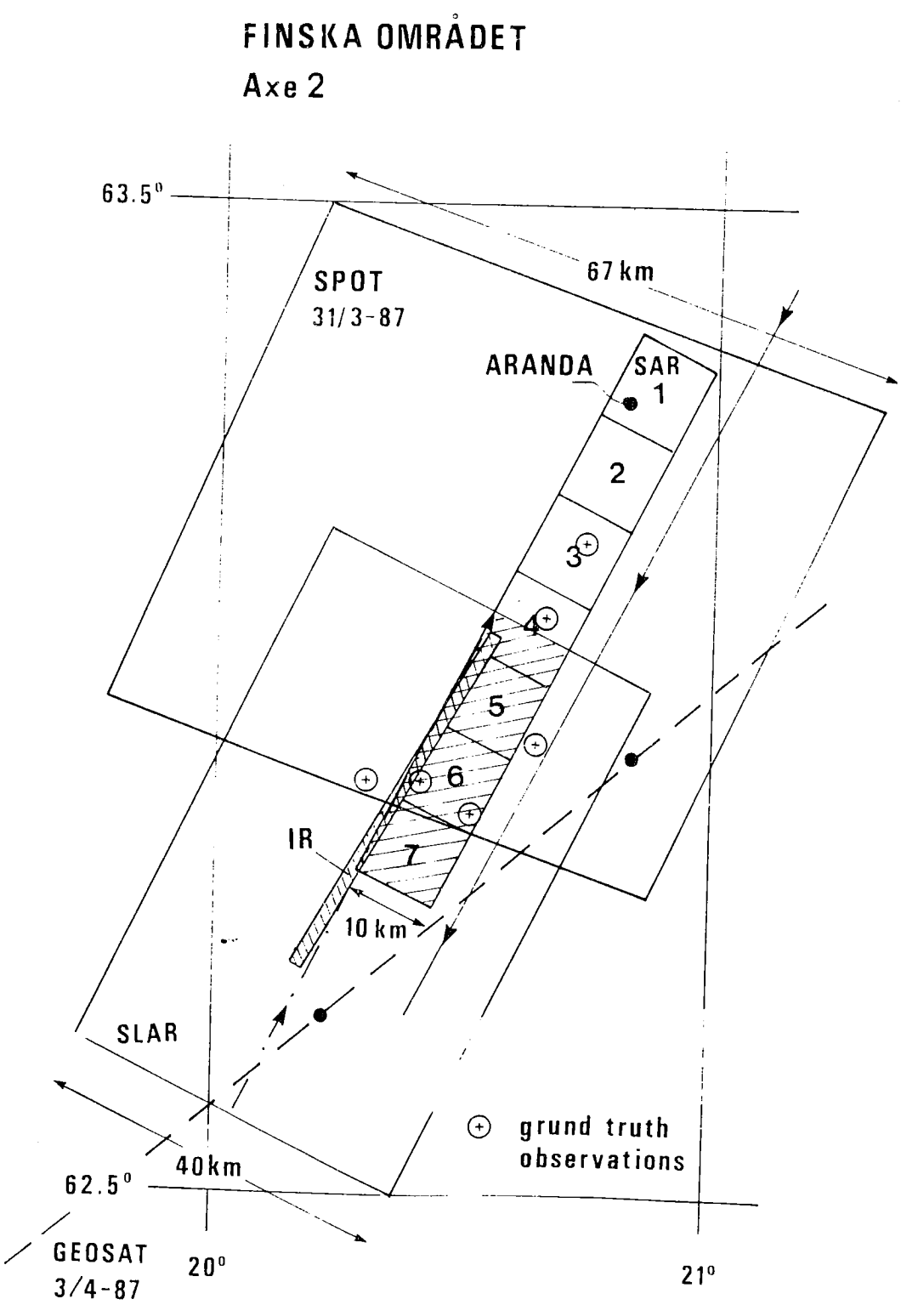

Figure 10a. Ground base II shown with the different sensors indicated as well as some of the ground truth observation sites.

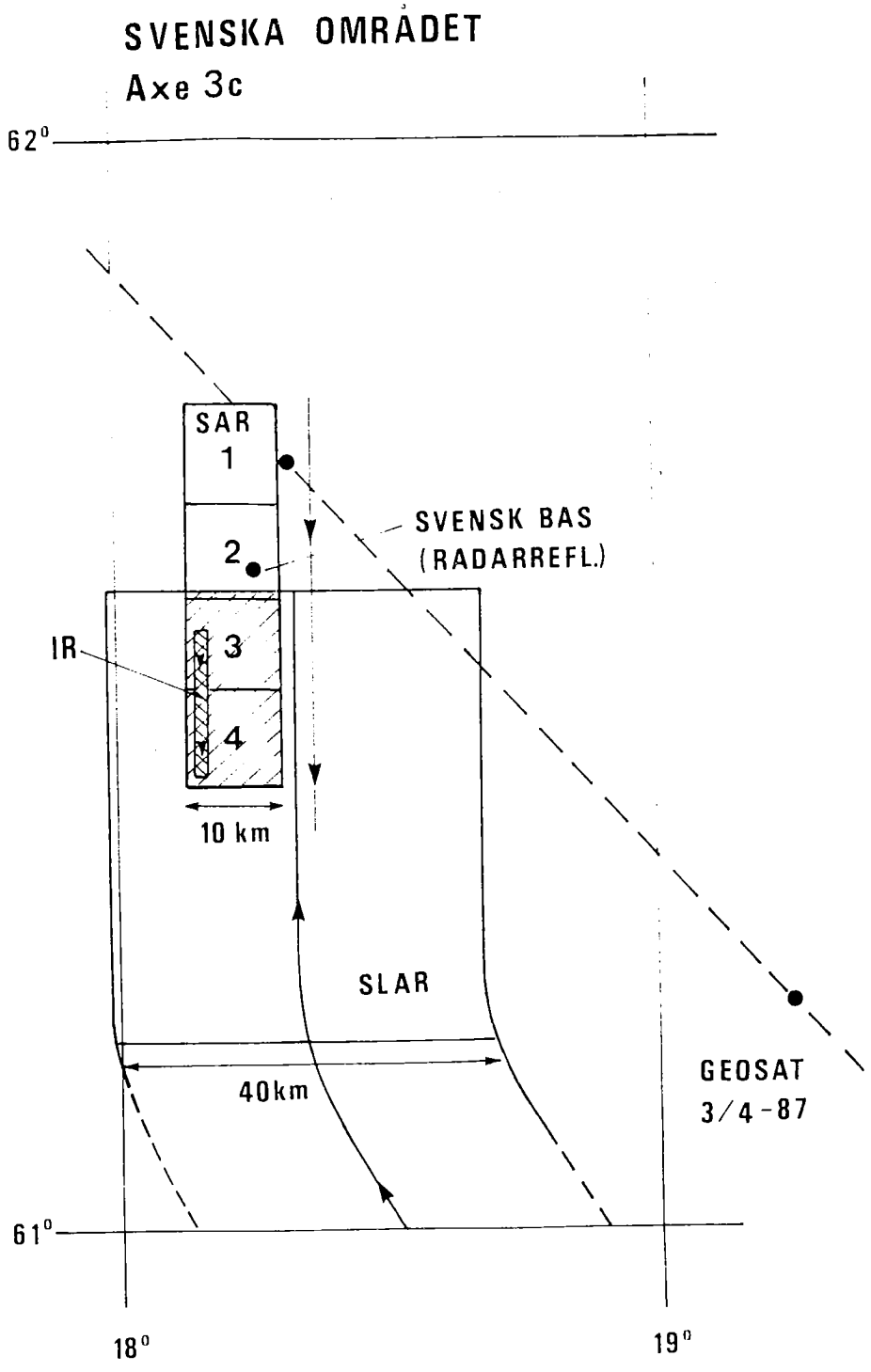

Figure 10b. Ground base III shown with the different sensors indicated as well as some of the ground truth observation sites.

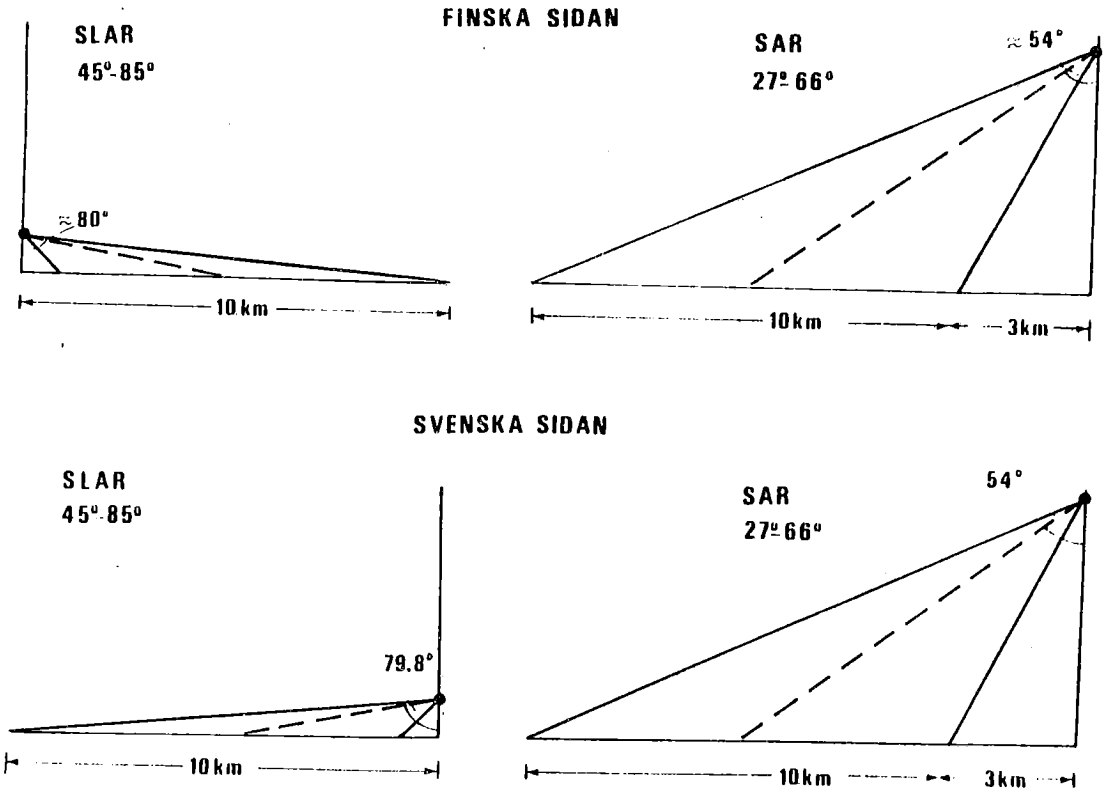

Figure 11. Geometry of SAR and SLAR mapping in area II and III together with the incidence angles used.

5.2 Area II

In Figs. 12a and 12b overlapping SLAR and SAR data are shown, the SLAR to the left and the SAR to the right. The Figs. correspond to SAR scene number 4 and 6 as indicated earlier in Fig. 10a. Note that the SLAR scene is displayed with negative contrast.

Ground truth measurements were done (see paper IV) at the points indicated, and an ice classification over the whole area was also done. In Fig. 12a the ice was quite thin (25 - 40 cm) and the surface was covered with snow only at the ice ridges. The temperature was just above zero degrees and the salinity approximately 0.7 per mille. Fig. 12b was recorded at the boundary of the thin and thick ice fields. Both bare and snow covered areas occurred and fractures were more frequent than in the thin ice fields.

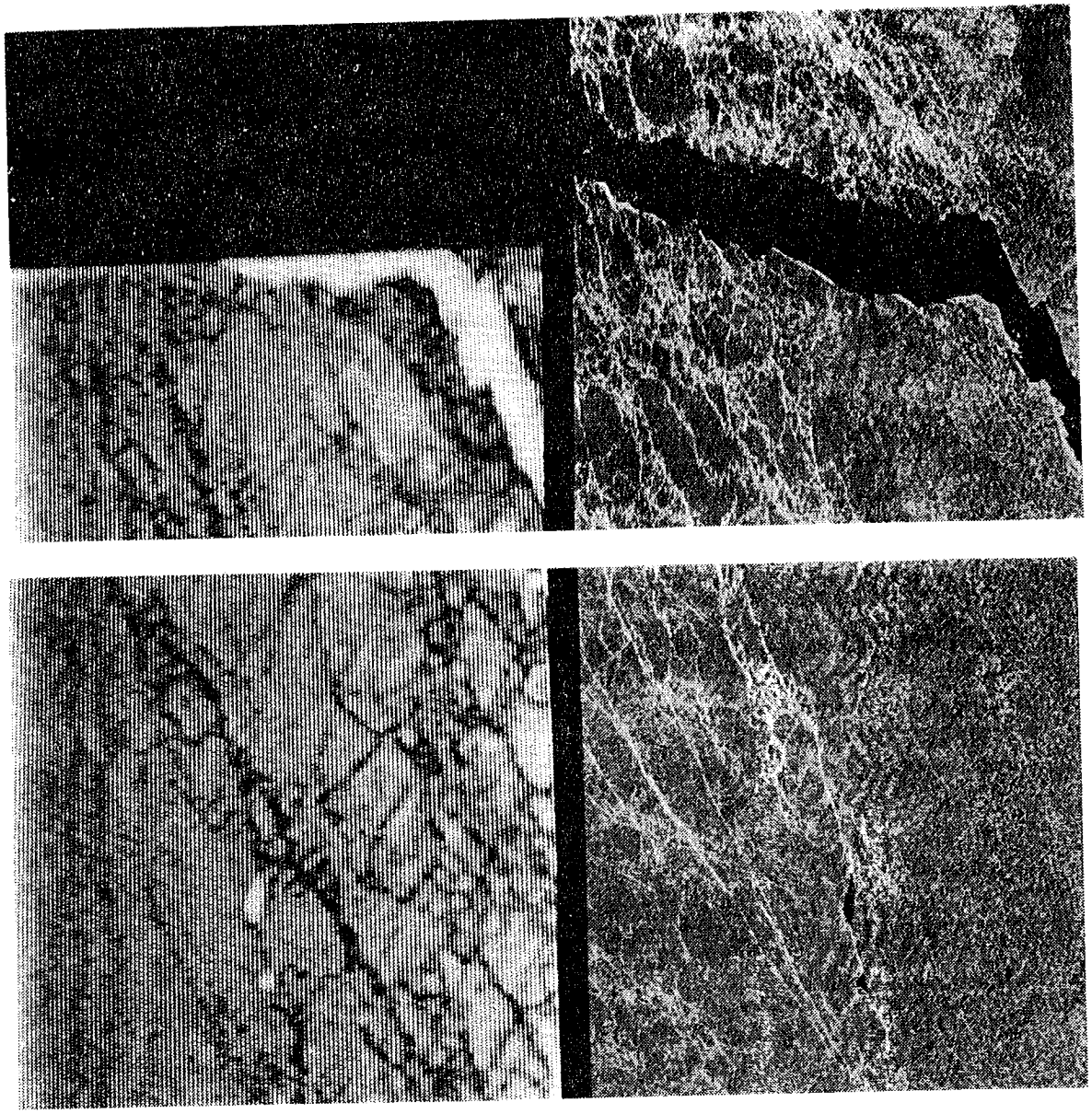

Figure 12. Overlapping SLAR (negative) and SAR data in area II corresponding to SAR scene 4 (a) and 6 (b).

Fig. 12a shows a big lead approximately 1 - 2 km wide, which is easily seen in both the SLAR and the SAR image. A comparison with the SPOT scene two days earlier showed that the lead was only one or two days old. It is also easy to see the bright strips crossing downwards in the left part of the image (dark in the SLAR image). This can be either ice ridges, ship channels, floe boundaries or fractures in the ice. According to observations (see paper IV, section 2) it was mostly ice ridges and some fractures.

If we look at the SLAR image it is possible to see some ridges in the middle and to the right, which can not be seen in the SAR image. To explain this we recall Fig. 10a showing the geometry and the incidence angle ranges. Because the SAR has its smallest incidence anlge to the right and its largest to the left the ice ridges will be more pronounced to the left side on the SAR image while the opposite is true for the SLAR.

In the upper right hand corner of the SAR image the fast ice boundary is seen. This part was not recorded by the SLAR so any comparison cannot be made

The effect of the incidence angle dependence is much more pronounced in Fig. 12b than in Fig. 12a. We can clearly see dark linear features crossing downwards to the right in the SLAR image which are barely seen in the SAR image.

The most obvious feature of the SLAR and SAR images is that it is easy to distinguish between open water (or possibly thin ice) of low intensity from the surrounding first-year ice of higher intensity. This is of great importance if the ice concentration is to be determined.

5.3 Area III

The overlapping SLAR and SAR data shown in Fig. 13 corresponds to SAR scene number 3 (see Fig. 10b). No ground truth measurements of ice classification were done in this area which makes it difficult to interpret the images. However, in both images it is easy to see large ice floes surrounded by thin ice (or possibly open water). The SAR image also shows the possibility to delineate small ice blocks which is impossible in the SLAR image due to its poorer resolution.

As can be seen the SLAR is more sensitive to ice ridges and floe boundaries than the SAR, mainly depending on the larger

incidence angles. It is however difficult to determine whether it is ridges or floe boundaries. This might be easier in the SAR image due to its higher resolution.

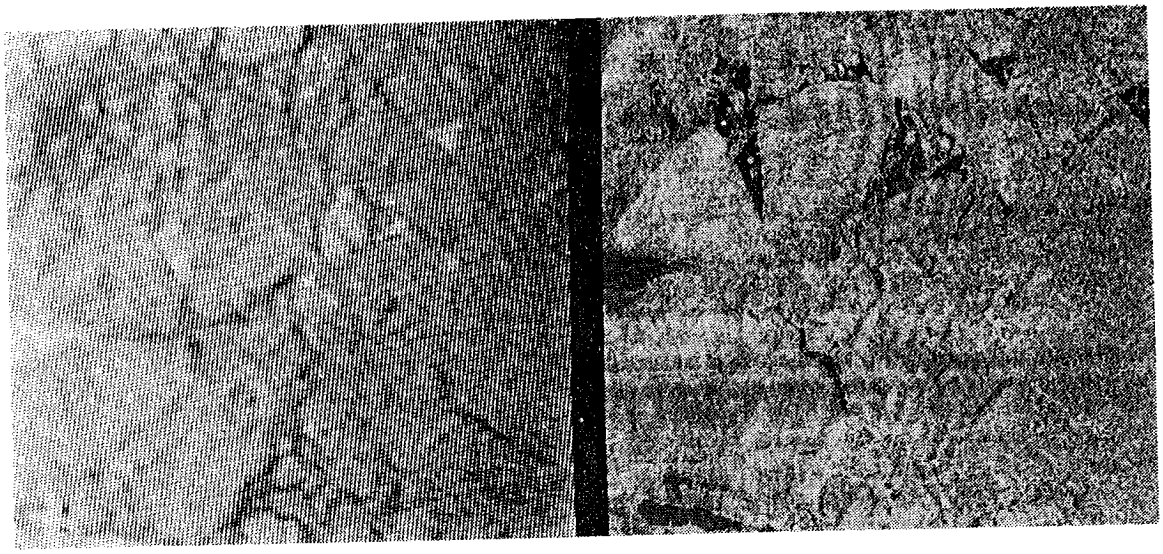

Figure 13. Overlapping SLAR (negative) and SAR data in area III corresponding to SAR scene 3.

6. CONCLUSIONS

Open water (or possibly thin ice) can be distinguished from the surrounding ice in both the SLAR and the SAR image.

Ice ridges, floe boundaries, ship channels and fractures are more easily detected in the SLAR image.

The four trihedral corner reflectors with a square base were successfully deployed in the field and detected in the SAR imagery. However, due to severe saturation of the SAR system no attempt has been made to perform an absolute calibration of the system. The information however, may be of use for rectification of the SAR imagery.

Absolute calibration of one SAR image was attempted using scene 2 of area 4 utilizing the wind-roughened ocean as a reference level. The backscatter coefficient for the ocean was obtained using other measurements at X-band and HH-polarization (Daley, 1973), but corrected for the wind direction.

Comparison with the theoretical models given is difficult since no ground truth data are available. However, some general characteristics of sea ice backscattering may be shown in the Figs. presented.

7. RECOMMENDATIONS FOR BEPERS 88

- Absolute calibration should be based on both
  (1) corner reflectors (point targets) and
  (2) area-extended reference targets.

- Several sizes of corner reflectors should be used to cover the range from the minimum detectable signal to system saturation. The design should incorporate a mechanism for adjusting the pointing angle to assure that the maximum effective area is used. The RCS of the reflectors should also be validated prior to the experiment in the laboratory.

  The corner reflectors should be deployed in area of low background σ° in order to maximize the signal-to-clutter ratio. The site should be chosen in order to avoid multiple reflections into the reflectors. Also, they should be placed with a sufficient offset in range and azimuth relative to each other in order to minimize the influence from nearby reflectors.

- Area-extended targets such as level and homogenous ice or the open ocean should be selected and used as a complementary method of absolute calibration. A ground- or helicopter-based scatterometer should measure the

backscatter coefficient as a function of incidence angle to enable calibration. These measurements should be made during the SAR flight to minimize the effects of changing surface conditions, e.g. snow wetness. The main advantage of using area-extended targets is that the effects of saturation, antenna side-lobes and defocussing are eliminated, which are major problems when using point targets. Note especially that the SAR focus tends to vary during the flight due to e.g. turbulence.

In order to evaluate the backscatter models against measurements it is of vital importance that the radar is calibrated. However, an extensive ground truth program is also needed to measure all the model parameters. The parameters are given below.

Level ice and ice ridges

σ = surface height standard deviation
l = correlation length
S = ice salinity
ϱ = ice density
d = ice thickness
T = ice temperature
ϵ = dielectric constant of the ice
distribution and radius of both air bubbles and brine inclusions.

Additional parameters for ice ridges

φ_s = slope angle of the triangular geometry
S_θ = standard deviation of the normally distributed ice blocks
A_{ridge} = area of the ice ridge
A_{coh} = area of specularly oriented ice blocks.

Snow

σ = surface height standard deviation
l = correlation length
ϱ = snow density
d = snow thickness
T = snow temperature
ϵ = dielectric constant of the snow
distribution and size of snow grains.

8. REFERENCES

Daley, J.G., 1973: Wind dependence of radar sea return, J. Geophys. Res., Vol 78, No. 33, p. 7823.

Guinard, N.W., 1971: Variation of the NRCS of the sea with increaseng roughness, J. Geophys. Res., Vol 76, No. 6, p. 1525.

Hallikainen, M., 1984: Microwave Remote Sensing of Snow, Helsinki University of Technology, Radio Laboratory, Helsinki, Finland.

Johansson, R. and J. Askne, 1987: Modelling of radar backscattering from low-salinity ice with ice ridges, Radio and Space Science, Chalmers University of Technology, Gothenburg, Sweden.

Kim, Y., R.G. Onstott and R.K. Moore, 1984: The Effect of a Snow Cover on Microwave Backscatter from Sea Ice, IEEE Journal of Oceanic Engineering, OE-9, NO 5, 383.

Massonet, D., 1987: Conclusions about the campaign over the Gulf of Bothnia, Image Processing Division, C.N.E.S.

Robertson, S.D., 1947: Targets for microwave radar navigation, Bell System Tech. J., 26:852-869.

Rott, H., 1984: The Analysis of Backscattering Properties from SAR Data of Mountain Regions, IEEE Journal of Oceanic Engineering, OE-9, NO 5, 347.

Schroeder, L.C., D.H. Boggs, G. Dome, I.M. Halberstam, W.L. Jones, W.J. Pierson and F.J. Wentz, 1982: The relationship between wind vector and normalized radar cross-section used to derive SEASAT-A Satellite Scatterometer winds, J. Geophys. Res., 87:3318-3336.

Ulaby, F.T., R.K. Moore and A.K. Fung, 1981: Microwave Remote Sensing, Vol. 1. (Reading, Massachusetts: Addison-Wesley).

Ulaby, F.T., R.K. Moore, and A.K. Fung, 1982: Microwave Remote Sensing, Vol. 2 (Reading, Massachusetts: Addison-Wesley).

Ulaby, F.T., R.K. Moore, and A.K. Fung, 1986: Microwave Remote sensing, Vol 3 (Dedham, Massachusetts: Artech House).

APPENDIX A.

The Kirchhoff model under the scalar approximation is given by (Ulaby et al. 1982):

$$\sigma^\circ_{surface} = \left(|R_{pp}|^2 \cos^2\theta + 2\sin\theta |R_{pp}|^2 \sin^2\theta + \mathrm{Re}(R_{pp} R_{pp1}^*)\cos\theta \right) \cdot k^2 \ell^2 \exp(-g) \cdot \Sigma \frac{g^n}{n!n} f(n, l \cdot qt) \qquad (A1)$$

where

k = $2\pi/\lambda$
λ = wavelength
σ = surface height standard deviation
ℓ = correlation length
R_{pp} = Fresnel reflection coefficient
R_{pp1} = modified Fresnel refl. coeff. due to surface slopes
g = $4k^2\sigma^2\cos^2\theta$
q_t = $2k\sin\theta$

$$f(n, l \cdot q_t) = \begin{cases} \exp(-(l \cdot q_t)^2/4n) & \text{for } \rho = \exp(-x^2/l^2) \\ \dfrac{2n^2}{(n^2 + (l \cdot q_t)^2)^{3/2}} & \text{for } \rho = \exp -|x/l| \end{cases}$$

Restrictions: $kl > 6$

$l^2 > 2.76 \cdot \sigma \cdot \lambda$

rms slope < 0.25.

APPENDIX B.

The volume scattering σ°_{volume} is given by the expression (Ulaby et al. 1981):

$$\sigma^\circ_{volume} = \frac{N\sigma_b \cos\theta'}{2k_e} \left(1 - \frac{1}{L^2} \right) \qquad \text{(B1)}$$

where

K_e = volume extinction coefficient
N = number density of inclusions
σ_b = backscattering cross section of inclusions
θ' = angle of refraction

$$L = \exp \left(- \int_0^{d/\cos\theta'} k_e dz \right)$$

d = ice thickness

Restriction: The Rayleigh approximation has been used which means that the inclusions have to be small compared to the wavelength.

APPENDIX C.

To calculate the backscatter coefficient from a snow free ice ridge, σ°_{ridge}, two different contributions have been considered. The first one is a specular component due to ice blocks oriented towards the radar and with zero incidence angle. The second one is a mean value obtained from the ice ridge (Johansson and Askne 1987):

$$\sigma^\circ_{coh} = \frac{k^2}{\pi}|R(0)|^2 e^{-g} \cdot A_{coh} \qquad (C1)$$

$$E(\sigma^\circ) = \int_{-\pi/2}^{\pi/2} \sigma^\circ(\theta_i)\, p(\theta)\, d\theta \qquad (C2)$$

where

A_{coh} = total area of specularly oriented ice blocks
$\sigma^\circ(\theta_i)$ = backscatter coefficient (surface + volume scattering)
θ_i = incidence angle
$p(\theta)$ = gaussian probability density function.

The incidence angle, θ_i, can be expressed in the radar incidence angle, θ_r, the sail inclination, φ_s, and the block orientation angle, θ:

$$\theta_i = \theta + (\varphi_s - \theta_r) \qquad (C3)$$

The final expression for the backscatter coefficient from an ice ridge then is (if $A_{coh} << A_{ridge}$):

$$\sigma^\circ_{ridge} = E(\sigma^\circ) + \sigma^\circ_{coh} \frac{A_{coh}}{A_{ridge}} \qquad (C4)$$

where A_{ridge} = area of the ice-ridge.

In: BEPERS Pilot Study. Data Report. Styrelsen för Vintersjöfartsforskning/Winter Navigation Research Board, Rep. No 45, p. 149-151. Helsinki 1988.

X HELICOPTER IMPULSE RADAR MEASUREMENT

By Peter Ulriksen

Lund Institute of Technology
Box 118, S-22100 Lund, Sweden

Performed: April 1, 1987
Purpose: To develop methods suitable for calibration of SAR data.

IMPULSE RADAR OPERATION

The impulse radar is installed in a helicopter, the antenna pointing straight down. An extremely short signal is transmitted and will reach the snow/ice surface. When the signal changes its velocity a portion of the energy is reflected. This will typically happen at the air/snow-, air/ice-, snow/ice- and ice/water interface.

Flight 1 (Data sets 1 - 6)

In this area, profiles are oriented in a triangle defined by WASA lighthouse, R/V Aranda and the islet Östra Norrskär.

The profiles were measured with the radar operating in two different modes of polarization. The first set of three profiles has a standard polarization with the E field transmitted and received in direction perpendicular to the line of flight. In the second set another antenna is used to receive the depolarized signal oriented parallel to the line of flight.

The purpose of cross polarized measurements is to see if polarization may be a good ice surface roughness indicator.

A video camera pointing at boresight is operated during the data takes. The radar and video signals are recorded simultaneously on a VCR.

Flight 2 (Data sets 7, 8)

This flight is used to obtain two sets of data with different vertical resolution. The profiles are located along the northern profile in the triangle, i.e. between R/V Aranda and WASA lighthouse. The standard polarization mode is used for both data sets.

Flight 3 (Data set 9)

A single profile stretching from a point just south of R/V Aranda to the Decca fix J74 Violet/E10.8 Red. The purpose was to get a data set covering the contact zone between the fast ice and the drift ice.

On ice (Data set 10)

Just north of R/V Aranda five pits were dug in the snow on the ice. The antenna was placed in each hole. Drillings obtained the ice thickness necessary to calculate the velocity of radio waves. In one pit the antenna was rotated through 180 degrees to obtain the polarization properties of the ice, which allows determination of the c-axis orientation of the ice.

EVALUATION

Helicopter altitude variations will be eliminated from the recorded data by low pass filtering. The remaining range variations are attributed to the ice surface roughness and compared to the video record.

The envelope and instantaneous frequency of the ice surface echo will be calculated via a Hilbert transform. These parameters will be correlated to phenomena visible in the video record. Ice thickness variations will be studied in the data sets with a high vertical resolution.

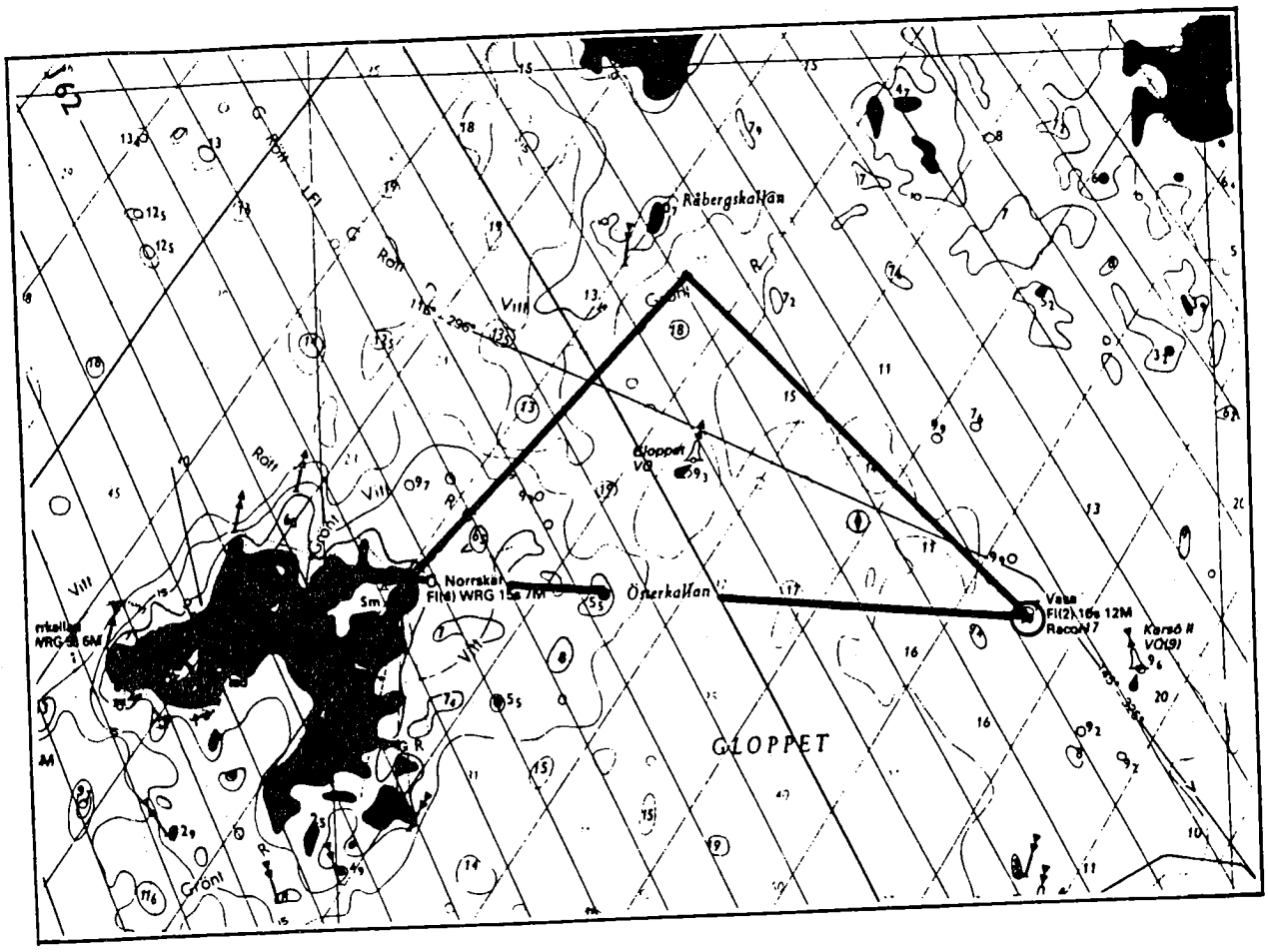

Chart showing the trajectories of flights 1, 2 and northern part of flight 3. Aranda is moored in the northern point of the triangle.

In: BEPERS Pilot Study. Data Report. Styrelsen för Vintersjöfartsforskning/Winter Navigation Research Board, Rep. No 45, p. 153-159. Helsinki 1988.

XI SATELLITE DATA

By Hanna Kemppainen[1)] and Bertil Håkansson[2)]

1) Finnish Institute of Marine Research
P.O. Box 33, SF-00931 Helsinki, Finland

2) Swedish Meteorological and Hydrological Institute
S-60176 Norrköping, Sweden

ABSTRACT

The satellite data set used in BEPERS Pilot Study consists of SPOT and NOAA AVHRR images. Sea ice surface conditions and concentration in the Gulf of Bothnia are inferred from the NOAA AVHRR visible and infrared imagery. The surface temperatures extracted from channel 4 intensities are so uniform in the area that even open water area is difficult to distinguish. With the help of a colour composite clouds obscuring the ice are distinguished clearly as well as open water and snow cover which can be seen uniform near the coast line. The reason for incorporating a SPOT scene in data set is its suitability for complementing the aerial photography for SAR and SLAR verification. However, the time delay of two days between the SPOT and SAR image acquisition limits a comprehensive comparison of these images.

1. INTRODUCTION

NOAA AVHRR imagery has been demonstrated to be useful for ice mapping purposes by several investigators (e.g. Dey 1981). AVHRR data have an advantage of frequent acquisition and quite high resolution of 1.1 km at the nadir. AVHRR provides an image in 5 spectral intervals: 0.58 - 0.68, 0.725 - 1.10, 3.55 - 3.93, 10.30 - 11.30 and 11.30 - 12.50 μm. Visual, near infrared and thermal infrared channels are best suited for observing ice conditions. In 1992 channel 3A (1.57 - 1.78 μm) will be suited for daytime snow/cloud discrimination (Fusco and Muirhead, 1987).

AVHRR quick look images from Tromsoe Telemetry Station for the period March 30 to April 4 have been valued and the results are summarized in Table 1. Scenes from March 30 1338 GMT and March 31 1147 GMT as well as April 2 1306 GMT and April 4 1658 GMT have been acquired on magnetic tape. The Swedish Space Corporation delivered a SPOT image of March 31 1987 which covers the Northern Quark. The geometric resolution in multispectral mode is 20 meters. In this mode SPOT provides an image with 3 spectral bands: 0.50 - 0.59, 0.615 - 0.68 and 0.79 - 0.89 μm. They correspond to green and red in the visual part of the electromagnetic spectrum and near infrared. The SPOT satellite repeats it's orbit configuration every 26th day. It can change the incidence angle of observation if required. In this way a particular area can be viewed more often than what is usually obtained.

Table 1. AVHRR scenes used in BEPERS Pilot Study

Date	Time (GMT)	Quality	Comments Area I	Area II	Area III	Acq.
30.3.	0710	2	cloudy no daylight	cloudy	cloudless	
30.3.	1158	2	cloudy	cloudy	cloudy 2/8	
30.3.	1338	3	"	"	cloudless	*
31.3.	1147	5	cloudless	cloudless	"	*
31.3	1326	4	as 1147 but in the edge of the swath			
1.4.	1137	3	cloudless	cloudy	cloudy 4/8	
1.4.	1317	1	"	"	cloudy	
2.4.	1306	3	"	"	"	*
3.4.	0723	0	no daylight,	cloudy		
3.4.	1242	0	cloudy	cloudy	cloudy	
4.4.	1658	3	"	"	" 1-2/8	*

Quality: 0 = poor
5 = very good

2. THE AVHRR IMAGERY OF 31 MARCH 1987

In the NOAA-9 AVHRR image of 31 March every study area except of area IV (Southern Sea of Bothnia) is seen without clouds obscuring the ice. The passage is 11.47 GMT.

A colour composite can be used to study the ice situation. Colour composites are used to display three images of a scene. Each waveband is coloured with a primary colour. The variations in the spectral response of objects in these three wavebands result in colour differences which aid in the identification of the object. Thus features can be distinguished which in one single channel would have the same signature and therefore look the same. This is the case expecially with clouds which are difficult to distinguish in channel 4 of AVHRR but which are clearly seen in a colour composite. By projecting channel 1 in red, the difference between channel 1 and channel 2 in green and channel 4 in blue, the following features can be distinguished:

- blue is open water
- blue-white is ice
- pink is low clouds of fog.

An example of the processed RGB picture is shown in Fig. 1.

Figure 1. An RGB picture of the Gulf of Bothnia. R is channel 1, G is the difference between channel 1 and channel 2 while B is channel 4.

3. INTERPRETATION OF AVHRR CHANNEL 4 IMAGES

An AVHRR thermal infrared (TIR) image of channel 4 represents the spatial distribution of radiation emitted by the surface of the Earth as well as the atmosphere. Objects that are not at absolute zero temperature radiate energy over all wavelengths in the electromagnetic spectrum. In the infrared region, radiation temperature varies with the physical temperature of the object and the emissivity of the surface and thus the distribution of the radiant energy emission is not a linear function of the surface physical temperature. The radiant temperature measured by AVHRR is a function of the emissivities of the water, snow and ice, and the physical temperatures of their surface layers.

Since AVHRR senses the temperature of the upper snow or ice surface, one might think that TIR imagery could be used to estimate ice thickness since the surface of thin ice is warmer that that of thicker ice. Surface temperature is, anyhow, also dependent on the thickness and density of snow cover and changing meteorological conditions. An additional problem encountered with AVHRR imagery is the presence of clouds which obscure sea ice, and also can be warmer or colder than the ice. The advantage of TIR imagery is that it is not limited by darkness.

The AVHRR channel 4 image of 31 March 1147 GMT shows that the surface temperature is quite uniform in the whole sea area. Even the open water area in the Southern Sea of Bothnia is hard to distinguish. This may be due to melting snow and ice surface because of quite high air temperatures. Air temperature measurements carried out in the meteorological observation stations in the neighborhood of study areas are summarized in Table 2. On March 31 the wind was very weak and that is why the surface of open water may be even warmer than that of snow and ice. AVHRR image of April 2 1306 GMT for study area II shows similarly very limited surface temperature distribution.

Table 2. Air temperatures in the neighborhood of the study areas on 31 March 1500 EET (Finnish Meteorological Institute, 1987).

Observation station	Air temperature °C
Kemi	3
Hailuoto	2
Mässkär	3
Valassaaret	2
Vaasa	6
Pori	6
Mariehamn	6
Utö	1

4. SPOT IMAGE 31 MARCH

The SPOT image was taken over the area II where R/V aranda was located. The image corner parameters are:

C1	N 633006	E 201222
C2	N 631843	E 212013
C3	N 630003	E 194603
C4	N 624852	E 205255

It should be mentioned that March 31 is classified as a cloudfree day according to quick-look AVHRR data. A careful analysis of the AVHRR image in full resolution indicates, however, that low clouds or fog are present in the northern part of the Bothnian Sea (see Fig. 1) which may influence the SPOT image data.

SPOT data over sea ice have so far not been used. The main reason for incorporating this data set in the BEPERS Pilot Study is its potential to complement the aerial photography for SAR and SLAR verification schemes. Before this can be done, however, the SPOT image has to be carefully interpreted with respect to the various wavelength responds to different ice types.

5. CONCLUSIONS

It is indeed difficult to obtain different kinds of remotely sensed data on a timely basis. The SPOT scene and the SAR images were sampled with two days of delay. During this period ice movements have changed the ice situation, limiting the possibility of a comprehensive comparison. However, the SPOT and AVHRR images of March 31 are coincident and a comparative study between these data sets are indeed possible.

In the BEPERS-88 the SAR flights are planned to be carried through during a six day period with a total of three flights.

This will increase the possibility to obtain coincident remotely sensed data from AVHRR and LANDSAT-TM with the SAR, both with respect to orbit configuration and weather conditions.

6. REFERENCES

Dey, B. 1981: Monitoring winter sea ice dynamics in the Canadian arctic with NOAA-TIR images. - J. Geophys. Res. Vol 86. No C4. pp. 3223-3235.

Finnish Meteorological Institute, 1987: Statistical table of meteorological observations of 31 March 1987. - Published on 1 April 1987, 3 p.

Fusco, L. and K. Muirhead, 1987: AVHRR data services in Europe - the Earthnet approach. - ESA Bulletin No 49, pp. 9-19.

In: BEPERS Pilot Study. Data Report. Styrelsen för Vintersjöfartsforskning/Winter Navigation Research Board, Rep. No 45, p. 161-165. Helsinki 1988.

XII AVAILABILITY OF GEOSAT DATA DURING THE BEPERS PILOT STUDY

By Lars M.H. Ulander

Department of Radio and Space Science
Chalmers University of Technology
S-412 96 Göteborg, Sweden

The U.S. Navy satellite Geosat carries a radar altimeter which is the successor to altimeters flown on Skylab (1973), GEOS-3 (1975) and Seasat (1978). Launched in March 1985, it has generated global and long term measurements of mean sea level, significant wave height and wind speed. Since September 30, 1986, the data has been unclassified when the orbit was altered to match the Seasat orbit to within a few kilometres. 244 orbital revolutions generate the repeat cycle of 17.05 days providing a spacing of 164 km at the equator; the inclination of 108 degrees provides a coverage ut to 72 degrees latitude (Cheney et al. 1987). One ascendeing node is located at longitude E 0.985 degrees (Kilgus and MacArthur 1987).

Spaceborne altimeters were originally developed for oceanographic applications. Recent studies have also shown a

potential for sea ice applications. Dwyer and Godin (1980) showed that the location of the sea ice edge could be determined to within a few kilometres, whilst Rapley (1984) used altimeter data to detect penetrating swell into the Antarctic pack ice. Recently, Ulander (1987) has shown that the normal incidence backscatter coefficient indicates the ice type. However, the altimeter has the potential of providing several other sea ice parameters, such as ice concentration, ridging etc., but the lack of an accepted backscatter theory and simultaneous altimeter and surface truth observations has sofar inhibited progress.

The coverage of Geosat data during the BEPERS pilot study has been studied using GDR (Geophysical Data Records) data spanning 34 days from March 24 to April 26, 1987. The GDR is the final altimeter data product which has undergone several stages of data reduction. However, it contains no data of the radar pulse echoes which are required for studies over sea ice and was merely used for identifying interesting data segments for detailed studies. For further studies SDR (Sensor Data Records) and WDR (Waveform Data Records) are required to complement the GDR data. Note that 24 hours of GDR, SDR and WDR require 4 Mbyte, 22 Mbyte and 56 Mbyte of storage.

Figure 1 illustrate the interesting subsatellite tracks during 3 weeks spanning the BEPERS pilot study. April 3 was selected for more detailed studies. Hence, SDR and WDR data have been requested but not yet received and analysed. Figure 2 illustrates the expected coverage of Geosat during the BEPERS study, which is presently scheduled for March 3-9, 1988.

It is believed that the analysis will increase the understanding of the backscatter mechanism over ice and provide data for evaluating the extraction of sea ice parameters. Also, it will provide the first altimeter data acquired over low-salinity sea ice in the Baltic Sea.

REFERENCES

Cheney, R.E., Douglas, B.C., Agreen, R.W., Miller, L., Poter, D.L., Doyle, N.S. 1987: Geosat altimeter geophysical data record user handbook, NOAA Technical Memorandum NOS NGS-46, Rockville, Maryland.

Dwyer, R.E. and Godin, R.H. 1980: Determining sea-ice boundaries and ice roughness using GEOS-3 altimeter data, NASA Contractor Report 156862, 47 pp.

Kilgus, C.C. and MacArthur, J.L. 1986: Development in radar altimetry - the Navy Geosat mission, Proc. IGARSS'86, ESA SP-254.

Rapley, C.G. 1987: Interpretation of Seasat radar altimeter data over sea ice using near-simultaneous SAR imagery, accepted for publication in Int. J. Remote Sensing.

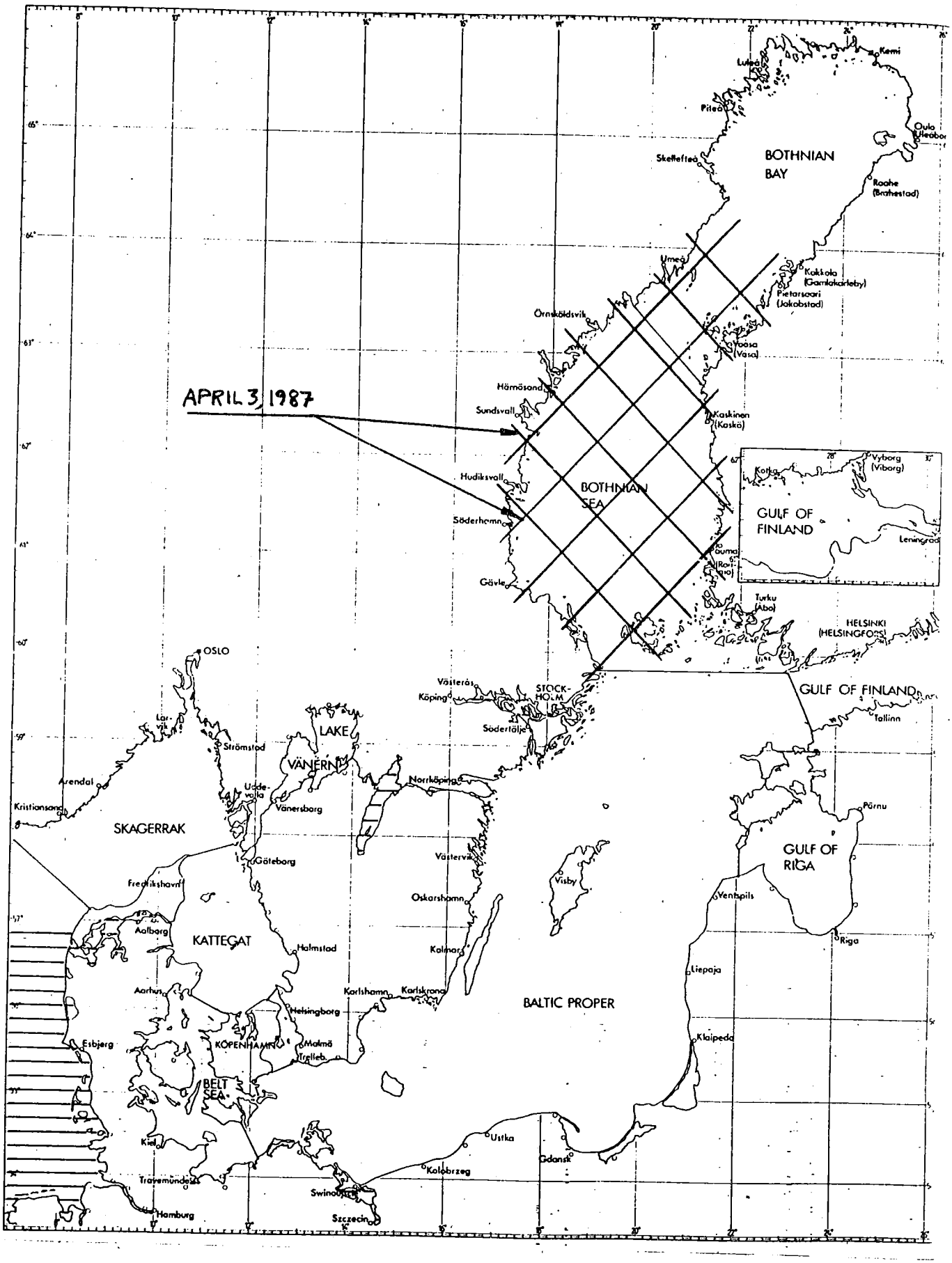

Figure 1. Geosat tracks during the BEPERS Pilot Study.

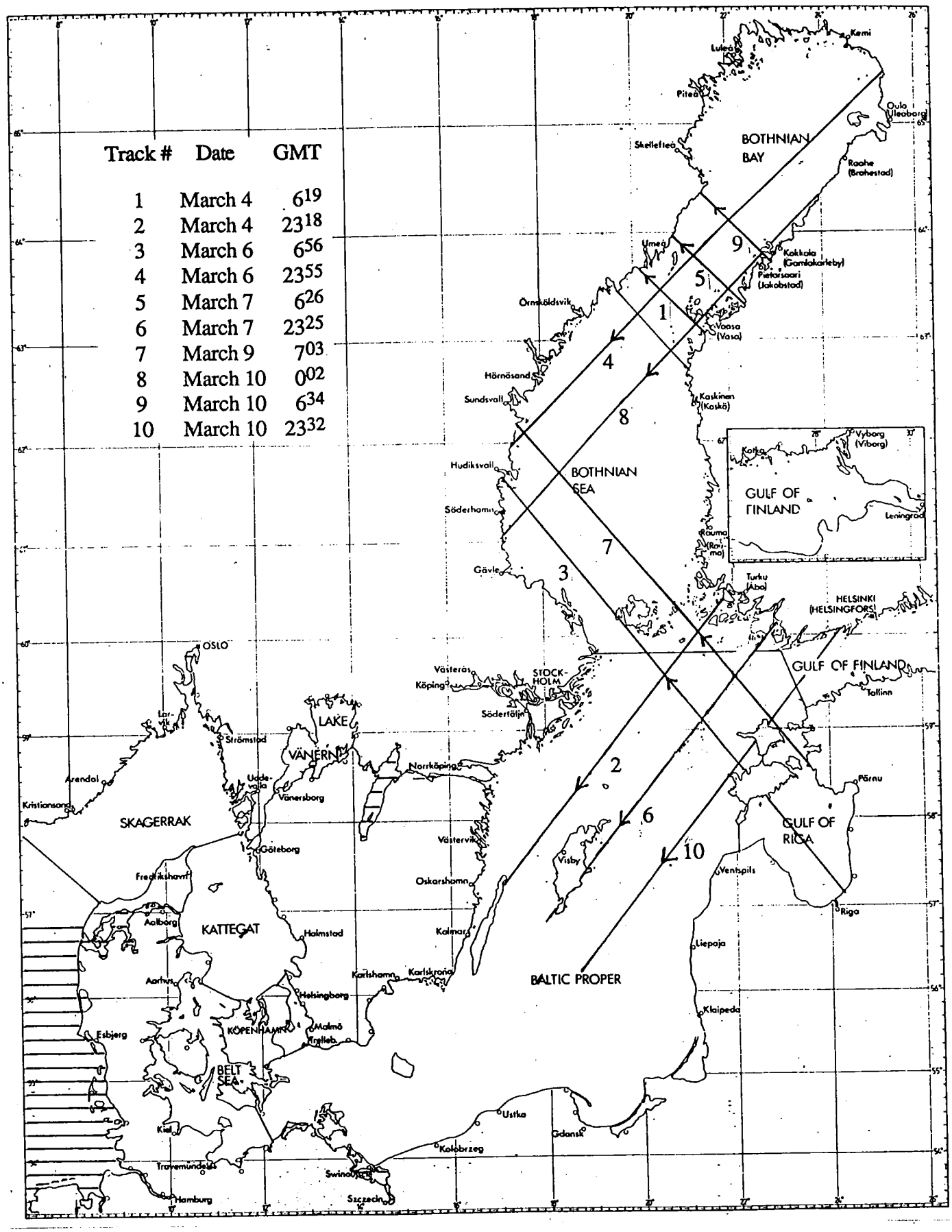

Figure 2. Extrapolated Geosat tracks during the BEPERS campaign 1988.

880501R

Helsinki 1988. Valtion painatuskeskus

ISBN 951-47-1278-1